Characteristics of the marine CO_2 system in Arctic waters.

International Environmental Doctoral School

Fernando Aguado Gonzalo

Marine Chemistry and Biochemistry Department

Institute of Oceanology Polish Academy of Sciences

&

International Environmental Doctoral School associated with the Centre for Polar Studies at the University of Silesia in Katowice

A PhD dissertation under the supervision of

Assoc. Prof. Karol Kuliński

Sopot 2026

Charakterystyka morskiego systemu węglanowego w wodach Arktyki.

Fernando Aguado Gonzalo

Zakład Chemii i Biochemii Morza

Instytut Oceanologii Polskiej Akademii Nauk

&

Międzynarodowa Środowiskowa Szkoła Doktorska przy Centrum Studiów Polarnych przy Uniwersytecie Śląskim w Katowicach

Rozprawa doktorska przygotowana pod kierunkiem

dr. hab. Karol Kulińskiego, prof. IO PAN

Sopot 2026

Table of Contents

Acknowledgments

First and foremost, I would like to express my most sincere gratitude to my supervisor, Karol Kuliński, for his guidance throughout this fantastic journey and for his eternal patience in answering all my questions and supporting all my "great" ideas. I want to thank Katarzyna Koziorowska and Marcin Stokowski for spending countless hours teaching me how to use the instrumentation and how not to break it. I would also like to thank the three of them for being the best travel companions you could ever wish for. Thank you for holding my hand through this journey.

I would also like to thank the Institute of Oceanology of the Polish Academy of Sciences and all the staff working on it for their cooperation over all these years, especially my colleagues in the chemistry department, who helped me turn this complicated journey into a pleasant walk.

To all the wonderful scientists and students I met during these years, and to the countless happy moments I shared with them.

Estoy eternamente agradecido de mi familia quien me enseño los valores de la educación e invirtieron su tiempo y su paciencia en asegurarse que nunca me faltase de nada, especialmente a mis padres, quienes tuvieron que despedirse de su hijo con 18 años para que pudiese perseguir sus sueños.

Finally, and most importantly, I would like to thank the two people who were always behind me, who helped me overcome stressful and difficult moments, who supported me in embarking on this adventure, and who helped me get back up every time I fell. To my wife, Alexandra Loginova, and to my son, Gorka Aguado Loginov, you were the light in this journey.

There were many difficult moments when things didn't work or failed, but thanks to all of you, I found the courage to say, "I will try again tomorrow." Until.. I succeed.

Thank you all!

Funding

The author declares that financial support was received for the research, authorship, and publication of this work.

First publication: The sampling, chemical analyses, and data interpretation related to the marine CO2 system structure and variability were financially supported by the Polish National Science Center, grant no. 2019/34/E/ST10/ 00167, under the project PROSPECTOR. The analysis of the interrelationships between sea ice extent and chlorophyll a distribution was supported by the European Union within the Horizon Europe programme, project 101136480 — SEA-Quester. The interpretation of the seawater freshening was supported by the Norwegian Financial Mechanism 2014–2021 (85%) and National Science Centre (15%) within the GRIEG Programme, grants no. 2019/34/H/ST10/00504 and 2019/34/H/ST10/00645. Additionally, the contribution of PK to the study was supported by the Polish National Science Center, grant no. 2020/37/B/ST10/02905.

Second publication: The study was performed within the framework of grant no. 2019/34/E/ST10/00167 financed by the Polish National Science Center. In addition, some sampling and chemical analyses were financially supported by the Norwegian Financial Mechanism 2014–2021 (85%) and National Science Centre (15%) within the GRIEG Programme, grants no. 2019/34/H/ ST10/00504 and 2019/34/H/ST10/00645. The interpretation of the results in terms of their contextualization was supported by the European Union's Horizon Europe research and innovation programme under Grant Agreement No. 101136480 (SEA-Quester).

Third publication: The study was conducted within the framework of Grant No. 2019/34/E/ST10/00167 (Arctic data), 2021/41/B/ST10/00946 (Baltic Sea pCO2 data), and 2023/49/B/ST10/02690 (TA, DIC, and pH data); all three of them financed by the Polish National Science Centre. The interpretation of the results in terms of their contextualization was supported by the European Union's Horizon Europe research and innovation programme under Grant Agreement No. 101136480 (SEA-Quester).

Publications included in this dissertation

1. Aguado Gonzalo, F., Stokowski, M., Koziorowska-Makuch, K., Makuch, P., Beszczyńska-Möller, A., Kukliński, P. and Kuliński, K., 2024. Key processes controlling the variability of the summer marine CO_2 system in Fram Strait surface waters. *Frontiers in Marine Science*, *11*, p.1464653. doi.org/10.3389/fmars.2024.1464653.

2. Aguado Gonzalo, F., Koziorowska, K., Szymczycha, B. and Kuliński, K., 2026. The internal consistency between calculated and measured variables of the marine carbonate system in Arctic open and coastal waters, case study: Atlantic Arctic. *Marine Chemistry*, p.104604. doi.org/10.1016/j.marchem.2026.104604.

3. Aguado Gonzalo, F., Koziorowska, K., Bromboszcz-Szczypior, L., Loginova, A. and Kuliński, K., 2026. High vertical resolution measurements of pH, pCO_2, Total Alkalinity and Dissolved Inorganic Carbon using a new approach: the carbonate profile. *Oceanologia*, 68(1), 68101. doi.org/10.5697/VMDA8631.

Summary

Introduction and Rationale

Seawater carbonate chemistry is described by the concentration and the reactions in seawater of the different carbonate species: CO_2 (carbon dioxide), HCO_3^- (bicarbonate ion), and CO_3^{2-} (carbonate ion). Part of the CO_2 gas ($CO_{2(g)}$) entering the water column remains in the form of dissolved gas ($CO_{2(aq)}$), while part reacts with H_2O to form carbonic acid (H_2CO_3), which rapidly dissociates into H^+ (hydrogen ion) and HCO_3^- that can further dissociate to CO_3^{2-}, releasing another H^+ (Eqs. 1, 2, and 3) (Dickson et al., 2007). Both these dissociation stages are described by the temperature-, pressure- and salinity-dependent dissociation constants k_1 and k_2 (Eqs. 4 and 5) (Millero, 2010).

$$CO_{2(g)} \rightleftharpoons CO_{2(aq)} \quad (1)$$

$$CO_{2(aq)} + H_2O \rightleftharpoons H^+ + HCO_3^- \quad (2)$$

$$HCO_3^- \rightleftharpoons H^+ + CO_3^{2-} \quad (3)$$

$$k_1 = \frac{[CO_2^*]\,[H^+]}{[HCO_3^-]} \quad (4)$$

$$k_2 = \frac{[HCO_3^-]\,[H^+]}{[CO_3^{2-}]} \quad (5)$$

where CO_2^* is a total concentration of $CO_{2(aq)}$ and an undissociated form of carbonic acid, H_2CO_3. Therefore, the dissociation of $CO_{2(aq)}$ increases H^+ concentration in seawater and thus reduces its pH ($pH = -\log_{10}[H^+]$).

The total sum of the concentrations of the different inorganic carbon species in seawater is denoted as the dissolved inorganic carbon (DIC) (Eq. 6).

$$DIC = [CO_{2(aq)}] + [H_2CO_3] + [HCO_3^-] + [CO_3^{2-}] \quad (6)$$

In the surface ocean, at a temperature of 17°C and a salinity of 35, approximately 92% of the DIC is in the form of bicarbonate ions, around 7% exists as carbonate ions, the other two species ($CO_{2(aq)}$ and H_2CO_3) constitute together only 1%, from which, 0.1 % is in the short living form of H_2CO_3. Thus, H_2CO_3 is not considered directly relevant for chemical or biological processes (e.g., Riebesell et al., 2010).

Although $CO_{2(aq)}$ represents only about 1% of the DIC pool, its concentration relative to the atmospheric level is crucial for the direction of the air-sea CO_2 gas exchange. When the concentration of CO_2 in the ocean surface is lower than in the atmosphere, there is a net flux of CO_2 to the seawater, while it is released from the seawater when its concentration is higher than in the atmosphere.

Since 1850, about 25% of total anthropogenic CO_2 emissions have been taken up by the oceans (Friedlingstein et al., 2025). As a consequence, the global ocean DIC inventory has increased, and the seawater pH has decreased, a phenomenon known as ocean acidification (OA). The pH decrease, which is currently about 0.017 per decade (IPCC, 2019), would be even larger if it were not for the presence of strong bases in the seawater (Ma et al., 2023), which capture some of the H^+ ions in the buffer reaction. Typically, this reaction is illustrated with carbonate ions (Eq. 7).

$$CO_{2(aq)} + CO_3^{2-} + H_2O \rightleftharpoons 2HCO_3^- \quad (7)$$

Although carbonate chemistry is most crucial for regulating ocean pH, other ions in seawater can also act as proton acceptors, controlling the pool of free protons in water. The excess of proton acceptors

over proton donors in seawater (or bases over acids), approximating the oceanic buffering capacity, is defined as the total alkalinity (TA) (Wolf-Gladrow et al., 2007). The TA in seawater is quantified as:

$$TA = [HCO_3^-] + 2[CO_3^{2-}] + [B(OH)_4^-] + [OH^-] + [HPO_4^{2-}] + 2[PO_4^{3-}] + [H_3SiO_4^-] + [NH_3] + [HS^-] - [H^+] - [HSO_4^-] - [HF] - [H_3PO_4] - [HNO_2] + [\text{minor bases - minor acids}] \quad (8)$$

Since TA is to a large extent salinity-dependent, it is relatively constant in open waters, whereas in coastal waters it shows significant temporal and spatial variability. Regardless of the total concentration and location, the dominant share of TA is mostly bicarbonates and carbonates, usually about 90%. In open waters, borates contribute a few percent to the TA, while other substances play a rather minor role and are often considered irrelevant. In coastal, estuarine, and fjord systems, however, these commonly negligible substances become more important either because of their unusual contribution and/or elevated concentrations (ion anomalies), and can largely contribute to TA. For instance, the contribution of organic compounds with acid-base properties in waters rich in dissolved organic matter can have a large contribution to the TA (Hunt et al., 2011; Kerr et al., 2021; Kuliński et al., 2017; Yang et al., 2015).

Commonly, four measurable parameters are used to describe the structure of the carbonate system in seawater (also denoted as marine CO_2 system) . The mass conservation is defined by (1) the DIC. The charge balance is parametrized by (2) the TA. The speciation of inorganic carbon species is controlled by (3) the pH. And the potential to transfer inorganic carbon between the atmosphere and the ocean surface is determined by (4) the partial pressure of seawater CO_2 (pCO_2) (Dickson et al., 2007).

In the well-characterized carbonate system of the open ocean, these four measurable variables (TA, DIC, pH and pCO_2) can be calculated using ion-pairing models through the set of thermodynamic and mass-balance equations (e.g. Lewis et al., 1998). For these calculations, two of the four variables are needed as input parameters, along with temperature and salinity. Besides TA, DIC, pH, and pCO_2, these models can also estimate the contributions and concentrations of different inorganic carbon species, including CO_3^{2-}. The concentration of CO_3^{2-} is ultimately used to determine the saturation states of aragonite (Ωar) and calcite (Ωcal), two crystal forms of calcium carbonate ($CaCO_3$) used by calcifying organisms to build their exoskeletons, therefore they are key parameters for understanding ecosystem health and sensitivity against OA. However, in coastal waters, the presence of unparametrized components in the ion-pairing models (such as organic compounds with acid-base properties) can induce errors (sometimes above the limits to resolve regional and short-term variability in the marine CO_2 system), expressed as over- or underestimations of the calculated parameters, including Ωar and Ωcal.

The Arctic Ocean is particularly efficient at absorbing anthropogenic CO_2 due to the higher solubility of the gas in its cold waters, which, on the other hand, makes the region especially sensitive to OA (von Schuckmann et al., 2024). Moreover, rising temperatures are increasing the extent and duration of sea ice-free areas, thereby enhancing air-sea CO_2 fluxes. The effect of OA is further amplified by seawater freshening caused by meltwater inflow from sea ice and glaciers, which is responsible for reducing TA and the buffer capacity in surface water layers (Zhang et al., 2020). Furthermore, river runoff remains a significant source of freshwater to the Arctic Ocean. Although the Arctic Ocean accounts for only 1% of the total oceanic volume, it receives approximately 11% of the global continental runoff, and this effect has been exacerbated in recent decades by the increase in precipitation in drainage basins (e.g. Capelle et al., 2020 and reference therein). On the other hand, the expansion of ice-free, open waters and the increase in nutrient supply have increased net primary production (NPP). This mechanism reduces CO_2 concentration and increases pH in the photic layer, counteracting OA.

Therefore, there is a direct feedback mechanism between anthropogenically driven changes in the Arctic cryosphere, air-sea CO_2 fluxes, and NPP, all of which transform the carbonate equilibrium of surface

waters and thus influence OA in different directions. **To quantify present and project future changes in OA, carbon cycling, and carbon inventory in the Arctic, it is necessary to accurately measure changes in the marine carbonate system and attribute the main drivers of these changes. Despite the significant exposure of Arctic waters to OA, the contributions of individual drivers to changes in its surface pH remain poorly quantified**.

Moreover, due to the harsh environmental conditions and logistical constraints, measurements of the carbonate system in Arctic waters are scarce. In most cases, only two (out of four) variables of the carbonate equilibrium are measured, and the others are calculated using ion-pairing balance models. This is despite the Arctic region being heavily influenced by meltwater, continental runoff, and enhanced primary production, all of which have the potential to cause atypical seawater composition and thus affect the quality of results estimated by the models. **Even though it is suspected that the accuracy of the calculated variables is likely reduced, to date, there have been no dedicated assessments demonstrating the uncertainty of the calculated values in Arctic coastal areas. There is also no study reporting clear guidelines about how to obtain high-quality calculated values of the carbonate system, which are ultimately the backbone for OA studies, ecosystem health and carbon inventory in the Arctic region.**

The scarcity of measurements and potential limitations in the quality of mathematically determined carbonate system variables are not the only problems. The high spatial (including vertical) and temporal variability of the marine carbonate system in Arctic coastal waters makes its characterization, and thus OA studies, a difficult task. Sampling of different carbonate system (and other biogeochemical) parameters is most often performed by collecting water with traditional Niskin-bottle-based devices, offering only sparse vertical resolution. **The lack of a system allowing for continuous, high-resolution water-column sampling of different variables of the marine carbonate system limits our ability to explore the rapid biogeochemical transformations in the photic zone, where melted sea ice, continental runoff, CO_2 air-sea gas exchange, and primary production interact simultaneously and have the most significant impact.**

Research hypotheses

Taking into account the actual state of knowledge on the marine carbonate system in Arctic waters, as well as research needs related to gaps in understanding, the following **research hypotheses** have been proposed:

1) Despite the direct influence of sea ice meltwater on TA and DIC, NPP is the main driver of pH changes in the surface layer of the Arctic open waters during the summer season.
2) The accuracy of the calculated carbonate system parameters using ion-pairing models is reduced in Arctic coastal areas compared to open ocean waters, limiting the quality of OA studies.
3) High-resolution vertical sampling of the marine carbonate system parameters reveals fine-scale biogeochemical variability in the surface layer induced by continental runoff and sea ice/glacier meltwater in Arctic coastal areas.

Goals

The main overarching aim of this PhD dissertation was to provide new insights into the structure and variability of the marine carbonate system in understudied Arctic waters, including the biogeochemically complex coastal areas. This was done considering the limitations of the possible sampling area and the challenges of providing high-quality, high-resolution data to link the variability of the marine carbonate system to the influence of continental runoff, sea ice meltwater, primary production, and temperature, with special focus on the Atlantic sector of the Arctic region. The specific **research goals** included:

I. To characterize the interannual spatial variability of the marine carbonate system in surface waters of the Fram Strait and to identify and quantify the main physical and biological drivers behind these transformations.
II. To identify quality limitations in the use of thermodynamic ion-pairing models to calculate TA, DIC, pH, and pCO_2 in open and coastal Arctic waters and to provide concise guidelines for obtaining high-quality data on the carbonate system.
III. To provide a solution for simultaneous sampling of all four carbonate system parameters (and other biogeochemical variables) with high vertical resolution in stratified, biogeochemically complex Arctic coastal waters.

Study area

The study has been mostly conducted in the North Atlantic region, and particularly in the Greenland Sea and the Fram Strait, as well as on the west shelf of Svalbard, including its adjacent fjords. This region has been recognized as one of the most effective areas in absorbing atmospheric CO_2 (e.g. Land et al., 2013) and, at the same time, one of the most productive areas in the Arctic (Cherkasheva et al., 2025; Slagstad et al., 2015). It is also known for its intensive water and heat exchange, where the East Greenland Current transports cold, low-salinity waters, together with sea ice, southwards along the Greenland shelf slope. On the other hand, the West Spitsbergen Current carries warm, more saline waters northward along the continental slope of the Archipelago of Svalbard (Beszczynska-Möller et al., 2012). Moreover, the Greenland Sea is the main gateway for Arctic sea ice (Spreen et al., 2020), and the resulting sea ice meltwater reduces surface water salinity. All this means that the surface waters in this region, which are so actively absorbing CO_2 and thus heavily exposed to OA, are characterized by dynamic interactions among different water masses with a wide range of physical, biological, and chemical properties (e.g., temperature, salinity, nutrient concentrations, and NPP). This provides an ideal setup for decoupling and quantifying the influence of different factors shaping spatial and temporal variability of the marine carbonate system in open waters – a feature that has been explored in Publication 1.

Moreover, the significant inflow of freshwater into the coastal zone of Svalbard (sea ice/glacier meltwater and continental runoff), and into the open waters of the Greenland Sea (sea ice meltwater), entails a decrease in TA, and therefore in the buffering capacity of seawater, increasing the vulnerability of these areas to OA. Simultaneously with the enhanced OA effect, freshwater inflow can complicate OA research itself by causing ion anomalies and introducing inorganic and organic non-parameterized substances, which can introduce errors when thermodynamic ion-pairing models are used to calculate carbonate system parameters. This phenomenon has been addressed in Publication 2.

Furthermore, the spread of freshwater is often accompanied by sharp salinity and biogeochemical gradients and by water column stratification, making precise water sampling of the carbonate system parameters challenging. The latter aspect has been investigated in Publication 3, which, in addition to the research in the waters of the North Atlantic, was enriched with additional measurements carried out in the Baltic Sea - a basin characterized by high riverine runoff and steep biogeochemical gradients in the water column.

Methods

The three publications included in this dissertation are largely based on my own measurements of temperature, salinity, pH, pCO_2, TA, and DIC taken in the East Greenland Sea and the Fram Strait (during summer 2021 and 2024), the continental shelf and fjords of the west coast of Svalbard (summer 2021 and 2022), and the Baltic Sea (spring 2024). In the case of Publication 1, the open waters data I collected during 2021 were merged with an existing database covering the same set of variables measured in 2019 and 2020 in the same region.

The analytical methodology I used in my experimental doctoral research included:

- The pCO_2 measurements were obtained from the headspace of a bubble-type equilibrator equipped with an additional spray-type water diffuser using a cavity ring-down spectroscope (CRDS) G210-I (Picarro) – the system described in detail by Stokowski et al. (2021). The equilibrator was receiving a constant flow of seawater from a pump located in Kingstone (surface water) and/or from a submersible pump ("carbonate profiler") in the case of Publication 3. To estimate temperature changes during the transport through the pipeline, temperature was always recorded at the inlet of the system and in the equilibrator.
- The pH was measured on a total pH scale (Clayton and Byrne, 1993) using a spectrophotometric method based on m-cresol purple (m-CP) dye using a HydroFIA pH (CONTROS, 4H JENA Engineering GmbH).
- The concentration of DIC (µmol kg^{-1}) was determined by acidifying the samples and measuring the resulting CO_2 (Chen et al., 2015). This was done using an automated DIC analyzer (Apollo SciTech Inc.) equipped with a Li7815 CO_2 detector.
- The TA concentration in the samples (µmol kg^{-1}) was estimated by closed-cell potentiometric titration as described by Dickson et al. (2007). Importantly, all TA and DIC measurements have been performed against certified reference materials provided by the Marine Physical Laboratory of the Scripps Institution of Oceanography, University of California, San Diego (Dickson et al., 2003).
- Underway salinity and temperature were measured with an SBE 21 SeaCAT thermosalinograph and an additional temperature probe SBE 38 located at the water inlet and measuring in situ temperature (Sea-Bird Scientific), while water column temperature and salinity data were measured using the CTD-rosette (SBE9/11, Sea-Bird Scientific).
- Calculations of the marine carbonate system components (DIC, TA, pH, and pCO_2) were done using the EXCEL version 2.3 of the ion-pairing model CO2SYS (Publication 1) and the updated version of the EXCEL CO2SYS provided by Orr et al. (2018) (Publication 2 and 3).

A detailed description of the sampling procedure, sample preservation, and analytical techniques was provided in the individual publications. This also refers to ancillary variables (e.g., concentration of phosphate, silicate, and oxygen saturation). Furthermore, some data from 2019 and 2020 were measured using different analyzers (but the same methodology). Related analytical details are described in Publication 1.

Overview of the results

This summary contains only brief descriptions of the results. More detailed information may be found in the individual publications that make up this PhD dissertation.

To achieve the first research goal, the spatial and interannual variabilities of the carbonate system data (TA, DIC, pH, and pCO_2), temperature, and salinity collected during 2019, 2020, and 2021 in the surface waters of the Fram Strait and the Eastern Greenland Sea were analyzed and presented in Publication 1. The results show that the study area was characterized by significant spatial hydrodynamic variability, which is reflected in changes in salinity (from 30.0 to 35.2) and temperature (from -0.5 °C to 8.5 °C). The TA concentrations clearly followed the distribution pattern of salinity, which suggests conservative mixing of TA. Extrapolation of the strong linear correlation between these two parameters indicates that the TA concentration for the zero-salinity end-member amounted to 420 µmol kg^{-1}. This agrees with previously reported values for sea ice (441 µmol kg^{-1}) (Rysgaard et al., 2007), indicating sea ice meltwater as the main driver of TA changes in the area.

To describe the influence of sea ice meltwater on DIC, previously reported data for sea ice DIC as the zero-salinity end-member (Rysgaard et al., 2007) and winter surface DIC as the high salinity end-member were used to determine the linear relationship between DIC and salinity (see Publication 1 and references therein). Then, the DIC determined by this function from measured salinity has been compared with measured DIC (Publication 1, Figure 5), and the difference between the two has been

attributed to (NPP). The results showed that NPP plays an important but secondary role in the spatial and interannual variability of DIC in surface waters and has a rather minor effect on TA changes.

Moreover, the interannual spatial distribution of salinity and temperature was correlated with the percentage of the study area covered by sea ice. The results showed that the year with the lowest sea ice cover (2021, with 16.7% of the study area covered by sea ice) was also the year with the lowest surface temperatures and the lowest surface water salinity. In the same way, the year with the largest area covered with sea ice (2019 with 49.9%) was also the year with the highest surface salinity and temperature. This revealed that the volume of summer-melted sea ice plays the main role in interannual changes in the distribution of sea surface temperature, salinity, and, by extension, TA and DIC in the study area.

Since the clear and strong influence of meltwater from sea ice on TA and DIC variability was confirmed, a thermodynamic ion pairing model (CO2SYS) was used to verify hypothesis 1) and to check whether this variability still has a lower potential than NPP to influence seawater pH. The calculations performed revealed that NPP was indeed the primary process driving pH variability in the region (Publication 1, Figure 9). Due to high interannual variability, NPP was responsible for pH changes in surface waters ranging from 0.10 in some years to 0.22 in others. Temperature and salinity variability in the study area were responsible for pH changes of up to 0.14 and 0.1, respectively. The calculations also showed that some minor part of pH variability in the region (up to 0.02) can be due to unparametrized processes and/or atypical seawater constituents not included in the commonly used thermodynamic models (denoted as inconsistencies in publication 1).

In Publication 1, the first research goal was achieved, and the reported results confirmed the first hypothesis: the high spatial and interannual variabilities of surface TA and DIC during summer in the North Atlantic, being driven by salinity (or volume of sea ice meltwater) changes, are not the primary drivers of the pH (and pCO_2) variability that is principally regulated by NPP.

In addition to the results used to test the first hypothesis, Publication 1 also provided high spatial resolution pCO_2 data collected during 2019, 2020, and 2021, which showed that other medium- and small-scale physical processes (e.g., mesoscale/submesoscale eddies) may contribute to rapid changes in pCO_2 and thus in the marine carbonate system. However, the mechanisms responsible for them cannot be understood solely from surface measurements. To describe and quantify these processes, it would be necessary to sample pCO_2, as well as other carbonate system variables, with high vertical resolution in the upper water column. Therefore, these results confirm the validity of the third hypothesis and the third research objective, pointing to the need for fine-scale water-column measurements (in this case, pCO_2) to understand the mechanism behind the variability of the carbonate system in the surface water layer.

The results from Publication 1 also clearly showed that the thermodynamic ion-pairing model can produce errors in pH calculations due to unparametrized processes and seawater constituents – a feature addressed in the second hypothesis and the second research goal. In Publication 1, pH was calculated from DIC and TA, as planned in the study. However, in such calculations, which are often the basis of OA studies, various combinations of all four carbonate system variables can be used, and the final errors may differ depending on the initial pair of carbonate variables used. To summarize and understand the limitations of the commonly used thermodynamic ion-pairing model, as proposed in the second research objective, the oceanic and coastal data collected in 2021 were used to compare the calculated values of TA, DIC, pH, and pCO_2 to the in situ measurements of the same values (Publication 2). The dispersion of the difference between measured and calculated values is commonly reported in similar studies as the average of the differences between measured and calculated values, together with their standard deviation. However, this statistical approach does not accurately reflect the data's dispersion around the "real values". In Publication 2, as part of the guideline for OA studies, it was proposed to use the 68th percentile, along with the rationale for this choice.

Together with the error reporting method, Publication 2 proposed a reference for distinguishing between "good quality" and "bad quality" data based on the weather-quality threshold for OA studies established by Newton et al. (2014). In our dataset, the threshold between good quality and low quality corresponds to a relative standard uncertainty of 10 μmol kg^{-1} for DIC and TA, 0.020 for pH, and 7 μatm for pCO_2.

The detailed analysis of estimated errors from Arctic coastal and ocean samples is presented in Publication 2, while the summary of the quality assessment is provided in Table 4 of this publication. The results indicate that high-quality calculated values can generally be obtained from oceanic samples. Only pH and pCO_2 as an input pair should be strictly avoided in calculations. On the other hand, values calculated from coastal samples generally produce low-quality datasets. Only pH and pCO_2 can be calculated with satisfying accuracy: for pH, using as input pairs TA and pCO_2 or DIC and pCO_2, and for pCO_2, using as input pairs DIC and pH.

In addition to the input carbonate system parameters, it is also recommended to include the concentrations of phosphates and silicates, as they can directly influence the carbonate equilibrium and thus the quality of the calculations. The evaluation of the contribution of these two input parameters demonstrates that not including them in the calculations generate an error between 1.9% and 7.2%.

The development of sensors capable of collecting in-situ pH and pCO_2 data with high temporal resolution has opened new possibilities to study OA in Arctic waters. Unfortunately, our study shows that pH and pCO_2 cannot be used together as input data for calculating other parameters. Therefore, in publication 2, we evaluate the feasibility of using TA calculated from salinity (TA_s) using a linear relationship developed from the collected dataset. Results demonstrate that applying TA_s together with either pH or pCO_2 produces slightly larger errors (than when using measured TA) but generally good-quality data. This opens new perspectives for long-term studies of OA, carbon inventory, and ecosystem health in Arctic coastal areas.

The results obtained in Publication 2 show that the absolute uncertainty in the calculations of the marine carbonate system is significantly larger in coastal regions than in oceanic waters, thereby positively verifying hypothesis 2. In addition to highlighting limitations in the use of thermodynamic ion-pairing models in Arctic coastal and oceanic waters, Publication 2 also provides concise guidelines for the research community to conduct high-quality OA-related research in this OA-sensitive region.

To achieve the third research objective and obtain high-resolution vertical measurements of the carbonate system parameters (including pCO_2) in highly stratified environments (e.g., near continental and glacier runoff), a new sampling approach was proposed (Publication 3). The system consists of a commonly used CTD profiler (Sea-Bird 19plus, Sea-Bird Electronics, Inc., Bellevue, Washington, USA), coupled with a submersible pump and hose to form a PUMP-CTD, which was then combined with a traditional underway equilibrator-based pCO_2 measuring unit. The system, denoted as the "carbonate profiler", can measure temperature and salinity in situ and transport seawater from selected depths to laboratories on a research vessel, enabling continuous measurements of temperature, salinity, pH, and pCO_2 and simultaneous discrete sampling for TA and DIC (and other biogeochemical variables) with high vertical resolution throughout the water column.

To demonstrate the capabilities of the carbonate profiler, a consistency test similar to the one presented in Publication 2 was performed in the ocean waters of the North Atlantic (Publication 3, Figure 3). Excellent agreement was demonstrated between measured pCO_2 in the water column and the pCO_2 calculated from water-column TA and pH, with a mean difference of $\bar{x}$ (SD) = 0.9 (±4.5) μatm, confirming the high quality of the coupling of both continuous measurements and discrete sampling.

A second sampling quality test was performed in the estuarine waters of the Vistula River (Baltic Sea). Four profiles (one every 6 hours) of TA, DIC, pH, pCO_2, salinity, and temperature were collected (Publication 3, Figure 5). The high performance of the carbonate profiler was assessed by reproducibly

precise estimation of the TA freshwater end-member (4069 µmol kg^{-1}, SD ±12 µmol kg^{-1}) based on the four vertical profiles.

Furthermore, sampling of turbidity plumes in high Arctic fjords demonstrated that the carbonate profiler can reveal rapid biogeochemical changes driven by freshwater inflow in the upper 5 meters of the water column (Hypothesis 3). The results demonstrate not only excellent performance of this sampling method but also provide evidence that a vertical resolution of 0.5 m is achievable for all carbonate system parameters (Publication 1, Figure 6). Moreover, the relationship between TA and salinity estimated from data collected with the carbonate profiler provides new insights into the freshwater TA end-members, ranging from 790 to 1240 µmol kg^{-1}, showing that continental runoff and glacier meltwaters in the Svalbard archipelago lower the buffer capacity of the seawater, reducing its potential to uptake atmospheric CO_2, and enhancing OA.

The studies presented in Publication 3 confirm that implementing simple modifications to sampling techniques enables the acquisition of high vertical resolution data on the carbonate system in stratified, biogeochemically complex coastal areas, and for resolving its rapid variability with high accuracy, thus confirming hypothesis 3.

Conclusions

The results and conclusions provided in the three publications compiled in this doctoral thesis successfully achieve all the objectives and positively verify the three research hypotheses. Furthermore, this work makes a groundbreaking contribution to Arctic research, with the following key findings:

- The mixing of sea ice meltwater and Atlantic water is the main driver for TA and DIC changes in the surface layer of the Fram Strait and the Greenland Sea.
- Although NPP exhibits strong interannual variability, it is the primary factor influencing pH in the Greenland Sea and Fram Strait surface waters. Temperature and salinity play a secondary (but also important) role.
- Determining marine carbonate system variables using the ion-pairing model generates significantly larger errors for Arctic coastal waters than for oceanic waters.
- Only three combinations of input parameters generate good quality data using the ion-pairing model in Arctic coastal waters: TA and pCO_2, DIC and pCO_2, and DIC and pH; other combinations should be avoided, and especially the pair of pCO_2 and pH.
- TA derived from salinity together with pCO_2 measurements can be used to calculate pH with high accuracy, which opens new possibilities for long-term OA studies in Arctic coastal waters.
- The influence of continental runoff and glacier/sea ice meltwater generates complex, sharp biogeochemical gradients in the surface layers of Arctic coastal waters and lowers the buffer capacity of seawater, reducing its potential to absorb atmospheric CO_2 and increasing ocean acidification.
- Easy-to-implement and inexpensive sampling system modifications combining a CTD profiler, a submersible pump and an underway pCO_2 measurement system fill a technology gap in studying changes in carbonate chemistry in stratified Arctic coastal waters.

Streszczenie

Wprowadzenie i uzasadnienie

System węglanowy wody morskiej opisują stężenia oraz reakcje poszczególnych form węgla nieorganicznego: CO_2 (dwutlenku węgla), HCO_3^- (jonu wodorowęglanowego) oraz CO_3^{2-} (jonu węglanowego). Część gazowego CO_2 ($CO_{2(g)}$) wnikającego do wody pozostaje w formie rozpuszczonego gazu ($CO_{2(aq)}$), natomiast część reaguje z H_2O, tworząc kwas węglowy (H_2CO_3), który ulega dysocjacji na jony H^+ (jon wodorowy) i HCO_3^-, a te z kolei mogą dalej dysocjować do CO_3^{2-}, uwalniając kolejny proton H^+ (równania 1, 2 i 3) (Dickson i in., 2007). Oba etapy dysocjacji opisują stałe dysocjacji k_1 i k_2 (równania 4 i 5), które są zależne od temperatury, ciśnienia i zasolenia (Millero, 2010).

$$CO_{2(g)} \rightleftharpoons CO_{2(aq)} \quad (1)$$

$$CO_{2(aq)} + H_2O \rightleftharpoons H^+ + HCO_3^- \quad (2)$$

$$HCO_3^- \rightleftharpoons H^+ + CO_3^{2-} \quad (3)$$

$$k_1 = \frac{[CO_2^*]\,[H^+]}{[HCO_3^-]} \quad (4)$$

$$k_2 = \frac{[HCO_3^-]\,[H^+]}{[CO_3^{2-}]} \quad (5)$$

gdzie CO_2^* jest sumarycznym stężeniem $CO_{2(aq)}$ i niezdysocjowanej formy kwasu węglowego, H_2CO_3.

Zatem dysocjacja rozpuszczonego CO_2 powoduje wzrost stężenia jonów H^+ w wodzie morskiej, a tym samym obniżenie jej pH ($pH = -\log_{10}[H^+]$).

Całkowita suma stężeń wszystkich form węgla nieorganicznego w wodzie morskiej określana jest jako rozpuszczony węgiel nieorganiczny (DIC – ang. *dissolved inorganic carbon*) (równanie 6).

$$DIC = [CO_{2(aq)}] + [H_2CO_3] + [HCO_3^-] + [CO_3^{2-}] \quad (6)$$

W warstwie powierzchniowej oceanu, przy temperaturze 17°C i zasoleniu 35, około 92% DIC występuje w formie HCO_3^-, około 7% w formie CO_3^{2-}, a pozostałe dwie formy ($CO_{2(aq)}$ i H_2CO_3) stanowią łącznie zaledwie 1%, z czego 0,1% przypada na krótkotrwały H_2CO_3. Z tego względu H_2CO_3 nie jest uznawany za bezpośrednio istotny w procesach chemicznych lub biologicznych (np. Riebesell i in., 2010).

Choć $CO_{2(aq)}$ stanowi jedynie około 1% puli DIC, jego stężenie względem stężenia w atmosferze ma kluczowe znaczenie dla kierunku wymiany gazowej CO_2 między atmosferą a morzem. Gdy stężenie CO_2 w warstwie powierzchniowej oceanu jest niższe niż w atmosferze, CO_2 jest pochłaniany przez wodę morską; w przeciwnym razie gaz jest uwalniany z wody do atmosfery.

Od 1850 roku około 25% całkowitej antropogenicznej emisji CO_2 zostało pochłonięte przez morza i oceany (Friedlingstein i in., 2025). W konsekwencji globalne stężenie DIC w oceanach wzrosło, a pH wody spadło – zjawisko to nazywane jest zakwaszaniem oceanów (OA – ang. *ocean acidification*). Spadek pH, który obecnie wynosi około 0,017 na dekadę (IPCC, 2019), byłby jeszcze większy, gdyby nie obecność w wodzie silnych zasad (Ma i in., 2023), które wychwytują część jonów H^+ w reakcji buforowej, zazwyczaj ilustrowanej z udziałem jonów węglanowych (równanie 7).

$$CO_{2(aq)} + CO_3^{2-} + H_2O \rightleftharpoons 2HCO_3^- \quad (7)$$

Mimo że to węglany i wodorowęglany są kluczowe dla regulacji pH oceanów, inne jony mogą również pełnić rolę akceptorów protonów. Nadmiar akceptorów protonów nad ich donorami (czyli zasad nad kwasami), opisujący pojemność buforową wody morskiej, definiuje się jako zasadowość całkowitą (TA – ang. *total alkalinity*) (Wolf-Gladrow i in., 2007). TA w wodzie morskiej jest wyznaczana jako suma stężeń zasad (wodorowęglanów, węglanów, boranów, krzemianów itd.) pomniejszona o stężenia kwasów (równanie 8).

$$TA = [HCO_3^-] + 2[CO_3^{2-}] + [B(OH)_4^-] + [OH^-] + [HPO_4^{2-}] + 2[PO_4^{3-}] + [H_3SiO_4^-] + [NH_3] + [HS^-] - [H^+] - [HSO_4^-] - [HF] - [H_3PO_4] - [HNO_2] + [\text{pozostałe zasady} - \text{pozostałe kwasy}] \quad (8)$$

Ponieważ TA w dużej mierze zależy od zasolenia, pozostaje ona relatywnie stała w wodach otwartych, podczas gdy w wodach przybrzeżnych wykazuje znaczną zmienność czasową i przestrzenną. Dominujący udział w TA (zazwyczaj ok. 90%), niezależnie od lokalizacji, mają wodorowęglany i węglany. Jednak w wodach przybrzeżnych, estuariach i fiordach inne substancje, które są zazwyczaj pomijalne, mogą odgrywać istotną rolę ze względu na ich podwyższone stężenia. Przykładem takich substancji są związki organiczne o właściwościach kwasowo-zasadowych, które w wodach o podwyższonym stężeniu materii organicznej mogą mieć istotny udział w TA (Hunt i in., 2011; Kuliński i in., 2017).

Do opisu struktury układu węglanowego w wodzie morskiej zazwyczaj stosuje się cztery mierzalne parametry. Zachowanie masy definiuje (1) DIC. Bilans ładunków charakteryzuje (2) TA. Specjację nieorganicznych form węgla kontroluje (3) pH. Potencjał wymiany węgla nieorganicznego między atmosferą a wodą morską jest określany przez (4) ciśnienie cząstkowe CO_2 w wodzie morskiej (pCO_2) (Dickson i in., 2007).

W dobrze scharakteryzowanych wodach oceanu otwartego te cztery zmienne można obliczać za pomocą równań równowagowych sprzężonych z modelami termodynamicznymi (tzw. ang. *ion-pairing models*). Do obliczeń wymagane są dwie z czterech zmiennych oraz temperatura i zasolenie. Oprócz TA, DIC, pH i pCO_2, modele te pozwalają również oszacować udział i stężenie różnych nieorganicznych form węgla, w tym CO_3^{2-}. Stężenie CO_3^{2-} jest z kolei wykorzystywane do określenia poziomów nasycenia wód aragonitem (Ωar) i kalcytem (Ωcal), które są formami krystalicznymi węglanu wapnia ($CaCO_3$) wykorzystywanymi przez organizmy kalcyfikujące do budowy ich egzoszkieletów. Powoduje to, że oba te parametry są jednocześnie kluczowe dla zrozumienia stanu ekosystemu i jego wrażliwości na OA. Jednak w wodach przybrzeżnych obecność składników wody morskiej niescharakteryzowanych w modelach parowania jonów (takich jak np. związki organiczne o właściwościach kwasowo-zasadowych) może powodować błędy (czasami duże), wyrażające się w przeszacowaniu lub niedoszacowaniu obliczanych parametrów, w tym Ωar i Ωcal.

Ocean Arktyczny jest szczególnie wydajny w pochłanianiu antropogenicznego CO_2 ze względu na podwyższoną rozpuszczalność gazów w jego zimnych wodach, co z kolei sprawia, że region ten jest również wyjątkowo wrażliwy na zakwaszanie (von Schuckmann i in., 2024). Co więcej, rosnące temperatury zwiększają zasięg obszarów wolnych od lodu morskiego i wydłużają czas trwania okresów bezlodowych, co wzmaga wymianę CO_2 między morzem a atmosferą. Zakwaszanie jest dodatkowo wzmacniane przez wysładzanie wody morskiej spowodowane napływem wód z topniejących lodowców i lodu morskiego, co prowadzi do zmniejszenia stężenia TA, a tym samym pojemności buforowej w powierzchniowej warstwie wód (Zhang i in., 2020). Ponadto istotnym źródłem wody słodkiej dla Oceanu Arktycznego pozostaje dopływ rzeczny. Mimo że Ocean Arktyczny stanowi zaledwie 1% całkowitej objętości oceanów, to dociera do niego około 11% globalnego spływu z lądu, a efekt ten dodatkowo nasilił się w ostatnich dekadach na skutek wzrostu opadów w zlewniach (np. Capelle i in., 2020 i cytowana tam literatura). Z drugiej strony, zwiększająca się powierzchnia wolnych od lodu, otwartych wód i wzrost dopływu składników odżywczych zwiększyły produkcję pierwotną netto (NPP– ang. *net primary production*). Mechanizm ten zmniejsza stężenie CO_2 i podnosi pH w warstwie eufotycznej, przeciwdziałając OA.

Istnieje zatem bezpośredni mechanizm sprzężenia zwrotnego między zmianami w kriosferze Arktyki, wymianą CO_2 przez powierzchnię morza oraz NPP, które przesuwają równowagę węglanową, a tym samym oddziałują na OA, w różnych kierunkach. **Aby ilościowo określić obecne i prognozować przyszłe zmiany w obiegu węgla w Arktyce, a także zmiany pH wód morskich, konieczne jest zidentyfikowanie zmian w morskim systemie węglanowym i przypisanie głównych czynników napędzających te zmiany. Pomimo znacznego narażenia wód powierzchniowych Arktyki na OA, wpływ poszczególnych czynników na zmiany pH pozostaje nierozpoznany.**

Ponadto, ze względu na trudne warunki środowiskowe i ograniczenia logistyczne, nadal mało jest bezpośrednich pomiarów systemu węglanowego w wodach Arktyki. W większości przypadków mierzy się tylko dwie (z czterech) zmienne opisujące równowagę węglanową, a pozostałe oblicza się za pomocą modeli termodynamicznych. Dzieje się tak pomimo silnego wpływu wód roztopowych i rzecznych oraz zwiększonej produkcji pierwotnej, które mogą powodować nietypowy skład wody morskiej, wpływając tym samym na jakość wyników modelowych. **Chociaż podejrzewa się, że dokładność modeli termodynamicznych może być ograniczona, szczególnie w obszarach przybrzeżnych Arktyki, do tej pory nie przeprowadzono żadnych specjalistycznych analiz określających niepewność obliczanych wartości. Brakuje również badań przedstawiających jasne wytyczne w zakresie uzyskiwania miarodajnych danych systemu węglanowego z wykorzystaniem metod numerycznych. Wytyczne te mogłyby stanowić podstawę dla dalszych badań nad OA, strumieniami węgla oraz oceną stanu ekosystemów morskich w regionie Arktyki.**

Niewystarczająca liczba pomiarów i potencjalne ograniczenia jakości matematycznie określonych zmiennych systemu węglanowego to nie jedyne problemy. Wysoka zmienność przestrzenna (w tym pionowa) i czasowa morskiego systemu węglanowego w arktycznych wodach przybrzeżnych sprawiają, że jego charakterystyka, a tym samym badania OA, są trudne. Pobieranie próbek różnych parametrów systemu węglanowego (i innych parametrów biogeochemicznych) najczęściej odbywa się przy użyciu batometrów, które ograniczają rozdzielczość pionową zbieranych próbek. **Brak systemu umożliwiającego ciągłe i o wysokiej rozdzielczości pionowej pobieranie próbek wody dla różnych zmiennych morskiego systemu węglanowego ogranicza możliwości badania szybkich przemian biogeochemicznych w strefie eufotycznej, gdzie topniejący lód morski, spływ kontynentalny, wymiana CO_2 między morzem a atmosferą oraz produkcja pierwotna oddziałują jednocześnie i mają największy wpływ.**

Hipotezy badawcze

Biorąc pod uwagę obecny stan wiedzy na temat morskiego systemu węglanowego w wodach Arktyki, a także potrzeby badawcze wynikające z niedostatków w jego zrozumieniu, postawiono następujące hipotezy badawcze:

1. Pomimo bezpośredniego wpływu wód z topnienia lodu morskiego na TA i DIC, to produkcja pierwotna netto jest głównym czynnikiem warunkującym zmiany pH w warstwie powierzchniowej otwartych wód Arktyki w sezonie letnim.
2. Dokładność parametrów systemu węglanowego obliczanych przy użyciu modeli termodynamicznych jest niższa w arktycznych obszarach przybrzeżnych w porównaniu z wodami otwartego oceanu, co ogranicza jakość badań nad zakwaszaniem oceanów (OA).
3. Pomiary i pobieranie z dużą rozdzielczością pionową próbek charakteryzujących morski system węglanowy ujawniają drobnoskalową zmienność biogeochemiczną w warstwie powierzchniowej, wywołaną przez dopływ rzeczny oraz topnienie lodu morskiego/lodowców w arktycznych obszarach przybrzeżnych.

Cele

Głównym i nadrzędnym celem niniejszej rozprawy doktorskiej było dostarczenie nowej wiedzy na temat struktury i zmienności morskiego systemu węglanowego w niedostatecznie zbadanych wodach Arktyki, w tym w złożonych biogeochemicznie obszarach przybrzeżnych. Badania skupiły się na dostarczeniu wysokiej jakości danych z atlantyckiego sektora Arktyki, aby umożliwić powiązanie zmienności morskiego systemu węglanowego z wpływem wód rzecznych i roztopowych, produkcji pierwotnej oraz temperatury. Szczegółowe cele badawcze obejmowały:

I. Charakterystykę międzyrocznej zmienności przestrzennej morskiego systemu węglanowego w wodach powierzchniowych Cieśniny Fram oraz identyfikację i ilościowe określenie głównych fizycznych i biologicznych czynników odpowiedzialnych za te przemiany.
II. Identyfikację ograniczeń jakościowych w stosowaniu termodynamicznych modeli do obliczania TA, DIC, pH i pCO_2 w otwartych i przybrzeżnych wodach Arktyki oraz opracowanie zwięzłych wytycznych na temat sposobu uzyskiwania wysokiej jakości danych o systemie węglanowym.
III. Opracowanie rozwiązania do jednoczesnego zbierania próbek wszystkich czterech mierzalnych parametrów systemu węglanowego (oraz innych zmiennych biogeochemicznych) z wysoką rozdzielczością pionową w uwarstwionych, złożonych biogeochemicznie wodach przybrzeżnych.

Obszar badań

Badania przeprowadzono głównie w regionie północnego Atlantyku, a w szczególności w Morzu Grenlandzkim i Cieśninie Fram, a także na zachodnim szelfie Svalbardu, w tym w przyległych fiordach. Region ten jest uznany za jeden z obszarów najefektywniej pochłaniających atmosferyczny CO_2 (np. Land i in., 2013), a jednocześnie za jeden z najbardziej produktywnych obszarów Arktyki (Cherkasheva i in., 2025; Slagstad i in., 2015). Znany jest on również z intensywnej wymiany ciepła i mieszania różnych mas wodnych, gdzie prąd wschodniogrenlandzki transportuje zimne, nisko zasolone wody wraz z lodem morskim na południe wzdłuż szelfu Grenlandii. Z drugiej strony, prąd zachodniospitsbergeński niesie ciepłe, bardziej słone wody na północ wzdłuż szelfu kontynentalnego archipelagu Svalbard (Beszczyńska-Möller i in., 2012). Co więcej, Morze Grenlandzkie stanowi główną drogę eksportu dla arktycznego lodu morskiego (Spreen i in., 2020), a powstająca w wyniku tego woda roztopowa zmniejsza zasolenie wód powierzchniowych. Wszystko to sprawia, że wody powierzchniowe w tym regionie, tak aktywnie absorbujące CO_2 i tym samym silnie narażone na zakwaszanie, charakteryzują się dynamicznymi interakcjami między różnymi masami wodnymi o szerokim zakresie właściwości fizycznych, biologicznych i chemicznych (np. temperatura, zasolenie, stężenie biogenów oraz produkcja pierwotna netto). Stanowi to idealny układ do rozdzielenia i ilościowego określenia wpływu różnych czynników kształtujących przestrzenną i czasową zmienność morskiego systemu węglanowego w wodach otwartych – zagadnienie to zostało zgłębione w Publikacji 1.

Ponadto znaczny dopływ słodkiej wody do strefy przybrzeżnej Svalbardu (rzeki oraz woda z topnienia lodu morskiego/lodowców) oraz do otwartych wód Morza Grenlandzkiego (woda z topnienia lodu morskiego) powoduje spadek TA, a tym samym obniżenie zdolności buforowej wody morskiej na zmiany pH, co zwiększa podatność tych obszarów na OA. Jednocześnie wraz z nasilonym efektem zakwaszania, dopływ słodkiej wody może komplikować same badania nad OA, powodując anomalie jonowe i dostarczając substancje nieorganiczne i organiczne o niescharakteryzowanych właściwościach kwasowo-zasadowych. Może to prowadzić do błędów przy wyznaczaniu parametrów systemu węglanowego, z wykorzystywaniem modeli termodynamicznych. Badania w tym zakresie są opisane w Publikacji 2.

Co więcej, rozprzestrzenianiu się wysłodzonej wody towarzyszą często gwałtowne zmiany zasolenia i parametrów biogeochemicznych oraz stratyfikacja kolumny wody, co sprawia, że precyzyjne

próbkowanie parametrów systemu węglanowego jest wyzwaniem. Ten ostatni aspekt został zbadany w Publikacji 3, która, oprócz badań na wodach Północnego Atlantyku, została wzbogacona o dodatkowe pomiary przeprowadzone w Morzu Bałtyckim – basenie charakteryzującym się wysokim spływem rzecznym i znacznymi gradientami biogeochemicznymi w kolumnie wody.

Metody

Trzy publikacje wchodzące w skład niniejszej rozprawy opierają się w dużej mierze na moich własnych pomiarach temperatury, zasolenia, pH, pCO_2, TA i DIC, przeprowadzonych we wschodniej części Morza Grenlandzkiego i w Cieśninie Fram (latem 2021 i 2024 r.), na szelfie kontynentalnym i w fiordach zachodniego wybrzeża Svalbardu (latem 2021 i 2022 r.) oraz w Morzu Bałtyckim (wiosną 2024 r.). W przypadku Publikacji 1, zebrane przeze mnie w 2021 r. dane z wód otwartych zostały połączone z istniejącą bazą danych obejmującą ten sam zestaw zmiennych z 2019 i 2020 r. w tym samym regionie.

Metodyka analityczna wykorzystana w moich eksperymentalnych badaniach doktoranckich obejmowała:

- Pomiary pCO_2 uzyskano z fazy gazowej (ang. *headspace*) ekwilibratora przepływowego wyposażonego w dodatkowy natryskowy rozpylacz wody, przy użyciu detekcji CRDS w spektroskopie G210-I (Picarro) – system ten został szczegółowo opisany przez Stokowskiego i in. (2021). Do ekwilibratora doprowadzano w sposób ciągły wodę morską z pompy umieszczonej w kingstonie (woda powierzchniowa) i/lub z pompy zanurzalnej (ang. „*carbonate profiler*") w przypadku Publikacji 3. Aby oszacować zmiany temperatury podczas transportu rurociągiem od ujęcia w morzu do laboratorium, temperaturę rejestrowano na wlocie do układu oraz w ekwilibratorze, gdzie przeprowadzane były pomiary.
- pH mierzono na skali całkowitej (Clayton i Byrne, 1993) metodą spektrofotometryczną z wykorzystaniem purpury m-krezolowej (m-CP) przy użyciu systemu HydroFIA pH (CONTROS, 4H JENA Engineering GmbH).
- Stężenie DIC (µmol kg^{-1}) oznaczano poprzez zakwaszenie próbek i pomiar powstałego CO_2 (Chen i in., 2015). Wykorzystano do tego automatyczny analizator DIC (Apollo SciTech Inc.) wyposażony w detektor CO_2 Li7815.
- Stężenie TA w próbkach (µmol kg^{-1}) oznaczono metodą potencjometrycznego miareczkowania w układzie zamkniętym, zgodnie z założeniami Dicksona i in. (2007). Co istotne, wszystkie pomiary TA i DIC zostały wykonane w odniesieniu do certyfikowanych materiałów referencyjnych (CRM) dostarczonych przez Marine Physical Laboratory, Scripps Institution of Oceanography, University of California, San Diego (Dickson i in., 2003).
- Ciągłe pomiary zasolenia i temperatury w ruchu statku (ang. *underway*) wykonywano za pomocą termosalinografu SBE 21 SeaCAT oraz dodatkowego czujnika temperatury SBE 38 umieszczonego na wlocie wody do systemu, mierzącego temperaturę *in situ* (Sea-Bird Scientific). W przypadku badań w kolumnie wody, dane o temperaturze i zasoleniu zostały zebrane za pomocą sondy SBE9/11, Sea-Bird Scientific.
- Obliczenia zmiennych morskiego systemu węglanowego (DIC, TA, pH i pCO_2) wykonano przy użyciu programu CO2SYS w wersji EXCEL 2.3 (Publikacja 1) oraz zaktualizowanej wersji EXCEL CO2SYS udostępnionej przez Orr i in. (2018) (Publikacje 2 i 3).

Szczegółowy opis procedur pobierania próbek, ich konserwacji oraz technik analitycznych został zawarty w poszczególnych publikacjach. Dotyczy to również zmiennych pomocniczych (np. stężenia fosforanów, krzemianów i nasycenia tlenem). Ponadto niektóre dane z lat 2019 i 2020 mierzono przy użyciu innych analizatorów (lecz przy zastosowaniu tej samej metodologii) - szczegóły analityczne w tym zakresie opisano w Publikacji 1.

Przegląd wyników

Niniejsze streszczenie zawiera jedynie krótkie opisy uzyskanych wyników. Bardziej szczegółowe informacje można znaleźć w poszczególnych publikacjach składających się na tę rozprawę doktorską.

Aby zrealizować pierwszy cel badawczy, w Publikacji 1 przeanalizowano i przedstawiono przestrzenną oraz międzyroczną zmienność systemu węglanowego (TA, DIC, pH i pCO_2), oraz temperatury i zasolenia na podstawie danych zebranych w latach 2019, 2020 i 2021 w wodach powierzchniowych Cieśniny Fram i wschodniej części Morza Grenlandzkiego. Wyniki pokazują, że obszar badań charakteryzował się znaczną przestrzenną zmiennością hydrodynamiczną, co odzwierciedlały zmiany zasolenia (od 30,0 do 35,2) i temperatury (od -0,5°C do 8,5°C). Stężenia TA wyraźnie podążały za zmianami zasolenia, co sugeruje konserwatywne mieszanie TA. Ekstrapolacja silnej korelacji liniowej między tymi dwoma parametrami wskazuje, że stężenie TA w wodzie słodkiej wynosiło 420 µmol kg^{-1}. Jest to zgodne z wcześniej raportowanymi wartościami dla lodu morskiego (441 µmol kg^{-1}) (Rysgaard i in., 2007), co wskazuje na wody pochodzące z jego topnienia jako główny czynnik powodujący zmiany TA w tym obszarze.

Do opisania wpływu wód z topnienia lodu morskiego na DIC wykorzystano liniową zależność między wcześniej opublikowanymi danymi dla DIC w lodzie morskim (Rysgaard i in., 2007) a zimowym stężeniem DIC w wodach powierzchniowych (Publikacja 1 i cytowana tam literatura). Następnie stężenia DIC wyznaczone za pomocą tej funkcji na podstawie zmierzonego zasolenia porównano ze zmierzonymi wartościami DIC (Publikacja 1, Ryc. 5), a różnicę między nimi przypisano produkcji pierwotnej netto. Wyniki wykazały, że NPP odgrywa ważną, choć drugorzędną rolę w przestrzennej i międzyrocznej zmienności DIC w wodach powierzchniowych i ma raczej niewielki wpływ na zmiany TA.

Badania wykazały także, że międzyroczny rozkład przestrzenny zasolenia i temperatury w rejonie badań jest wyraźnie skorelowany z procentowym udziałem obszaru pokrytego lodem morskim. Rok o najmniejszej pokrywie lodowej (2021, z 16,7% powierzchni pokrytej lodem) był jednocześnie rokiem o najniższych temperaturach i najniższym zasoleniu wód powierzchniowych. Analogicznie, rok z największym obszarem pokrytym lodem (2019, 49,9%) był rokiem o najwyższym zasoleniu i temperaturze w powierzchniowej warstwie. Dowodzi to, że objętość stopionego latem lodu morskiego odgrywa główną rolę w międzyrocznych zmianach rozkładu temperatury powierzchni morza, zasolenia, a w konsekwencji również TA i DIC w obszarze badań.

Ze względu na wyraźny i silny wpływ wód z topnienia lodu morskiego na zmienność TA i DIC, użyto termodynamicznego modelu (CO2SYS) w celu weryfikacji hipotezy 1) i sprawdzenia, czy zmienność ta ma nadal mniejszy potencjał oddziaływania na pH wody morskiej niż NPP. Przeprowadzone badania wykazały, że NPP była w istocie głównym procesem warunkującym zmienność pH w tym regionie (Publikacja 1, Ryc. 9). Ze względu na dużą zmienność międzyroczną, NPP odpowiadała za zmiany pH w wodach powierzchniowych w zakresie od 0,10 w niektórych latach do 0,22 w innych. Z kolei zmienność temperatury i zasolenia w obszarze badań odpowiadała za zmiany pH odpowiednio do 0,14 i 0,1. Analizy wykazały również, że niewielka część zmienności pH w regionie (do ok. 0,02) może wynikać z procesów i/lub nietypowych składników wody morskiej, nieuwzględnionych w powszechnie stosowanych modelach termodynamicznych (określonych w Publikacji 1 jako niespójności).

Publikacja 1 realizuje pierwszy cel badawczy, a przedstawione wyniki potwierdzają pierwszą hipotezę: wysoka przestrzenna i międzyroczna zmienność TA i DIC latem w powierzchniowych wodach Północnego Atlantyku, będąca wynikiem zmian zasolenia (lub objętości wód dopływających z topnienia lodu morskiego), nie jest głównym czynnikiem kształtującym zmienność pH (oraz pCO_2), która z kolei jest regulowana przede wszystkim przez NPP.

Oprócz wyników wykorzystanych do zweryfikowania pierwszej hipotezy, Publikacja 1 dostarczyła również danych pCO_2 o wysokiej rozdzielczości przestrzennej zebranych w latach 2019, 2020 i 2021.

Wykazały one, że inne średnio- i małoskalowe procesy fizyczne (np. wiry) mogą przyczyniać się do gwałtownych zmian pCO_2, a tym samym w całym morskim systemie węglanowym. Mechanizmów odpowiedzialnych za te zmiany nie można jednak zrozumieć wyłącznie na podstawie pomiarów powierzchniowych. Aby opisać i określić ilościowo te procesy, konieczne byłyby pomiary pCO_2, a także zebranie innych zmiennych systemu węglanowego, z wysoką rozdzielczością pionową w górnej części kolumny wody. Wyniki te potwierdzają zatem zasadność trzeciej hipotezy i trzeciego celu badawczego, wskazując na potrzebę precyzyjnych pomiarów w kolumnie wody (w tym przypadku pCO_2) w celu zrozumienia mechanizmów kształtujących zmienność systemu węglanowego w warstwie powierzchniowej.

Wyniki Publikacji 1 pokazały również wyraźnie, że termodynamiczny model wody morskiej może generować błędy przy obliczeniach pH z powodu nietypowych procesów i składników wody morskiej – jest to zagadnienie poruszone w drugiej hipotezie i drugim celu badawczym. W Publikacji 1 wartość pH została obliczona na podstawie DIC i TA, zgodnie z planem badania. Jednak w takich obliczeniach, które często stanowią podstawę badań nad zakwaszaniem oceanów, można stosować różne kombinacje wszystkich czterech zmiennych systemu węglanowego, a ostateczne błędy mogą się różnić w zależności od wybranej pary parametrów wejściowych. Aby podsumować i zrozumieć ograniczenia powszechnie stosowanego modelu termodynamicznego, zgodnie z drugim celem badawczym, wykorzystano dane oceaniczne i przybrzeżne zebrane w 2021 r. (Publikacje 1 i 2) do porównania obliczonych wartości TA, DIC, pH i pCO_2 z pomiarami (Publikacja 2). Rozrzut różnic między wartościami zmierzonymi a obliczonymi jest powszechnie raportowane w podobnych badaniach jako wartość średnia różnic wraz z ich odchyleniem standardowym. Takie podejście statystyczne nie odzwierciedla jednak dokładnie rozproszenia danych wokół „wartości rzeczywistych". W Publikacji 2, w ramach wytycznych dla badań nad OA, zaproponowano zastosowanie 68. percentyla, wraz z uzasadnieniem tego wyboru.

Wraz z metodą raportowania błędów, w Publikacji 2 zaproponowano punkt odniesienia dla badań nad OA, rozdzielający dane „dobrej jakości" od danych „złej jakości", oparty na tzw. „progach jakości pogodowej" (ang. *weather-quality thresholds*) (Newton i in. 2014). W naszym zbiorze danych próg między dobrą a niską jakością odpowiadał niepewności wynoszącej odpowiednio 10 µmol kg^{-1} dla DIC i TA, 0,020 dla pH oraz 7 µatm dla pCO_2.

Szczegółowa analiza błędów oszacowanych dla próbek z przybrzeżnej i oceanicznej Arktyki została przedstawiona w Publikacji 2, natomiast podsumowanie oceny jakości znajduje się w Tabeli 4 tej publikacji. Wyniki wskazują, że wysoką jakość obliczeń można uzyskać dla próbek oceanicznych. W obliczeniach należy jednak bezwzględnie unikać pary wejściowej pH i pCO_2. Z kolei wartości obliczone dla obszarów przybrzeżnych zazwyczaj są niskiej jakości. Jedynie pH i pCO_2 mogą być obliczane z dużą dokładnością: dla pH przy użyciu par wejściowych TA i pCO_2 lub DIC i pCO_2, a dla pCO_2 przy użyciu pary wejściowej DIC i pH.

Oprócz parametrów wejściowych systemu węglanowego zaleca się również uwzględnienie stężeń fosforanów i krzemianów, ponieważ mogą one bezpośrednio wpływać na równowagę węglanową, a tym samym na jakość obliczeń. Ocena wkładu tych dwóch parametrów wejściowych wykazała, że ich pominięcie w obliczeniach generuje błąd od 1,9% do 7,2%.

Rozwój czujników zdolnych do zbierania *in situ* danych pH i pCO_2 z wysoką rozdzielczością czasową otworzył nowe możliwości badania OA w wodach Arktyki. Niestety nasze badania pokazują, że pH i pCO_2 nie mogą być stosowane jednocześnie jako parametry wejściowe do obliczania innych zmiennych. Dlatego w Publikacji 2 oceniamy możliwość wykorzystania TA oszacowanej z zasolenia (TA_s) przy użyciu liniowej zależności opracowanej na podstawie zebranego zbioru danych. Wyniki pokazują, że użycie TA_s wraz z pH lub pCO_2 generuje nieco większe błędy (niż przy wykorzystaniu zmierzonych wartości TA), ale ogólnie dane są dobrej jakości. Otwiera to nowe perspektywy dla długoterminowych badań nad OA, obiegiem węgla i stanem ekosystemów w przybrzeżnych obszarach Arktyki.

Wyniki uzyskane w Publikacji 2 pokazują, że niepewność bezwzględna dla obliczeń parametrów morskiego systemu węglanowego jest znacznie większa w rejonach przybrzeżnych niż w wodach oceanicznych, co pozytywnie weryfikuje hipotezę 2. Publikacja 2 nie tylko wskazuje na ograniczenia w stosowaniu modeli termodynamicznych w przybrzeżnych i oceanicznych wodach Arktyki, ale także dostarcza zwięzłych wytycznych dla społeczności naukowej, które mają pomóc w prowadzeniu wysokiej jakości badań nad OA w tym wrażliwym regionie.

Aby zrealizować trzeci cel badawczy i uzyskać pionowe profile zmiennych systemu węglanowego (w tym pCO_2) o wysokiej rozdzielczości w silnie stratyfikowanych wodach (np. w pobliżu ujść rzek i wód roztopowych z lodowców), zaproponowano nowe podejście do pobierania próbek (Publikacja 3). Zaprojektowany system składa się z powszechnie stosowanej w oceanografii sondy CTD (Sea-Bird 19plus, Sea-Bird Electronics, Inc., Bellevue, Waszyngton, USA) połączonej z pompą zanurzeniową, tworzących razem układ typu PUMP-CTD, który następnie zintegrowano z tradycyjną jednostką do pomiaru ciągłego pCO_2 opartą na ekwilibratorze przepływowym. System ten nazwano „profilerem węglanowym" (ang. *carbonate profiler*). Zestaw ten umożliwia pomiar temperatury i zasolenia *in situ* oraz transport wody morskiej z wybranych głębokości do laboratoriów na statku badawczym w celu ciągłego pomiaru pH i pCO_2 i jednoczesnego pobierania próbek TA i DIC (i innych zmiennych biogeochemicznych) z wysoką rozdzielczością pionową w kolumnie wody.

W celu zademonstrowania możliwości tak zaprojektowanego systemu do pobierania próbek, przeprowadzono w wodach oceanicznych Północnego Atlantyku test spójności podobny do tego przedstawionego w Publikacji 2 (Publikacja 3, Ryc. 3). Wykazano w nim doskonałą zgodność między pCO_2 zmierzonym w kolumnie wody a pCO_2 obliczonym na podstawie równolegle zbieranych próbek TA i pH z kolumny wody. Średnia różnica między obiema wartościami pCO_2 wynosiła zaledwie $\overline{x}$ (SD) = 0,9 (±4,5) µatm, co potwierdza wysoką jakość systemu pozwalającego na połączenie pomiarów ciągłych i zbierania próbek dyskretnych.

Drugi test jakości przeprowadzono w ujściu Wisły (Morze Bałtyckie). Zebrano próbki oraz wykonano pomiary TA, DIC, pH, pCO_2, zasolenia i temperatury z czterech profili pionowych (co 6 godzin) (Publikacja 3, Ryc. 5). Wysoka skuteczność profilera węglanowego została potwierdzona poprzez powtarzalne i precyzyjne oszacowanie TA dla wody rzecznej (4069 µmol kg^{-1}, SD ±12 µmol kg^{-1}) na podstawie ekstrapolacji wyników względem zasolenia z czterech pionowych profili.

Co więcej, pomiary i pobieranie próbek w mętnych wodach roztopowych fiordów wysokiej Arktyki wykazały, że dzięki zaprojektowanemu systemowi możliwe jest zaobserwowanie gwałtownych zmian biogeochemicznych wywołanych dopływem słodkiej wody w górnych 5 metrach kolumny wody (Hipoteza 3). Uzyskane wyniki nie tylko dowodzą doskonałej wydajności tej metody pobierania próbek, ale także dostarczają dowodów na to, że rozdzielczość pionowa 0,5 m jest możliwa do osiągnięcia dla wszystkich parametrów systemu węglanowego (publikacja 1, rysunek 6). Ponadto zależność między TA a zasoleniem oszacowana na podstawie danych zebranych za pomocą zaprojektowanego systemu do próbkowania dostarcza nowej i unikalnej wiedzy na temat zakresu stężeń TA w wodach słodkich (od 790 do 1240 µmol kg^{-1}). Wyniki te pokazują, że dopływ wód rzecznych i roztopowych w rejonie archipelagu Svalbard obniża zdolność buforową wody morskiej, redukując jej potencjał do pochłaniania atmosferycznego CO_2 i nasilając zakwaszanie wody morskiej.

Badania przedstawione w Publikacji 3 potwierdzają, że wdrożenie prostych modyfikacji do technik pobierania próbek pozwala na uzyskanie danych o wysokiej rozdzielczości pionowej dotyczących systemu węglanowego w stratyfikowanych, dynamicznych obszarach przybrzeżnych oraz na rozwiązanie ich znacznej zmienności biogeochemicznej, co tym samym potwierdza hipotezę 3.

Wnioski

Wyniki i wnioski przedstawione w trzech publikacjach składających się na niniejszą rozprawę doktorską pomyślnie realizują wszystkie cele i pozytywnie weryfikują trzy hipotezy badawcze. Ponadto praca ta wnosi nowatorski wkład w badania Arktyki, a jej kluczowe wnioski są następujące:

- Mieszanie się wód z topnienia lodu morskiego i wód atlantyckich jest głównym czynnikiem wpływającym na zmiany TA i DIC w warstwie powierzchniowej Cieśniny Fram i Morza Grenlandzkiego.
- NPP, mimo że wykazuje silną zmienność międzyroczną, jest głównym czynnikiem warunkującym pH w obszarach Morza Grenlandzkiego i Cieśniny Fram. Temperatura i zasolenie odgrywają rolę drugorzędną (ale również istotną) rolę.
- Wyznaczanie zmiennych morskiego systemu węglanowego z zastosowaniem modelu termodynamicznego jest obarczone znacznie większymi błędami dla wód przybrzeżnych Arktyki niż dla wód oceanicznych.
- Tylko trzy kombinacje parametrów wejściowych generują dane dobrej jakości za pomocą modelu parowania jonów dla wód przybrzeżnych Arktyki: TA i pCO_2, DIC i pCO_2 oraz DIC i pH; należy unikać innych kombinacji, a zwłaszcza pary pCO_2 i pH.
- TA wyznaczana z zasolenia razem z pCO_2 mogą być wykorzystywane do obliczania pH z wysoką dokładnością, co otwiera nowe możliwości dla długoterminowych badań nad OA w arktycznych wodach przybrzeżnych.
- Dopływ wody rzecznej oraz wód z topnienia lodowców i lodu morskiego generuje złożone gradienty biogeochemiczne w warstwach powierzchniowych arktycznych wód przybrzeżnych i obniża zdolność buforową wody morskiej, redukując jej potencjał do pochłaniania atmosferycznego CO_2 i nasilając zakwaszanie wody morskiej.
- Łatwe do wdrożenia i niedrogie modyfikacje systemu pobierania próbek, łączące sondę CTD, pompę zanurzeniową i system do pomiaru ciągłego pCO_2, wypełniają lukę technologiczną w badaniu zmienności systemu węglanowego w stratyfikowanych wodach przybrzeżnych Arktyki.

Bibliography

Beszczynska-Möller, A., Fahrbach, E., Schauer, U., and Hansen, E. 2012. Variability in Atlantic water temperature and transport at the entrance to the Arctic Ocean 1997 2010. ICES J. Mar. Sci. 69, 852–863. doi: 10.1093/icesjms/fss056

Capelle, D.W., Kuzyk, Z.Z.A., Papakyriakou, T., Guéguen, C., Miller, L.A., Macdonald, R.W., 2020. Effect of terrestrial organic matter on ocean acidification and CO2 flux in an Arctic shelf sea. Prog. Oceanogr. 185. https://doi.org/10.1016/j.pocean.2020.102319

Chen, B., Cai, W.J., Chen, L., 2015. The marine carbonate system of the Arctic Ocean: Assessment of internal consistency and sampling considerations, summer 2010. Mar. Chem. 176, 174–188. https://doi.org/10.1016/j.marchem.2015.09.007

Cherkasheva, A., Manurov, R., Kowalczuk, P., Loginova, A.N., Zabłocka, M. and Bracher, A., 2025. Adaptation of global primary production model to the Greenland Sea conditions: parameterization and monitoring for 1998-2022. Frontiers in Marine Science, 11, p.1491180.

Clayton, T.D., Byrne, R.H., 1993. Spectrophotometric seawater pH measurements: total hydrogen ion concentration scale calibration of m-cresol purple and at-sea results. Deep. Res. Part I 40, 2115–2129. https://doi.org/10.1016/0967-0637(93)90048-8

Dickson, A.G., Afghan, J.D., Anderson, G.C., 2003. Reference materials for oceanic CO2 analysis: A method for the certification of total alkalinity. Mar. Chem. 80, 185–197. https://doi.org/10.1016/S0304-4203(02)00133-0

Dickson, A.G.; Sabine, C.L. and Christian, J.R. (eds) 2007. Guide to best practices for ocean CO2 measurement. Sidney, British Columbia, North Pacific Marine Science Organization, 191pp. (PICES Special Publication 3; IOCCP Report 8). DOI: https://doi.org/10.25607/OBP-1342

Friedlingstein, P., O'Sullivan, M., Jones, M.W., Andrew, R.M., Bakker, D.C., Hauck, J., Landschützer, P., Le Quéré, C., Li, H., Luijkx, I.T. and Peters, G.P., 2025. Global carbon budget 2025. Earth System Science Data Discussions, 2025, pp.1-139.

Hunt, C.W., Salisbury, J.E., Vandemark, D., 2011. Contribution of non-carbonate anions to total alkalinity and overestimation of pCO2 in New England and New Brunswick rivers. Biogeosciences 8, 3069–3076. https://doi.org/10.5194/bg-8-3069-2011

IPCC Special Report on the Ocean and Cryosphere in a Changing Climate [H.-O. Pörtner, D.C. Roberts, V. Masson-Delmotte, P. Zhai, M. Tignor, E. Poloczanska, K. Mintenbeck, A. Alegría, M. Nicolai, A. Okem, J. Petzold, B. Rama, N.M. Weyer (eds.)], 2019. Cambridge University Press, Cambridge, UK and New York, NY, USA, 755 pp. https://doi.org/10.1017/9781009157964.

Kerr, D.E., Brown, P.J., Grey, A., Kelleher, B.P., 2021. The influence of organic alkalinity on the carbonate system in coastal waters. Mar. Chem. 237, 104050. https://doi.org/10.1016/j.marchem.2021.104050

Kuliński, K., Schneider, B., Szymczycha, B., Stokowski, M., 2017. Structure and functioning of the acid-base system in the Baltic Sea. Earth Syst. Dyn. 8, 1107–1120. https://doi.org/10.5194/esd-8-1107-2017

Land, P.E., Shutler, J.D., Cowling, R.D., Woolf, D.K., Walker, P., Findlay, H.S., 2013. Climate change impacts on sea–air fluxes of CO2 in three Arctic seas : a sensitivity study using Earth observation 8109–8128. https://doi.org/10.5194/bg-10-8109-2013

Lewis, E., Wallace, D. and Allison, L.J., 1998. Program developed for CO2 system calculations (No. ORNL/CDIAC--105). Brookhaven National Lab., Dept. of Applied Science, Upton, NY (United

States); Oak Ridge National Lab., Carbon Dioxide Information Analysis Center, TN (United States).

Ma, D., Gregor, L. and Gruber, N., 2023. Four decades of trends and drivers of global surface ocean acidification. Global Biogeochemical Cycles, 37(7), p.e2023GB007765.

Millero, F.J., 2010. Carbonate constants for estuarine waters. Marine and freshwater research, 61(2), pp.139-142.

Millero, F.J., 2007. The marine inorganic carbon cycle. Chem. Rev. 107, 308–341. https://doi.org/10.1021/cr0503557.

Newton, J.A., Feely, R.A., Jewett, E.B., Williamson, P., Mathis, J., 2014. Global Ocean Acidification Observing Network: requirements and governance Plan. Glob. Ocean Acidif. Obs. Netw. 5–28.

Orr, J.C., Epitalon, J.M., Dickson, A.G., Gattuso, J.P., 2018. Routine uncertainty propagation for the marine carbon dioxide system. Mar. Chem. 207, 84–107. https://doi.org/10.1016/j.marchem.2018.10.006

Riebesell, U., Fabry, V.J., Hansson, L., 2010. Guide to best practices for ocean acidification research and data reporting, European commission.

Rysgaard, S., Glud, R.N., Sejr, M.K., Bendtsen, J., Christensen, P.B., 2007. Inorganic carbon transport during sea ice growth and decay: A carbon pump in polar seas. J. Geophys. Res. Ocean. 112, 1–8. https://doi.org/10.1029/2006JC003572

Slagstad, D., Wassmann, P.F.J., Ellingsen, I., 2015. Physical constrains and productivity in the future Arctic Ocean. Front. Mar. Sci. 2, 1–23. https://doi.org/10.3389/fmars.2015.00085

Spreen, G., De Steur, L., Divine, D., Gerland, S., Hansen, E. and Kwok, R., 2020. Arctic sea ice volume export through Fram Strait from 1992 to 2014. Journal of Geophysical Research: Oceans, 125(6), p.e2019JC016039.

Stokowski, M., Makuch, P., Rutkowski, K., Wichorowski, M. and Kuliński, K., 2021. A system for the determination of surface water pCO2 in a highly variable environment, exemplified in the southern Baltic Sea. Oceanologia, 63(2), pp.276-282.

Von Schuckmann, K., Moreira, L., Cancet, M., Gues, F., Autret, E., Baker, J., Bricaud, C., Bourdalle-Badie, R., Castrillo, L., Cheng, L. and Chevallier, F., 2024. The state of the global ocean. State of the Planet, 4, pp.1-30.

Wolf-Gladrow, D.A., Zeebe, R.E., Klaas, C., Körtzinger, A., Dickson, A.G., 2007. Total alkalinity: The explicit conservative expression and its application to biogeochemical processes. Mar. Chem. 106, 287–300. https://doi.org/10.1016/j.marchem.2007.01.006

Yang, B., Byrne, R.H., Lindemuth, M., 2015. Contributions of organic alkalinity to total alkalinity in coastal waters: A spectrophotometric approach. Mar. Chem. 176, 199–207. https://doi.org/10.1016/j.marchem.2015.09.008

Zhang, Y., Yamamoto-Kawai, M., Williams, W.J., 2020. Two Decades of Ocean Acidification in the Surface Waters of the Beaufort Gyre, Arctic Ocean: Effects of Sea Ice Melt and Retreat From 1997–2016. Geophys. Res. Lett. 47, 1–11. https://doi.org/10.1029/2019GL086421

Publication 1

Aguado Gonzalo, F., Stokowski, M., Koziorowska-Makuch, K., Makuch, P., Beszczyńska-Möller, A., Kukliński, P. and Kuliński, K., 2024. Key processes controlling the variability of the summer marine CO_2 system in Fram Strait surface waters. *Frontiers in Marine Science*, *11*, p.1464653. doi.org/10.3389/fmars.2024.1464653.

frontiers | Frontiers in Marine Science

TYPE Original Research
PUBLISHED 11 November 2024
DOI 10.3389/fmars.2024.1464653

OPEN ACCESS

EDITED BY
Michele Giani,
National Institute of Oceanography and Applied Geophysics, Italy

REVIEWED BY
Matthew Buckley Alkire,
University of Washington, United States
Thiago Monteiro,
Universidade Federal do Rio Grande, Brazil

*CORRESPONDENCE
Karol Kuliński
kroll@iopan.pl

RECEIVED 14 July 2024
ACCEPTED 17 October 2024
PUBLISHED 11 November 2024

CITATION
Aguado Gonzalo F, Stokowski M, Koziorowska-Makuch K, Makuch P, Beszczyńska-Möller A, Kukliński P and Kuliński K (2024) Key processes controlling the variability of the summer marine CO_2 system in Fram Strait surface waters. *Front. Mar. Sci.* 11:1464653. doi: 10.3389/fmars.2024.1464653

Key processes controlling the variability of the summer marine CO_2 system in Fram Strait surface waters

Fernando Aguado Gonzalo[1], Marcin Stokowski[2], Katarzyna Koziorowska-Makuch[1], Przemysław Makuch[3], Agnieszka Beszczyńska-Möller[3], Piotr Kukliński[4] and Karol Kuliński[1]*

[1]Department of Marine Chemistry and Biochemistry, Institute of Oceanology of the Polish Academy of Sciences, Sopot, Poland, [2]Department of Genetics and Marine Biotechnology, Institute of Oceanology of the Polish Academy of Sciences, Sopot, Poland, [3]Department of Physical Oceanography, Institute of Oceanology of the Polish Academy of Sciences, Sopot, Poland, [4]Department of Marine Ecology, Institute of Oceanology of the Polish Academy of Sciences, Sopot, Poland

The aim of this study was to decouple and quantify the influence of various biological and physical processes on the structure and variability of the marine carbonate system in the surface waters of the eastern part of the Fram Strait area. This productive region is characterized by its complex hydrographic and sea ice dynamics, providing an ideal set up to study their influence on the variability of the marine carbonate system. Different variables of the marine CO_2 system: Total Alkalinity (TA), Dissolved Inorganic Carbon (DIC), partial pressure of CO_2 (pCO_2), and pH, were analysed together with temperature, salinity, sea ice extension, and chlorophyll *a* distribution during three consecutive summers (2019, 2020 and 2021), each of them having a unique oceanographic setting. The data revealed that TA and DIC are mostly controlled by the mixing of Atlantic water and sea ice meltwater. The combined effects of organic matter production/remineralization, calcium carbonate precipitation/dissolution, and air/sea CO_2 gas exchange cause deviations from this salinity-related mixing. The scale of these deviations and the proportion between the effects observed for TA and DIC suggest interannual shifts in net primary production and dominant phytoplankton species in the area. These shifts are correlated with the sea ice extent and the spread of the Polar Surface Waters in the region. Net primary production is the main factor controlling the temporal and spatial variability of pH and pCO_2 in the study area followed by the influence of temperature and, mixing of water masses expressed with salinity (seawater freshening). Surface waters of the Fram Strait area were generally undersaturated in CO_2. The lowest pCO_2 values, coinciding with an increase in oxygen saturation, were observed in areas of mixing of Arctic and Atlantic-derived water masses. However, as shown for 2021, a reduction of the sea ice extent may induce a westward shift of the chlorophyll maximum, resulting in pCO_2 increase and pH decrease in the eastern part. This indicates that sea ice extent and associated spread of Polar Surface Waters may be important factors shaping primary production, and thus pCO_2 and pH, in the Fram Strait area.

KEYWORDS

Marine CO_2 system, Arctic, Fram Strait, ocean acidification, pCO_2, pH, sea ice

1 Introduction

Due to climate change driven by anthropogenic forces, the Arctic Ocean is experiencing fast warming (Meredith et al., 2019). The sea ice concentration and extension in the Arctic have recently radically decreased in response to the increase in temperatures (Carmack et al., 2016; Comiso et al., 2011; Haine et al., 2015; Stroeve et al., 2012), and according to some future climate projections it may seasonally even completely disappear by mid-century (Peng et al., 2020). One of the expected consequences is the expansion of open waters favouring the air-sea CO_2 interchange. Up to today, between 116 ± 4 and 166 ± 60 TgC yr^{-1} of atmospheric CO_2 is being taken up by the Arctic Ocean (MacGilchrist et al., 2014; Yasunaka et al., 2023). Consequently, the uptake of CO_2 by the ocean is changing seawater chemistry, increasing dissolved inorganic carbon (DIC) concentration and reducing pH and calcium carbonate saturation state (Ω) (Ahmed et al., 2020; Bates and Mathis, 2009; Caldeira and Wickett, 2003; Manizza et al., 2019; Yasunaka et al., 2016), a process commonly known as Ocean Acidification (OA), which represents a direct threat to calcifying organisms (Wittmann and Pörtner, 2013; Kleypas, 2019).

The high solubility of CO_2 in cold polar regions makes them especially sensitive to ocean acidification, particularly in areas influenced by deep water upwelling (Qi et al., 2022), river runoff (Capelle et al., 2020; Fransson et al., 2009; Koziorowska-Makuch et al., 2023; Woosley and Millero, 2020), and sea-ice melting (Tynan et al., 2016; Zhang et al., 2020), with the latter two processes also reducing the buffer capacity of surface waters, inducing rapid pH changes. Moreover, the influence of sea-ice meltwater in surface waters enhances stratification, reducing vertical fluxes of nutrients and carbon, which has a direct impact on primary producers and CO_2 uptake and sequestration (e.g. Tremblay et al., 2015). Quick ice-melting events during summer are expected to become more frequent in the following decades due to the overall Arctic warming and the thinning of sea ice (e.g., Stroeve and Notz, 2018, and references therein), enhancing the influence of freshened, low alkalinity Arctic surface waters.

Moreover, the annual net primary production (NPP) in the Arctic Ocean has increased in the last decades (Lewis et al., 2020), a phenomenon that has been associated mostly with the expansion of open waters due to the sea ice loss (Carmack et al., 2016; Comiso et al., 2011; Haine et al., 2015; Stroeve et al., 2012). Corresponding to this change, biologically driven processes, such as primary production (PP) and remineralization of organic matter (OM), as well as the formation and dissolution of calcium carbonate, have a strong influence on all parameters of the carbonate system (Chierici et al., 2019; Wolf-Gladrow et al., 2007 and references therein), being especially important for CO_2 partial pressure (pCO_2) of surface waters and thus anthropogenic carbon sequestration (Devries, 2022 and references therein).

This all shows a strong interconnection between Arctic warming, sea ice extent, and NPP, and all these processes directly influence the marine carbonate system. Therefore, to estimate and project future changes in carbon sequestration and ocean acidification, it is necessary to understand and quantify spatial and temporal variations in the marine CO_2 system caused by these main drivers.

One of the most biologically productive sectors in the Arctic region is the Fram Strait area (Pabi et al., 2008; Slagstad et al., 2015). Being also the main gateway for sea ice export from the Arctic (e.g., Spreen et al., 2020), it provides a unique setting to study the influence of the changes in the cryosphere and the biological processes on the variability of the marine carbonate system in the surface waters. Furthermore, it was already reported that factors controlling changes in Fram Strait NPP are potentially associated with variations in ice-free zones during the growing season (Kahru et al., 2011; Arrigo and van Dijken, 2015), intensification of the water column stratification due to increased ice melting (Mayot et al., 2020), rising sea surface temperature (SST) (Cherkasheva et al., 2014), increase in nutrients availability (Krisch et al., 2020; Tuerena et al., 2021), and changes in the dynamics of the water masses (Arrigo et al., 2017; Joli et al., 2018; Marchese et al., 2019).

However, Fram Strait is also the main gateway for water masses and heat exchange between the Arctic Ocean and the North Atlantic (Beszczynska-Möller et al., 2012). The distribution of water masses and their interactions in Fram Strait are mainly controlled by the East Greenland Current (EGC) and the West Spitsbergen Current (WSC) (e.g., Beszczynska-Möller et al., 2012). The EGC brings cold and low saline waters and sea ice southward from the Arctic and follows the shelf slope east of Greenland (Halvorsen et al., 2015; Håvik et al., 2017). The WSC carries warm and more saline Atlantic-origin waters (AW) northward above the shelf break and continental slope along the western Spitsbergen coast. Although these main flows set up the water mass circulation in the area (Beszczynska-Möller et al., 2012), salinity distribution in the first meters of the water column is further modified by regional winds (Tsukernik et al., 2010; Halvorsen et al., 2015), storms (Brümmer et al., 2001; Graham et al., 2019), mesoscale eddies (Hattermann et al., 2016), sea ice melt (Marnela et al., 2013), recirculation of Atlantic Water (de Steur et al., 2014; Hattermann et al., 2016; Marnela et al., 2013; Richter et al., 2018; Hofmann et al., 2021) and evaporation-precipitation balance (Vihma et al., 2016). This complex oceanographical setup produces an intense spatial and temporal variation in NPP (Cherkasheva et al., 2014; Mayot et al., 2020), sea ice dynamics (Halvorsen et al., 2015; Spreen et al., 2020) and planktonic communities (Nöthig et al., 2015 and references therein), which add on top to the complexity of the carbonate system in the region and make understanding its spatio-temporal variability a challenging task.

The main goal of this study was to decouple and quantify the influence of various biological and physical processes on the structure of the marine carbonate system in the eastern Fram Strait surface waters, including its spatial and interannual variability. This was done by interpreting the results of the marine carbonate system from summer seasons of three consecutive years, each of which was analysed against the background of a unique oceanographical setting such as distribution of surface salinity and temperature, sea ice extent, as well as chlorophyll *a* distribution. The first part of the manuscript presents changes in total alkalinity (TA) and DIC, with particular emphasis on how biological processes may influence them. The

second part focuses on understanding and quantifying the main pH and pCO_2 distribution drivers and their spatial variability. The last part presents two hypothetical future scenarios, the first one where the surface waters are highly influenced by meltwater from sea ice and the second one with reduced influence of melted sea ice, providing an understanding of how the warmer, fresher, and sea-ice-reduced future will influence the marine carbonate system in the Fram Strait surface waters.

2 Methods

2.1 Sampling

In 2019, 2020, and 2021, biogeochemical and hydrographic data were collected from surface waters during the annually repeated research cruises of RV Oceania under the Institute of Oceanography Polish Academy of sciences (IOPAN) long-term Arctic research monitoring program (AREX). The sampling area covered the eastern part of the Fram Strait (Figure 1) extending from the west coast of Svalbard to approximately the Greenwich meridian and crossing the West Spitsbergen Current. The cruises of 2019 and 2021 were carried out from 21st June to 21st July, and in 2020, sampling was realized two weeks later, due to restrictions related to the Covid-19 pandemic, from 6th July to 8th August, all coinciding with the high melting season.

Surface seawater from a depth of 2.5 m was supplied with a specially designed, and previously used by Stokowski et al. (2021), plumbing system to the vessel's laboratories for both underway continuous measurements (salinity, temperature, pCO_2, oxygen saturation – O_2, and pH) and for collecting discrete samples for TA and DIC. The underway measurements of salinity, temperature, pCO_2 and O_2 were taken at a one-minute resolution along the cruise route, except for the year 2020, when salinity and temperature data (due to the malfunctioning of the thermosalinograph) were extracted from approx. 270 CTD profiles, taken at regular grid within the sampling trajectory of the RV Oceania (Figure 1). The set of high-resolution measurements was completed with pH measured every 30 minutes. To allow comparing the spatial pH, pCO_2, O_2, T and Sal distribution from different years and to calculate the average values for each of them, all measurements collected for each year were interpolated over a regular grid with a resolution of 0.002° x 0.007° (latitude x longitude) using the weighted-average gridding from Ocean Data View (Schlitzer, 2023).

In addition to the underway measurements, samples for TA and DIC were collected using 250 mL borosilicate bottles at approximately 30 stations homogeneously distributed across the sampling area (Figure 2). Immediately after sampling they were preserved using 100 µL $HgCl_2$ and stored in a refrigerator (between 2 and 5 °C) until they were analysed in the IOPAN laboratories.

Moreover, seawater sampling was supplemented by estimating the sea ice extent for the date when half of the sampling cruise was completed. This was done based on the data from the Advanced Microwave Scanning Radiometer 2 (AMSR-2), University of Bremen (seaice.uni-bremen.de, Spreen et al., 2008). The area with more than 10% Sea Ice Coverage (10% SIC) was compared to the total area of the investigated region. This was achieved by measuring the total surface (number of pixels) representing water in the chart and the surface of the area with SIC > 10%, the area was measured in pixels (px^2). The investigated region was defined as the area comprising approximately from the Fram Strait at 81.5°N to 74°N and from the Greenland coast to approximately the east coast of the Svalbard archipelago (-20°W to 25°E). For visual comparison of the SIC conditions in the sampling area, the 10% SIC line was overlaid on spatial maps to indicate the variability of sea ice cover in different years.

The surface chlorophyll distribution maps from July 2019, 2020, and 2021 are a satellite-derived MODIS-Aqua monthly average composite Chlorophyll *a* concentration (mg/m3) (NASA Ocean Biology Processing Group, 2023) retrieved from https://oceancolor.gsfc.nasa.gov/l3/.

2.2 Measurement techniques and laboratory analyses

2.2.1 Salinity and temperature

During 2019 and 2021, salinity and temperature were continuously measured in the flow of surface water using an SBE 21 SeaCAT thermosalinograph (SeaBird) installed on board and equipped with an additional temperature sensor SBE38 located at the water inlet, both sensors were calibrated in every cruise shortly before starting it. The temperature accuracy was ± 0.01°C in both instruments and the initial accuracy conductivity of the SBE 21

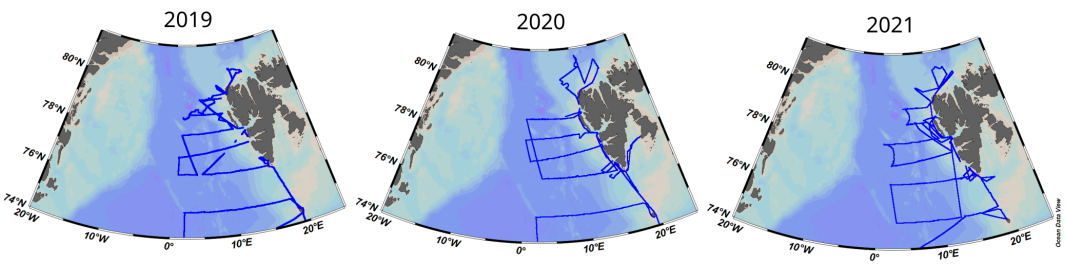

FIGURE 1
Location of the sampling area. The blue lines represent the trajectory of the RV Oceania, where continuous measurements were taken (temperature, salinity, pH, pCO_2, and O_2). Figure created with Ocean Data View (Schlitzer, 2023).

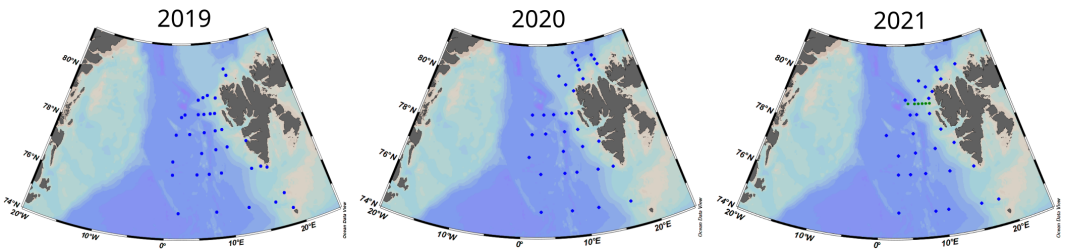

FIGURE 2
Study area with the location of the TA and DIC sampling locations (blue dots) during 2019, 2020 and 2021. The green dots in 2021 (right) show the location of the water column profiles extracted from the "CarbonBridge productivity regimes in the Arctic Ocean" project dataset (Paulsen et al., 2017) collected in January 2014. Figure created with Ocean Data View (Schlitzer, 2023).

SeaCAT-thermosalinograph was ± 0.001 S/m. In 2020, the surface salinity and temperature data were derived from CTD casts taken with the SBE9/11+ system (SeaBird) installed on a water carousel, which was calibrated shortly before the beginning of the cruise with a temperature (conductivity) accuracy of 0.01°C (± 0.001 S/m). All data was averaged using the same grid resolution as explained in section 2.1.

2.2.2 Partial pressure of CO_2

The pCO_2 was measured with a precision/accuracy of 1.3 µatm using a system equipped with a cavity ring-down spectroscope (CRDS) G2101-i (Picarro) connected to a bubble-type equilibrator with an additional spray-type water diffuser (see Stokowski et al., 2021 for a detail description of the method). The quality of the CRDS was assured by regular measurements of pure nitrogen (Linde 5.0) and artificial air with 205 and 507 ppm of CO_2. The temperature difference between the water inlet and equilibrator was corrected using the relationship between temperature and pCO_2 proposed by Takahashi et al. (1993).

2.2.3 Oxygen saturation

The O_2 measurements were performed in the same equilibrator as for pCO_2 using a Fibox 4 equipped with a dipping optode (PreSens GmbH, Germany). The optical sensor was calibrated using N_2 and ambient air. The response time was set to 10 seconds, and the measurements assured the precision of ± 0.3% of the saturation values.

2.2.4 pH

The pH was measured using the HydroFIA pH spectrophotometric system (CONTROS, 4H-JENA Engineering GmbH) from the same surface water flow used for other underway measurements. The quality of pH results was proved with repeated measurements (at 25°C) of the certified TRIS buffer (TRIS-CRM-T37) provided by A.G. Dickson (Scripps Institution of Oceanography, USA). The instrument yielded a precision of 0.002 pH units and an accuracy of 0.003.

2.2.5 Dissolved inorganic carbon

DIC samples from 2019 were measured on a Shimadzu TOC-L analyzer at the Institute of Oceanology of the Polish Academy of Sciences (IO PAN) in Poland. Samples collected in 2020 were measured at the Helmholtz-Zentrum Hereon (Germany) using a VINDTA 3C (Versatile INstrument for the Determination of Total dissolved inorganic carbon and Alkalinity) based on coulometric titration (Johnson et al., 2000). The samples collected in 2021 were measured on an automated DIC AS-C6L analyzer (Apollo SciTech) at the IOPAN.

2.2.6 Total alkalinity

The analysis of the samples collected in 2019 and 2021 for TA was made on an automated, open-cell potentiometric titration system developed by Andrew Dickson (Scripps Institution of Oceanography/UCSD, USA) (Dickson et al., 2007), while in 2020 using VINDTA 3C based on close-cell potentiometric titration.

For all DIC and TA measurements, the accuracy was ensured using certified reference materials (CRMs, batches no. #190 and #195) from A.G. Dickson (Scripps Institution of Oceanography, USA). These were also used for quantification of the precision for each of the used instruments, which was not worse than ± 3 µmol kg^{-1} for DIC and ± 4 µmol kg^{-1} for TA.

2.3 Calculations of the marine carbonate system.

Quantifying the influence of different biological and physical parameters on the marine CO_2 system was done for sampling locations for which the complete data set was collected, including DIC, TA, pH, pCO_2, salinity, and temperature. The computations of the carbonate system were done using version 2.3 of the CO2SYS program for Excel (Microsoft) (Lewis et al., 1998). Previous studies (Chen et al., 2015; Chierici and Fransson, 2009; Raimondi et al., 2019; Woosley et al., 2017) suggested that the carbonic acid dissociation constants guaranteeing the best consistency between calculations and observations of the marine CO_2 system in the Arctic waters are these by Mehrbach et al. (1973) as refitted by Dickson and Millero (1987) (later referenced as MER) and Lueker et al. (2000). Following these recommendations, and in agreement with Tynan et al. (2016), the carbonic acid dissociation constant of MER was selected.

The complete set of dissociation constants used in the computations included: MER for carbonic acid, Dickson et al. (1990) for HSO_4^-, Perez and Fraga (1987) for HF, and Dickson

et al. (1990) for borates. Additionally, boron concentrations have been approximated in the CO2SYS with the dependency by Lee et al. (2010), and the pH was reported on the total scale (pH = $-\log_{10}$ ($[H^+]$ + $[HSO_4^-]$) corresponding to our measurement technique.

2.3.1 Interannual biogeochemical variability

In order to compare biogeochemical changes between different years, it is necessary to select a reference value from which the annual change could be estimated. Therefore, the averages of the physical and chemical properties from the first 50 m of the Surface Winter Waters (SWW) in Fram Strait (Figure 2) were compared to the data obtained in this study during consecutive summers. The comparison of biogeochemical properties between winter (or pre-bloom) and summer (or post-bloom) waters has been used as a tool for tracing and quantifying biogeochemical changes in the area (e.g., Chierici et al., 2019). As the goal of this study was to compare the relative changes in the biogeochemistry of the entire region between consecutive years rather than to provide a net quantification of different biogeochemical processes at each sampling location, the SWW can be considered as a semi-arbitrary reference point to estimate the relative differences with respect to this point, giving simultaneously a tool to compare data collected during different years. A unique aspect of this approach is the possibility of quantifying the biogeochemical variability within the study area using the same reference point (for example, how latitudinal changes in temperature may influence pH in different years having different temperature gradients), but also considering the uncertainties that entail.

The winter data of temperature, salinity, TA, and DIC ($Temp_{wv}$, Sal_{wv}, DIC_{wv}, TA_{wv}) collected in January 2014 were obtained from the "CarbonBridge productivity regimes in the Arctic Ocean" project dataset (Paulsen et al., 2017). As presented before, these data do not represent the characteristics of the entire area but rather a semi-arbitrary point to compare biogeochemical differences between years. The mean values in the upper 50 m were obtained by averaging all the data from 2, 5, 11, 20, 30, and 50 m water depths from six water column profiles taken perpendicular to the west coast of Svalbard (see Figure 2 for more details). Furthermore, using the same dataset (Paulsen et al., 2017), the average values for the surface water layer (upper 50 m) have been compared with averages for 500 m (Table 1) and also with data collected below the photic zone (between 100 and 400 m) at selected locations during the 2021 sampling campaign (see Supplementary Table S1 for more details). The standard deviation for TA and DIC, between the three datasets mentioned in Table 1, was ± 4 µmol kg^{-1} for both of them (DIC and TA), which suggests a relative homogeneity of DIC and TA in the upper 500 m of water column after winter mixing and relatively small (negligible) interannual variability of DIC and TA in the region. Still, however, our data was only collected during one year (2021) and does not necessarily represent the values of TA and DIC from 2019 and 2020 which we cannot confirm to be within the variability of the already presented data.

The values of pCO_2 and pH (pCO_{2wv}, pH_{wv}) for SWW were calculated using version 2.3 of the CO2SYS program for Excel (Microsoft) (Lewis et al., 1998) using as input values $Temp_{wv}$, Sal_{wv}, DIC_{wv}, TA_{wv}.

2.3.2 Sea-ice as marine CO_2 system end member

During spring and summer, the winter water mixes in the surface layer mainly with sea ice meltwater (see section 3.1 for more details). To estimate TA and DIC changes due to this effect, the end member values of DIC_{ice} (355 ± 75 µmol kg^{-1}), TA_{ice} (441 ± 52 µmol kg^{-1}), and salinity (Sal_{ice} = 5.0 ± 0.9) for sea-ice were obtained from the study by (Rysgaard et al., 2007). These values have been obtained by averaging the results from 5-10 cm thick layers extracted from nine sea ice cores (0.9-1.9 m long), collected in Franklin Bay, N Canada (70°N, 126°W) in April 2004 and Young Sound, NE Greenland (74°N, 20°W) in March 2005. A detailed description of the methodology used during sampling and all the sea ice data is reported in Rysgaard et al. (2007).

2.3.3 Seasonal variations of TA and DIC

Relative changes in DIC and TA due to the mixing effect of SWW with sea ice meltwater (defined as DIC_{sal} and TA_{sal}) can be calculated as a function of salinity and expressed as a linear correlation between the two end members: sea surface DIC and TA during winter (DIC_{wv}, TA_{wv}) and melted sea ice (DIC_{ice}, TA_{ice}). TA_{sal} and DIC_{sal} at each sampling station can be calculated using Equations 1, 2.

$$TA_{sal} = 62.468 * (salinity) + 125.92 \quad (1)$$

TABLE 1 Average values of different parameters measured in the Fram Strait area during the winter of 2014 (Paulsen et al., 2017) Surface winter 2014 (SWW) is the average value of the first 50 m of the water column, while 500m winter 2014 is the value measured at 500 m at different locations of the sampling area (Figure 1). 100-400m summer 2021 are the average values from 16 measurements taken during the sampling campaign in 2021 at different depths (between 100 and 400 m), for more information see Supplementary Material (Supplementary Table S1).

	Salinity	Temperature (°C)	TA (µmol kg^{-1})	DIC (µmol kg^{-1})	pH (total scale)	pCO_2 (µatm)	Notation
Surface winter 2014	34.96	3.15	2309	2159	8.065	366	WW
500m winter 2014	35.06	2.90	2311	2166			$W14_{500}$
100-400m summer 2021	34.97	2.37	2301	2168			

$$DIC_{sal} = 60.367 * (salinity) + 49.052 \quad (2)$$

Therefore, the difference between TA and DIC measured in the consecutive summers (TA_{meas}, DIC_{meas}) and the calculated effect of mixing with meltwater (TA_{sal} and DIC_{sal}) should be the accumulated result of biological processes and air-sea CO_2 interchange (ΔTA_{bio} and ΔDIC_{bio}).

$$\Delta TA_{bio} = TA_{meas} - TA_{sal} \quad (3)$$

$$\Delta DIC_{bio} = DIC_{meas} - DIC_{sal} \quad (4)$$

2.3.4 Calculations of pH variations

Winter-to-summer changes in pH and pCO_2 were attributed to several processes: temperature (temp), inputs of freshwater from ice melting (sal), biological processes plus air-sea CO_2 fluxes (bio), and inconsistencies (inc). Variations in pH were calculated in CO2SYS using different combinations of the SWW variables reported in Table 1 ($Temp_{wv}$, Sal_{wv}, DIC_{wv}, TA_{wv}) and values obtained in this study for consecutive summers (TA_{meas}, DIC_{meas}, pCO_{2meas}, pH_{meas}, $temp_{meas}$, and sal_{meas}).

Changes in pH due to temperature variations (ΔpH_{temp}) were calculated assuming that temperature is the only variable changing between winter and summer. Thus, ΔpH_{temp} (Equation 5) was determined as the difference between winter pH (pH_{wv}, Equation 6) and the pH calculated as a function of winter salinity, DIC, and TA (Sal_{wv}, DIC_{wv}, TA_{wv}) and the measured temperature during summer.

$$\Delta pH_{temp} = pH_{calc} \quad f(temp_{meas}, sal_{wv}, DIC_{wv}, TA_{wv}) - pH_{wv}; \quad (5)$$

$$\text{Where } pH_{wv} = pH_{calc} \quad f(temp_{wv}, sal_{wv}, DIC_{wv}, TA_{wv}) \quad (6)$$

The influence of sea ice meltwater can change salinity and, therefore, TA and DIC in the surface waters, influencing pH. Thus, the pH changes due to the physical mixing of water masses (ΔpH_{sal}) were determined by subtracting the winter pH (pH_{wv}) from the theoretical pH_{sal} calculated by applying winter temperature ($Temp_{wv}$), summer salinities (sal_{meas}) and related to these salinities TA_{sal} and DIC_{sal} obtained from Equations 1, 2, respectively:

$$\Delta pH_{sal} = pH_{sal} - pH_{wv}; \quad (7)$$

$$\text{Where } pH_{sal} = pH_{calc} \quad f(temp_{wv}, sal_{meas}, DIC_{sal}, TA_{sal}) \quad (8)$$

The difference between TA and DIC measured in the consecutive summers (TA_{meas}, DIC_{meas}) and TA_{sal} and DIC_{sal} (Equations 1, 2) resulting from the physical mixing of water masses (or the influence of sea ice melting) can be attributed to the total effect of both biological processes (photosynthesis/respiration and calcification) and sea-air CO_2 exchange. Thus, the accumulated pH change corresponding to these effects (ΔpH_{bio}) can be calculated as:

$$\Delta pH_{bio} = pH_{calc} \quad f(temp_{wv}, sal_{meas}, DIC_{meas}, TA_{meas}) - pH_{sal} \quad (9)$$

To evaluate the consistency of the marine CO_2 system data presented in this study, the calculated pH from $temp_{meas}$, sal_{meas}, DIC_{meas}, and pCO_{2meas} was compared to the measured pH (pH_{meas}). The differences were attributed to the error propagation during calculations (Orr et al., 2018) and chemical components that may affect the equilibrium of the marine CO_2 system but are not yet parametrized in the mass balance equations used in the calculations (e.g., Kuliński et al., 2017)

$$pH_{inc} = pH_{calc} \quad f(temp_{meas}, Sal_{meas}, DIC_{meas}, pCO_{2meas}) - pH_{meas} \quad (10)$$

3 Results and discussion

3.1 Oceanographical settings

Surface temperature and salinity in the entire studied area during three years (2019, 2020, 2021) ranged between -0.5 and 8.5°C and between 30.0 and 35.2, respectively (Figures 3A, B). However, lower salinities were occasionally observed close to the ice margin. Sea surface salinity in the investigated area had generally quite similar distribution every year (Figure 3A). Warmer and more saline waters were found in this region in the southern part, which is related to the transformation of Atlantic Water during its northward transport in the WSC (Figure 4) (Hattermann et al., 2016). This effect was well reflected in our data by a surface patch of more saline waters extending northward and centred at 10°E. As AW flows northwards, surface waters experience intense cooling and freshening; the heat released during cooling enhances sea ice melting (Polyakov et al., 2010; Rippeth et al., 2015). Two frontal zones with stronger salinity and temperature gradients were identified in the surface layer based on the analyzed data set. One of them extending along the west coast of Svalbard represents the West Spitsbergen Polar Front (Nilsen et al., 2016) which separates Atlantic water in the WSC ($S > 34.8$) from the colder and fresher Arctic-type water ($S < 34.8$) originating from the South Cape Current (SCC) and carried northward along the West Spitsbergen shelf (Figure 4) (Saloranta and Svendsen, 2001; Nilsen et al., 2021). The second salinity/temperature front, which reflects a boundary between Atlantic and Polar waters in Fram Strait (Karpouzoglou et al., 2022), more winding, was located along the sea-ice margin with slight shifts from year to year, depending on the sea ice extension (Figure 3A). To determine the location of this front during different years we selected the isohaline 34.8 which coincides with the boundary of the frontal area with a strong salinity gradient in our data. In the central Fram Strait, it depicts the transition zone between the northward flowing Atlantic Water and Polar Water (PW) originating in the Arctic Ocean and carried southward by the East Greenland Current. Therefore, it can be considered an excellent tool to compare the front extension during consecutive years. As illustrated in Figure 3A, a smaller extension of the isohaline 34.8 was observed in 2021 compared to 2020 and 2019, which coincides well with the sea ice extension in the region. During

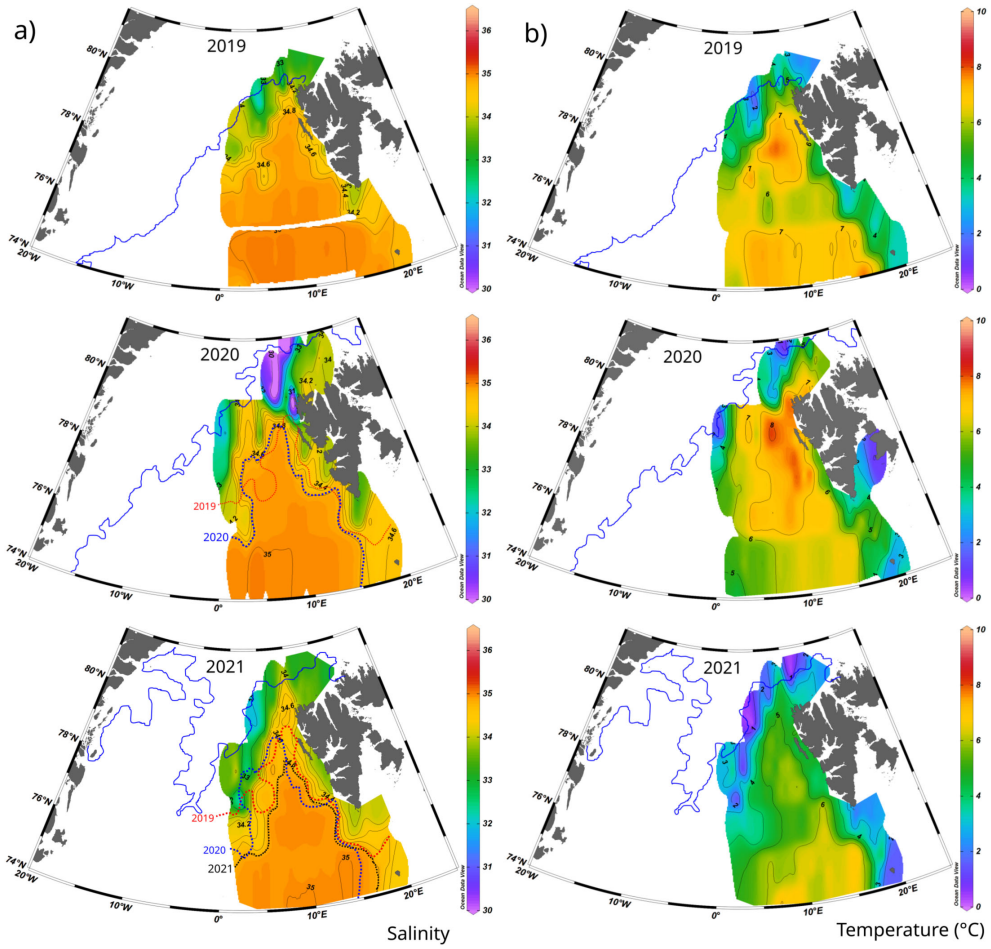

FIGURE 3
Surface salinity **(A)** and temperature **(B)** distribution in the study area during 2019, 2020 and 2021. As a reference, the isoline of 34.8 from previous years was marked in the salinity maps. The original surface data was extrapolated using the weighted-average gridding from Ocean Data View (Schlitzer, 2023). The blue line represents the 10% sea ice coverage (SIC), northern of this line the SIC is higher than 10%. The study area covered by SIC higher than 10% was 49.94% during 2019, 32.69% in 2020 and 18.68% in 2021. Detailed maps presenting the SIC are shown in the Supplementary Material (Supplementary Figure S1).

these three years, there was a strong variability in the area covered with sea ice as expressed with SIC higher than 10% (SIC > 10%). In July 2019 it was 49.94% of the investigated region, while in 2020 and 2021 it was 32.69% and 18.68%, respectively (Figure 3; Supplementary Material S1). The decrease in surface salinity can be linked to enhanced sea ice melting, providing more fresh water to the surface layer, and/or to changes in surface circulation. Unfortunately, our data only provide information on sea ice coverage and the relationship between sea ice melting and corresponding released freshwater volume and surface salinity distribution has to be corroborated in future studies. Independently of the prevailing mechanism, it is clear that the extent of waters with surface salinity higher than 34.8 was reduced in 2021, having thus less impact on surface processes.

Unlike the salinity distribution, the surface temperatures show a strong interannual variability (Figure 3B). A strong temperature gradient was observed in all studied years close to the sea-ice margin in the west/northwest part of the study area, with warmer waters following the direction of the WSC from the south and reaching up to 79°N. Still, the spatially averaged surface temperature (calculated as the average of the gridded data, with the same spatial distribution and the same extension between years, see methods) differed from one year to another, amounting to 5.2°C during 2019, 5.3°C in 2020, and 3.8°C in 2021. The spatial patterns of the temperature gradients also varied between different years. One of the main features that could be distinguished is a zonally extending pattern of lower surface temperature located at 76°N in 2019, at 75°N in 2020, and at 76°N in 2021 (Figure 3B). An explanation of causal mechanisms, responsible for complex and annually varying patterns of surface temperature is beyond this study. However, the average surface temperature clearly shows colder surface waters during 2021 than during 2019 and 2020, coinciding with a smaller extension of the AW surface pattern (defined as surface waters with S > 34.8) and reduced sea ice.

The surface temperature and salinity variability reflect the general large-scale patterns previously described for this area, where warmer and more saline AW is transported northwards in the WSC. As AW flows northward, it mixes with colder and fresher

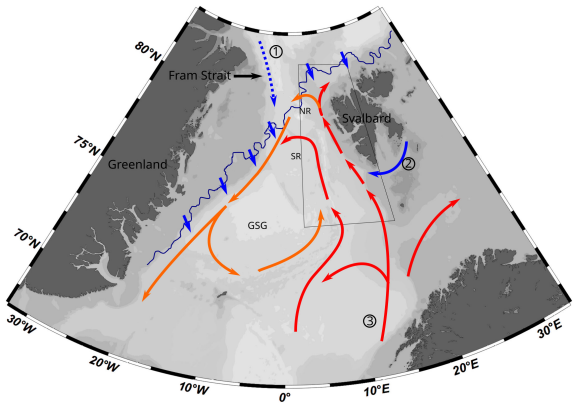

FIGURE 4
Schematic representation of the main surface currents encountered in the study area (based on Hattermann et al., 2016). The blue line represents the limit of the 10% sea-ice concentration (see methods). The black box delimit the study area. The color in the arrows represents a schematic view of the main water masses in the area and its transformations. Blue arrows represent the influence of Arctic waters, either as melted sea ice (small ones), as Arctic surface waters (1) or Arctic waters carried by the South Cape Current (SCC) (2). The red arrows represent the Atlantic Water (AW) carried by the West Spitsbergen Current (WSC) (3), orange Polar warm Surface Waters (PSWw). GSG, NR, and SR denote Greenland Sea Gyre, Northern Recirculation, and Southern Recirculation, respectively.

melted sea-ice waters, creating warm Polar Surface Waters (PSWw) (Rudels et al., 2005). Rudels et al. (2005) define PSWw in terms of temperature and potential density (warmer than 0°C and less dense than 27.7) but for the purpose of this study, we take advantage of the isohaline of 34.8 as a good delimiter of the surface boundary between the Atlantic and Arctic derived waters. Therefore, water with S > 34.8 will be denoted as AW and water with S < 34.8 will be described as PSWw.

PSWw sitting on the top of Atlantic water can flow eastward, following the north Svalbard circulation (Athanase et al., 2020), or westward and then southward along the sea-ice margin zone (Marnela et al., 2013; Hattermann et al., 2016). This recirculation pattern explains the high salinity gradient in our data between the AW flowing northward and PSWw moving southward. However, it was also possible to identify some isolated patches with S > 34.8 outside of the main AW inflow, probably originating from the mesoscale eddies generated in the eastern Fram Strait (Bashmachnikov, 2020; Bashmachnikov et al., 2023; Raj et al., 2016), which bring colder and more saline subsurface Atlantic waters to the surface, breaking the seasonal stratification.

The part of the western branch of the WSC recirculates in Fram Strait mainly along two routes: a Northern Recirculation (NR) around the Molloy Hole near 80°N (Hattermann et al., 2016) (Figure 4) or a Southern Recirculation (SR) located south of 79° N. The SR is mainly related to the eastern rim of the Greenland Sea Gyre (GSG) (de Steur et al., 2014; Beszczynska-Möller et al., 2012) (Figure 4). Variability in the AW temperature reaching the Fram Strait has been associated with changes in the GSG circulation (Chatterjee et al., 2018), where a stronger GSG circulation strengthens the AW inflow along the WSC. It can be reflected in surface waters in the southern Fram Strait, where a stronger GSG promotes a northern extension of the AW which in the upstream area extends to the surface before being transformed in PSWw as it mixes with meltwater.

Hence, interannual and spatial variations in surface temperature and salinities can be explained through changes in surface circulation and varying sea-ice extension and melting rates. Warmer and more saline waters, as observed for 2019 and 2020 (Figures 3A, B), correspond to a higher influence of AW in the surface waters or a reduction of the PSWw. On the other hand, cooler and fresher surface waters, as observed during 2021 along with a decrease in sea-ice extension (which was reduced from 43.94% of the region covered in 2019 to 18.68% in 2021), could be related to a higher volume of sea ice meltwater or/and varying intensity of recirculation, which would explain differences in the sea ice extension and the expansion of the area covered by PSWw.

3.2 The marine carbonate system

3.2.1 Distribution of TA and DIC

The data collected for TA and DIC from 2019 to 2021 are shown in Figure 5. The main changes in TA are closely correlated as a function of salinity. TA data shows a conservative mixing along the line drawn between the AW properties reported for winter (salinity 34.96 and TA = 2310 μmol kg^{-1}, Table 1) and the TA of the melted sea ice (salinity 5.0 and 441 μmol kg^{-1} TA) (see methods for details and references) revealing high variability, but similar to previously reported in the area (Chierici et al., 2019; Tynan et al., 2016). Tynan et al. (2016) were able to characterize two TA_0 zero salinity end-members, one lower (TA_0 = 403 μmol kg^{-1}) associated with sea ice melting and one higher (TA_0 = 1230 μmol kg^{-1}) related to the influence of Polar Waters. However, our data only shows the influence of one TA_0 with low values (~ 420 μmol kg^{-1}), supporting the idea that TA variations in this data set result only from the mixing between AW and sea ice meltwater.

Biological processes like organic matter photosynthesis/respiration (P/R) and calcification/carbonate dissolution (NCC) are expected to influence slightly TA concentration (Middelburg et al., 2020). In order to better understand the importance of these biological processes in the TA distribution, the differences between two end-members mixing line and the measured TA values (Figure 5) were calculated (ΔTA_{bio}) (see methods). Therefore, TA_{bio} represents the changes in TA which are not due to the mixing of AW with melted sea ice.

The average [± standard deviation (SD)] of ΔTA_{bio} for 2019 is 10.0 ± 8.5 μmol kg^{-1} (Figure 5). Data collected during 2020 also shows a positive shift ΔTA_{bio} of 4.2 μmol kg^{-1} (SD ± 9.9 μmol kg^{-1}). On the other hand, in 2021, the TA measured was the closest to the ideal mixing line (TA_{sal}), with a ΔTA_{bio} of 0.7 μmol kg^{-1}, SD ± 8.8 μmol kg^{-1}.

As for TA, the conservative mixing line (DIC_{sal}) formed by linking values for winter AW (salinity 34.96 and DIC_{wv} = 2160 μmol kg^{-1}, Table 1) and melted sea ice water (salinity 5.3 and DIC_{ice} =369 μmol kg^{-1}) is represented as a black line in Figure 5. The deviations from this line are caused due to other mechanisms besides the physical mixing of AW and sea ice meltwaters, namely

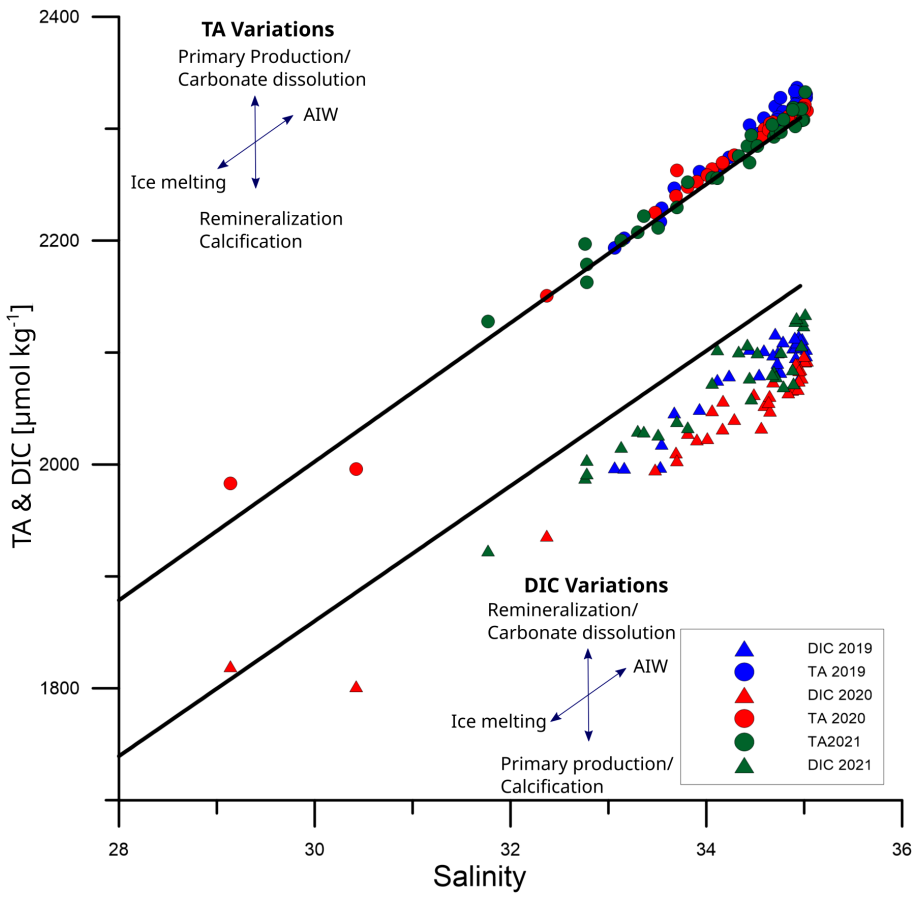

FIGURE 5
Concentration of TA and DIC against salinity. The black line represents the conservative mixing between Atlantic Water encountered in the study area during winter and melting sea ice. Triangles show DIC concentration, while circles are for TA. Data with blue colour were collected during July 2019, red during July 2020, and green during July 2021. Arrows represent the direction of change from the equilibrium due to different processes. Air-sea fluxes are not represented, but they change DIC concentration in the same direction as Remineralization and Primary Production.

organic matter photosynthesis/respiration, calcification/carbonate dissolution and CO_2 air-sea exchange (ΔDIC_{bio}).

All measured DIC values, ranging from 1800 to 2120 µmol kg^{-1}, were below this line and revealed variability higher than for ΔTA_{bio}. DIC data presented here have a wider range than previously recorded at 6m water depth for this area by Tynan et al. (2016) (from 2040 to 2120 µmol $kg^{-1)}$ and the data collected within the first 6m of the water column by Chierici et al. (2019) (from 1883 to 2084 µmol kg-1). This may indicate that, due to the high stratification in the surface waters, a shallower sampling depth (2.5m in this study) resulted in a wider range of DIC data. Therefore, the sampling depth should be taken into consideration, especially when estimating air-sea carbon fluxes. The mean ΔDIC_{bio} for 2019, 2020, and 2021 were -50.0, -73.4, and -42.9 µmol kg^{-1}, respectively (SD ±12.7 µmol kg^{-1} for 2019; SD ±18.7 µmol kg^{-1} for 2020; and, SD ±18.8 µmol kg^{-1}).

Both NCC and P/R modify DIC and TA in given proportions. P/R decreases approximately 6.3 moles of DIC for each 1 mol of TA increase, while NCC decreases DIC and TA in the molar proportion of 1:2 (e.g., Middelburg et al., 2020). However, the DIC concentrations, opposite to TA, are further modified by the air-sea CO_2 fluxes. Since the surface waters in Fram Strait were undersaturated in CO_2 with respect to the atmosphere (this study), the air-sea CO_2 fluxes always led to an increase in DIC concentration.

A positive ΔTA_{bio} (10.0 µmol kg^{-1}) and a negative ΔDIC_{bio} (-50.0 µmol kg^{-1}) were obtained for 2019. In previous studies P/R has been identified as the main factor influencing the marine carbonate system in the Fram Strait area (Chierici et al., 2019) and the adjacent Barents Sea (Fransson et al., 2001). Assuming that P/R is the primary process influencing also our data, the ΔTA_{bio} of 10.0 µmol kg^{-1} for 2019 should correspond to ΔDIC of -63 µmol kg^{-1}, which is a more significant decrease in DIC than the ΔDIC calculated in our study (-50.0 µmol kg^{-1}). This difference could be due to an uptake of atmospheric CO_2 increasing the DIC of the surface waters.

Using the same assumption of P/R as the most important process, the ΔTA_{bio} of 4,2 µmol kg^{-1} found for 2020 would correspond to -26.1 DIC µmol kg^{-1}, which is a much smaller DIC loss than the observed ΔDIC_{bio} (-73.4 µmol kg^{-1}). However, calcite formation during coccolithophorid blooms is a common phenomenon in the mixing zone of Atlantic and Arctic waters (PSWw) (Lalande et al., 2011), and this process counteracts the TA release by P/R. Thus, the contribution of biological calcium carbonate export from surface waters would explain the low

ΔTA_{bio} encountered for 2020 as compared to the highly negative values of ΔDIC_{bio}.

A similar pattern as for 2020 can be described for 2021, for which P/R alone cannot explain the DIC loss (ΔDIC_{bio} = -42.9 µmol kg^{-1}) based on ΔTA_{bio} (0.7 µmol kg^{-1}). The smallest DIC loss in 2021 (the lowest absolute ΔDIC_{bio} value compared to 2019 and 2020) may indicate a lower P/R that year and, in combination with low ΔTA_{bio}, may suggest a shift in the biological community towards the increase in the relative abundance of calcifying organisms. While diatoms have been reported as the dominant species in cold and nutrient-rich waters close to the sea ice front, coccolithophores are more abundant, particularly during summer, in the eastern ice-free part of Fram Strait (Lalande et al., 2013; Nöthig et al., 2015). In southern warmer areas, both of them are often replaced by nano- and picoplankton (Bauerfeind et al., 2009; Nöthig et al., 2015), which is related to faster nutrient recycling and lower carbon export (Forest et al., 2010). 2019 was characterized by warmer waters than 2021 and a farther northern extension of the surface AW signature, together with positive ΔTA_{bio} (10.0 µmol kg^{-1}) and a negative ΔDIC_{bio} (-50.0 µmol kg^{-1}). As a result, the ratio between nano-picoplankton and calcifiers as the main drivers for PP is expected to be higher during the warmer 2019 than during the colder 2021, characterized by much smaller ΔTA_{bio} (0.7 µmol kg^{-1}) but similar (ΔDIC_{bio} = -42.9 µmol kg^{-1}) as 2019.

Thus, the interannual shifts in dominating species can be proposed as an explanation for the variable ratios between ΔTA_{bio} and ΔDIC_{bio} in different years, when either the proximity of the sea ice front changes with respect to the study area (diatoms vs. coccolithophorids) or there are differences in seawater temperature (coccolithophorids vs. nano- and picoplankton species).

To sum up, the ratio between $\Delta DIC_{bio}/\Delta TA_{bio}$ suggests that during the warmer 2019 and 2020, there was a higher P/R in the area (this assumption is further supported by satellite chlorophyll data in the next section) than during the colder 2021. Besides that, it also indicates a shift in the ratio between calcifiers and nano-picoplankton, where warmer years could promote a reduction of calcifiers with respect to nano-picoplankton.

The changes in DIC and TA presented in this section are strongly connected to changes in pCO_2 and pH. Both of them play a key role as indicators of atmospheric carbon sequestration and ocean acidification. Due to the sampling strategy, pH and pCO_2 data were collected in higher resolution, providing not only information about their general distribution but also about mesoscale processes which could influence their variability.

3.2.2 Surface pCO_2

The pCO_2 measurements in all investigated years (2019-2021), with average values of 288, 271 and 286 µatm for 2019, 2020 and 2021, respectively, show that the entire study area was undersaturated with CO_2 relative to atmospheric levels which were, in annual average, 412, 414 and 417 ppm (data obtained from environmental monitoring of Svalbard and Jan Mayen; https://mosj.no), which is in agreement with other studies in Fram Strait and around Svalbard (e.g., Chierici et al., 2019; Fransson et al., 2017; Tynan et al., 2016; Yasunaka et al., 2018);. The pCO_2 values ranged from 170 µatm found near the sea-ice edge and were associated with the presence of colder, lower salinity waters, up to 350 µatm observed in the southern part under the influence of warmer and more saline Atlantic waters (Figure 6). The distribution of surface pCO_2 (Figure 6) shows a similar pattern as salinity (Figure 3A), with values decreasing from South to North and the highest values centred at approximately 10°E (similar to the AW surface patch area). The surface pCO_2 rapidly declined as we moved closer to the continental margin of Svalbard and the sea-ice edge.

In general, lower values of pCO_2 were found within the AW surface patch in 2020 (average pCO_2 303 µatm) than in 2021 (average pcO_2 329 µatm), while similar values have been found outside of this area (approx. 255 µatm). The lower pCO_2 in 2020 coincided with the lowest DIC concentrations found in our study, which could reflect higher P/R in the area that year (Figure 6). Figure 7 shows the monthly averaged distribution of chlorophyll *a* estimated from satellite observations (NASA Ocean Biology Processing Group, 2023). Higher chlorophyll *a* concentration are visible within the AW surface patch (10°E) in 2020 (average chlorophyll *a* in AW surface patch area of 1.14 mg m^{-3}) than in 2021(average chlorophyll *a* 0.82 mg m^{-3}), while in 2021, the maximum of PP (highest chlorophyll *a*) was located further west of the AW inflow area.

In 2019, the chlorophyll *a* distribution (average in the study area of 3.00 mg m^{-3}) was higher to that in 2020 (chlorophyll *a* 1.05 mg m^{-3}), with higher PP within the AW inflow (average of 2.21 mg m^{-3}). This feature is, however, not reflected so clearly in the DIC and pCO_2 – both being higher in 2019 (DIC_{bio} -50.0 µmol kg^{-1} and average pCO_2 289 µatm) than in 2020 (DIC_{bio} -73.4 µmol kg^{-1} and average pCO_2 271 µatm). The reason for that and the coinciding smaller DIC loss (lower absolute value of ΔDIC_{bio}) and relatively high accumulation of TA (reflected with ΔTA_{bio}) measured during 2019 could be related to a delay between the sampling time and the peak of high PP. The satellite images represent the monthly averaged chlorophyll *a* distribution while pCO_2 (as well as TA and DIC) was collected within days, which may generate a mismatch between both datasets.

To sum up, the lower pCO_2 was correlated with lower salinity waters. Areas influenced by AW (salinity greater than 34.8) had a strong interannual variability: during the investigated period we can distinguish between two years (2019 and 2020) characterized by a high signal of PP within the AW surface patch and, one year (2021) with low PP within the study area but high PP westward of the AW inflow (outside of the study area and only based on satellite data).

The pCO_2 data not only shows a general south-to-north gradient (Figure 6), but it is possible to recognize rapid and small/medium scale latitudinal and longitudinal changes of pCO_2 due to the higher resolution data. To depict them and understand the mechanism behind these variations, three surface pCO_2 transects from 2021 (a year for which both the south-to-north pCO_2 variability and pCO_2 data coverage were high) were selected and plotted in Figure 8:

- southern profile (76° N), with higher values of pCO_2 (between 270 µatm and 340 µatm) coinciding with high salinity.

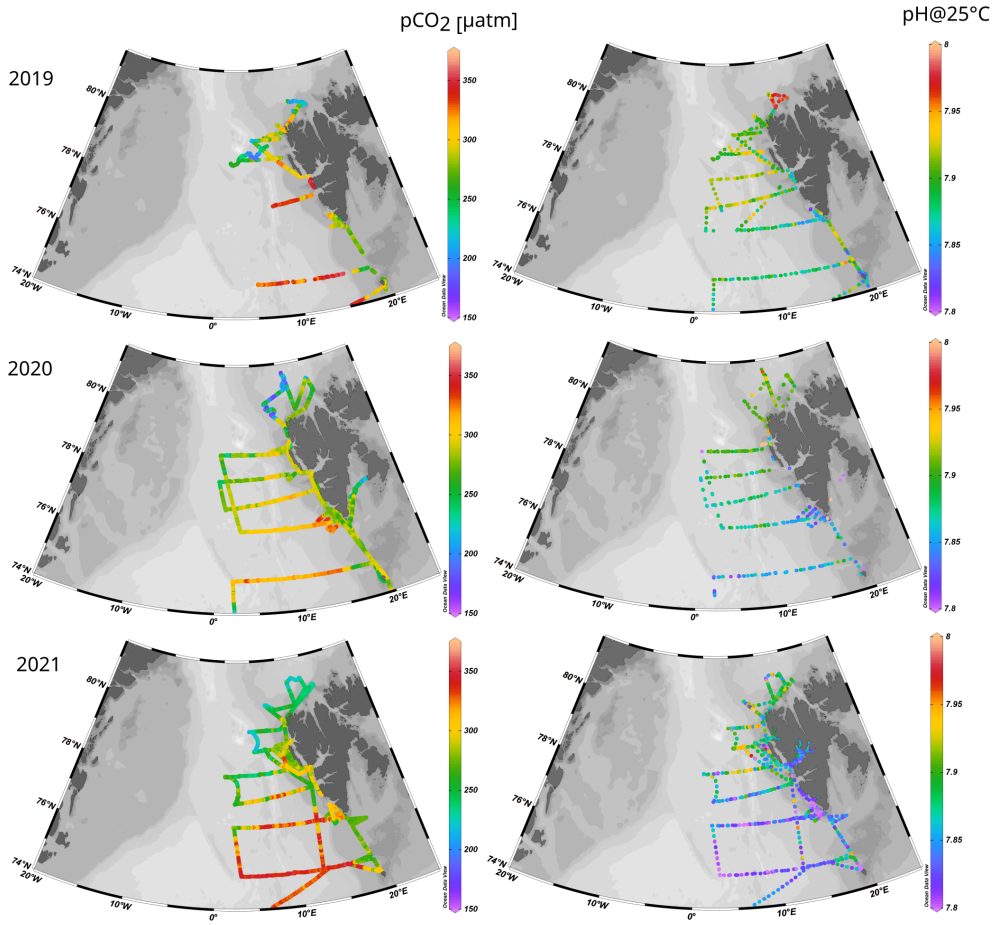

FIGURE 6
Surface distribution of pCO_2 (left) and pH at 25°C (right) from 2019 (top), 2020 (middle) and 2021 (bottom).

- middle profile (77° N), with strong spatial variations of surface pCO_2 (ranging between 240 µatm and 310 µatm), salinity, and temperature.
- northern profile (79° N), with significantly lower values of pCO_2 (from 230 µatm to 250 µatm) and a drastic latitudinal reduction of salinity due to the proximity of the sea ice.

The variability in pCO_2 along the latitudinal transects can be influenced by several factors: temperature, salinity (or mixing of different water masses), P/R, and upwelling of deeper waters with different pCO_2. To simplify the interpretation of this variability, the pCO_2 data was normalized to 5°C ($NpCO_2$) using the temperature dependence proposed by Takahashi et al. (2002). The $NpCO_2$ was plotted in Figures 8A–C with oxygen data as a proxy for P/R, and with salinity to understand the pCO_2 changes due to mixing effects.

In the southernmost transect (Figure 8C), two main features related to variations in pCO_2 can be recognized. First, there was a salinity reduction, a slight increase in the O_2 saturation, and a decrease in pCO_2 west of 5°E, probably related to the influence of PSWw along the GSG. The second feature was a correlation between the O_2 saturation and the pCO_2 but without large changes in salinity east of 5°E, indicating variability in P/R only. The increases in P/R without salinity changes could be due to the vertical transport of deeper water (e.g. from the chlorophyll maximum depth) to the surface. Theoretically, the mechanism explaining it could be the influence of eddy-driven upwelling or wind-driven increase in the mixed layer depth, which could bring a signal of higher P/R from deeper waters to the surface.

In the middle transect (Figure 8B), several areas with salinity drop can be identified. One is located between 2°E and 3°E and reflects the influence of PSWw, but with minor changes in oxygen and pCO_2. A second patch with a strong drop in salinity of 1 unit was located at 6.5°E, followed by an oversaturation of O_2 up to 108 µmol kg^{-1} and an intense reduction of pCO_2 by more than 50 µatm. The reason for this salinity drop was probably an intrusion of a filament of PSWw in the surface layer occupied by AW. The different O_2 and pCO_2 dynamics, thus also different P/R, observed for these two salinity perturbations could be related to nutrient availability. Previous studies showed that surface waters of Arctic origin are generally nitrate-limited, while AW is mostly Fe-limited (Krisch et al., 2020; Tuerena et al., 2021). The injection of PSWw into the mainstream of AW may cause a mixture of water masses, providing extra nitrate from AW to PSWw and Fe from PSWw to AW and inducing an intense P/R. This feature was well seen at 6.5°E but not at 3°E, maybe because the latter region does not represent a PSWw intrusion into AW (and mixing of both) but

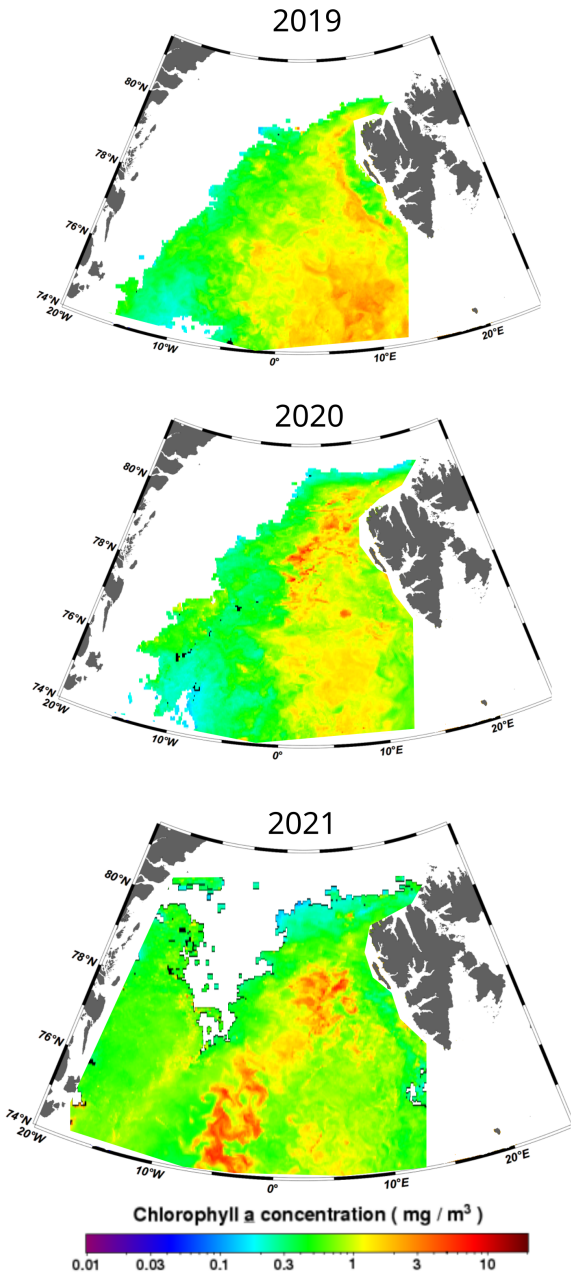

FIGURE 7
Satellite-derived MODIS-Aqua monthly average composite chlorophyll *a* concentration (mg/m^3) for July 2019, 2020, and 2021 (NASA Ocean Biology Processing Group., 2023).

rather the boundary between PSWw and AW with clear separation of both water masses properties. Still, an increase in O_2 saturation on the edge of the salinity drop (between 3°E and 4°E) is distinguishable and probably related to the mixing of PSWw and AW. Along the middle transect (Figure 8B), there was one more area with a salinity drop located east of 11.5°E and associated with an increase in O_2 saturation and a decrease in pCO_2, probably due to both the dilution effect and the P/R. In this case, it was connected to the influence of meltwater released from the Spitsbergen fjords and/or the influence of the South Cape Current that propagates northward along the west coasts of Spitsbergen. Interestingly, along the same latitude (Figure 8B) there was an area from 7.5°E to 11.5°E where the salinity remained constant, but the pCO_2 was highly variable and coupled with the O_2 saturation (the relationship between ΔpCO_2 and O_2 saturation is provided as Supplementary Material, Supplementary Figure S2). As postulated above, the eddy-driven upwelling of deeper waters (or the deepening of the mixed layer) from the maximum chlorophyll depth (typically located at 20-30m water depth) carrying a higher P/R signal, could explain this rapid phenomenon, although future studies correlating the variability of pCO_2 and O_2 in surface layers with changes in the mixed layer depth are needed to support this theory.

The northernmost transect (Figure 8A) was highly influenced by continental runoff, and sea-ice melted water.

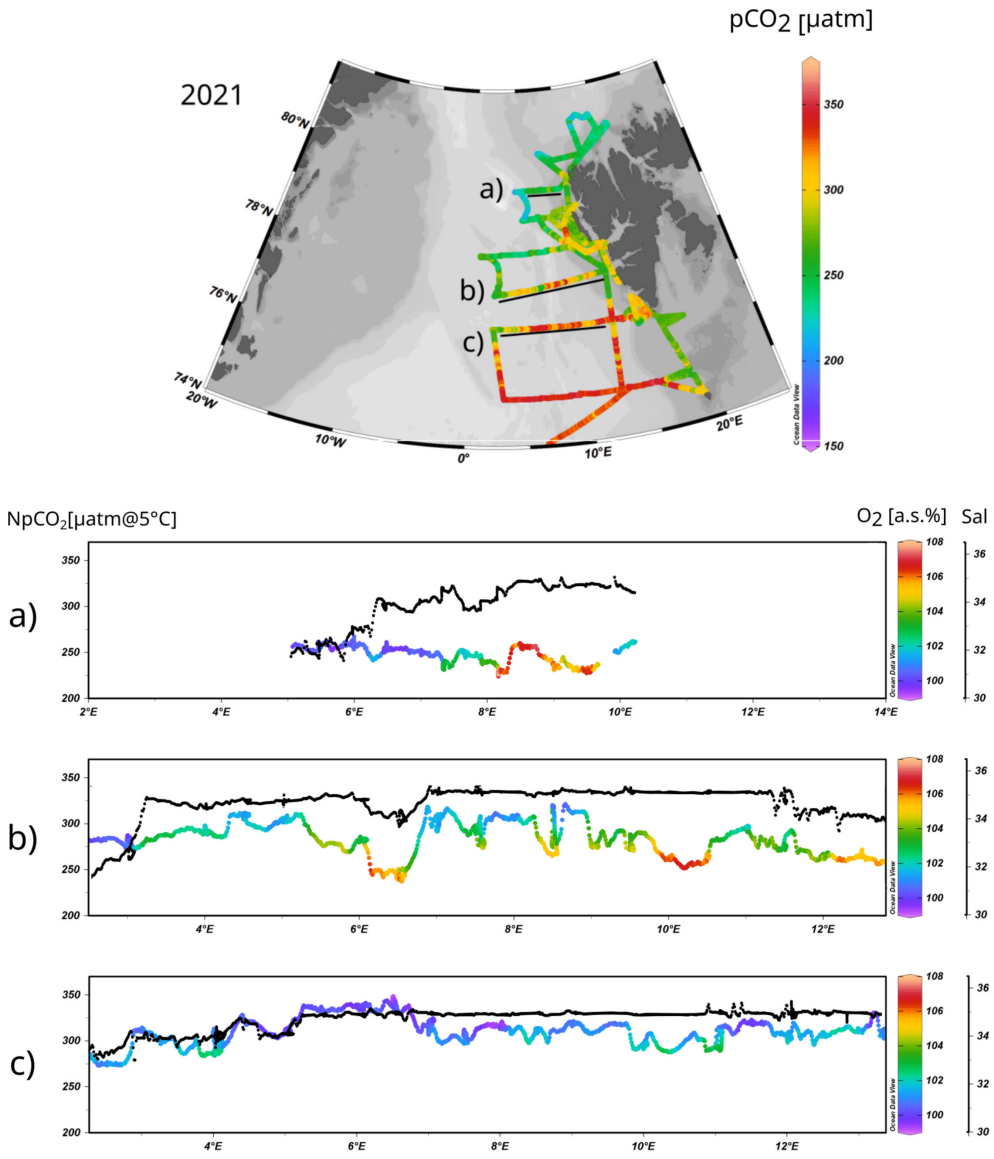

FIGURE 8
Surface distribution of pCO_2 (top) during the sampling campaign in 2021. The transects **(A–C)** marked in the surface pCO_2 distribution map are displayed at the bottom of the figure. The black line within the transects shows salinity variations, the colourful line represents $NpCO_2$ (normalized pCO_2 to 5°C), and the colour scale within the colourful line depicts O_2 (a.s.). All the transects display data collected during 2021.

From 5°E to 7°E, the dilution effect (salinity drop by approx. two units) maintained undersaturated levels of pCO_2 (250 µatm) with O_2 being close to the equilibrium with the atmosphere. East of 8°E, similarly low pCO_2 (250 µatm) was measured. However, in this case, it was a consequence of the intense P/R, indicated by an oversaturation in the water O_2 with respect to the atmospheric levels (up to 108%).

Altogether, four processes have been identified that potentially contribute to pCO_2 reduction in the studied region and thus enhance the water capacity to absorb atmospheric CO_2. These are: (1) the dilution effect due to PSWw's influence, (2) the P/R increase due to the mixing of nutrient pools of AW and PSWw, (3) wind-driven increase in the mixed layer bringing higher P/R signal from deeper waters, (4) the influence of lower salinity waters in the western coast of Spitsbergen.

3.2.3 Surface pH distribution

Along with temperature, salinity, and pCO_2, the pH distribution was affected by an intense latitudinal variation with lower pH values observed in the southern part associated with warmer waters having higher pCO_2, and higher pH values measured close to the sea ice and the continental margin (Figure 6). Importantly, pH was measured at 25°C; therefore, the distribution of pH presented in this study is not influenced by temperature variations, in contrast to pCO_2 distribution. Comparing the three consecutive years of investigations, 2021 had the lowest pH value (7.8), increasing up to 7.95 in the northern part; 2019 had the highest pH, ranging from 7.85 to 8.1, while in 2020, pH values were intermediate and ranged from 7.85 to 8.0.

Since inorganic carbon chemistry heavily influences the pH, it is expected that the processes triggering changes in pCO_2 can also be

traceable in the pH distribution (excluding temperature). Still, if the general trends in pH and other CO_2 system variables are compared within the area of AW surface expression, it can be concluded that higher values of pCO_2 were found in 2019 and 2021 than in 2020 (Figure 6). Both years (2019 and 2021) also had similar DIC concentrations, higher than in 2020 (Figure 5). However, this situation is not reflected in pH (Figure 6), where 2019 had higher values coinciding with the higher values of TA (Figure 5), followed up by 2020 and 2021, which had lower pH and lower TA. As postulated above, it could be due to a change in the characteristics of the plankton community, increasing the abundance of calcifying organisms in years with colder and fresher surface waters and consequently reduced alkalinity of surface waters, making them more sensitive to pH changes. Therefore, not only the pCO_2 distribution is important for understanding the pH variability in the Fram Strait area, but it is also essential to know the distribution of TA and biologically driven ΔTA_{bio}.

To better understand the pH variations in the region due to different physical and biological factors, their influences have been quantified, as described in section 2.2, and presented in Figure 9. The range of the temperature effect on pH (ΔpH_{temp}) is from a reduction of -0.08 in the warmer and more saline waters to an increase of 0.06 close to the sea ice (values represent the minimum and maximum from all the years). Importantly, these changes in pH due to temperature variations refer to a semi-arbitrary reference point ($Temp_{wv}$) established for winter conditions (see methods). Thus, the ΔpH values do not provide any valuable information other than the absolute difference between maximum and minimum. This difference reflects the variability in pH due to the temperature gradient between the warmer and colder waters in the region. As a result, the ΔpH_{temp} due to the temperature factor is approx. 0.14 and can be understood as the pH change due to the cooling of waters as they flow northwards. The effect of dilution (or seawater freshening) is defined as ΔpH_{sal} and is responsible for a pH increase in the region of approx. 0.1, with a wide range of ΔpH_{sal} values from 0.01 to 0.10 being inversely correlated with salinity. The ΔpH_{bio} is the integrated effect of the P/R, NCC, and air-sea fluxes. Its average values varied widely from year to year, with an average of 0.18, 0.22, and 0.10 for 2019, 2020 and 2021, respectively. Additionally, the consistency of the marine CO_2 system variables was presented as pH_{inc} as an expression of the variability in the data due to uncertainties derived from calculations and the propagation of errors during the analytical measurements. The average of pH_{inc} was 0.02 which is much lower than ΔpH_{bio} but also than ΔpH_{temp} or ΔpH_{sal}, suggesting that even though there are some uncertainties related to the calculations with the use of CO2SYS, they are usually lower than the effect of any of the factors influencing pH variability. Still, the effect of the inconsistencies in the marine CO_2 system should not be ignored in pH-oriented studies in this region, as depending on the scope of conducted research they may constitute an important source of uncertainty.

The results clearly show that ΔpH_{bio} is the main factor controlling the pH distribution in Fram Strait surface waters. Interestingly, the two years with greater ice extension (2019 and

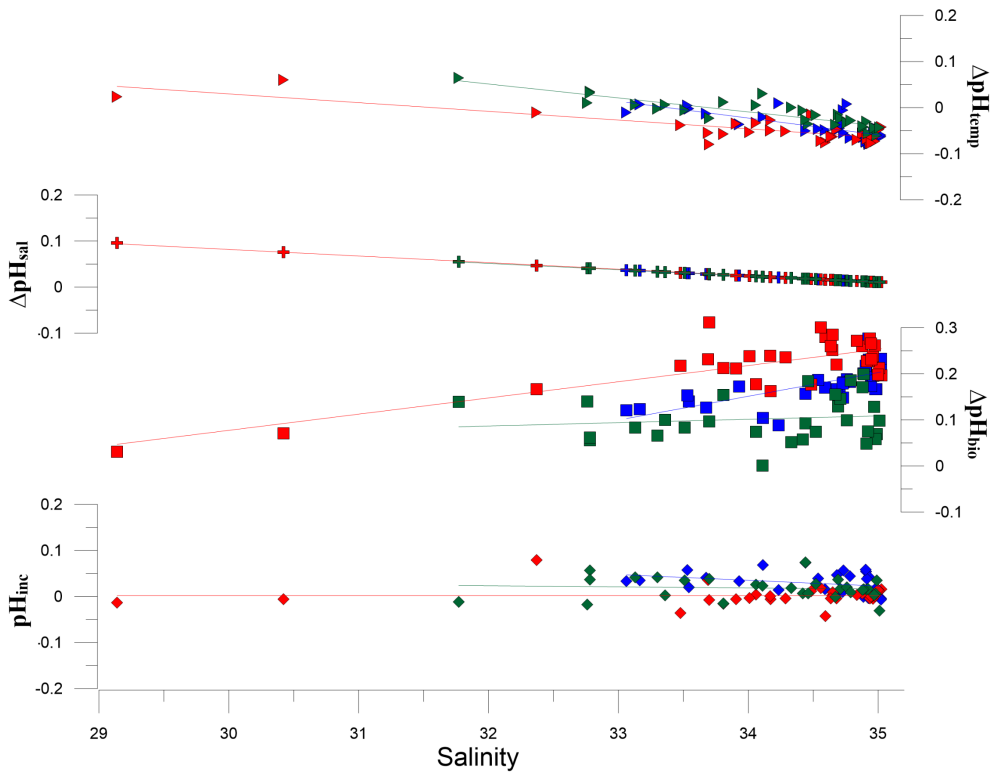

FIGURE 9
Correlation between different ΔpH (associated with temperature ΔpH_{temp}, salinity ΔpH_{sal}, the combined effect of NPP, NCC, and air-sea fluxes ΔpH_{bio}, and inconsistencies pH_{inc}) and salinity. Blue dots are data from 2019, red dots from 2020, and green dots from 2021.

2020) were also characterized by higher pH variation due to ΔpH_{bio}. It is also worth mentioning that the influence of dilution close to the sea ice margin can be similar in magnitude to the pH change due to the temperature variations, both creating rapid pH fluctuations and directly influencing the CO_2 system structure. Thus, with their combined effects, sea ice melting and temperature variability are unneglectable drivers affecting the distribution of surface pH in the eastern Fram Strait, which must be considered for investigating ocean acidification development under future climate scenarios.

3.3 Synthesis

Overall, 2019 and 2020 were characterized by warmer surface waters with a northern extension of the surface AW patch (seawater with salinity greater than 34.8), coincidentally with a broader sea ice extension. On the other hand, 2021 had colder waters, and the surface extent of AW was reduced in the study area, coinciding with the smaller sea ice extension. The mechanism to explain the temperature and salinity variability could be an increase in the PSWw influence on the area and/or a reduced surface expression of AW in years with enhanced sea ice melting due to the higher admixture of meltwater.

The results from DIC and TA indicate that it was possible to trace higher P/R in the AW-influenced area during warmer years (2019 and 2020), coinciding with a lower presence or abundance of calcifier organisms as suggested by the ratio $\Delta TA_{bio}/\Delta DIC_{bio}$. Furthermore, these results coincide with the distribution of surface pCO_2 and pH, where warmer years with higher P/R have also lower pCO_2 at the surface and higher pH, intensifying the capacity of the surface waters to absorb atmospheric CO_2, even though warmer surface waters have reduced CO_2 solubility. Satellite images of chlorophyll *a* distribution also support the idea of higher P/R within the eastern Fram Strait during warmer years. Our conclusions agree with previous findings which suggest that warmer waters may sustain the pycnocline in the surface layer for longer periods, favouring the development of primary producers (Cherkasheva et al., 2014).

Besides the general trends, the high-resolution data of pCO_2 indicate that other medium/small-scale processes may contribute to rapid changes in surface pCO_2. Several studies have shown the presence of mesoscale/submesoscale eddies in the region (Bashmachnikov, 2020; Ghaffari et al., 2018; Trodahl and Isachsen, 2018), which are especially abundant at the outer boundary of the AW inflow. These features can be likely identified in our dataset as local drops in the surface pCO_2 in the AW frontal zone, which may indicate an upwelling of nutrient-rich waters, enhancing P/R in the surface layers, and/or an upwelling of already low pCO_2 waters related to subsurface production, probably at the bottom of the surface mixed layer (Tuerena et al., 2021).

Our data also shows an intense decrease in surface pCO_2 (and an increase in O_2 saturation) in areas where PSWw meets AW. These areas are characterized by an intrusion of cold waters into the warmer layer, indicating that mixing of PSWw and AW in some sectors may enhance P/R. The differences in nutrient limitation between Arctic and Atlantic-derived surface waters have been previously postulated (Krisch et al., 2020; Tuerena et al., 2021), bringing the idea that the mixing between nitrate-limited Arctic-derived waters (in this study, sea-ice-derived meltwater), and Fe-limited Atlantic-derived waters could create the ideal "nutrient-soup" to enhance P/R.

But this initial enhancement of P/R due to the mixing of water masses could create also a negative effect, as seen in 2021, where chlorophyll data shows that the intense PP area was moved westward. Therefore, the reduction of sea ice would move the PP westward, and, an expansion of PSWw (already depleted in nitrates) could create a colder nitrate-limited surface layer, which will produce, as observed in 2021 higher DIC and pCO_2 in the surface layer. These waters may intensify the seasonal pycnocline, deepening it or reducing the eddy-driven upwellings. Consequently, years with colder (or rather higher influence of melted sea ice) surface waters may result in reduced P/R in the eastern part of the Fram Strait.

The mechanism to explain how a higher volume of PSWw may influence the study area is not clear and cannot be fully explained with the data presented in this study. Nevertheless, it can be hypothesised that due to the direct mixing or by the influence of the GSG, more meltwater is incorporated within the surface waters of the eastern part of Fram Strait. With this idea in mind, and based on our biogeochemical data, Figure 10 shows a theoretical concept connecting the main factors influencing the carbonate system in the eastern Fram Strait in two hypothetical scenarios: the first one with a lower influence of melted sea ice waters and lower extension of PSWw within the WSC (Figure 10A) and the second one with a wider extension of PSWw due to higher volume of sea ice meltwater (Figure 10B).

In the scenario with a lower influence of melted sea ice waters (Figure 10A), there is a high P/R in the eastern Fram Strait, which is likely associated with larger vertical nutrient fluxes linked to more abundant mesoscale eddies. Alternatively, the intrusion of PSWw in the surface layer occupied by AW may also enhance P/R by mixing waters with different nutrient limitations. Consequently, enhanced P/R, a higher abundance of nano-pico plankton, and a reduced influence of calcifiers would result in elevated alkalinity and enhanced capacity to capture anthropogenic CO_2 in surface waters.

In the high PSWw scenario and a strong influence of sea ice meltwater on the surface layers, P/R is concentrated close to the sea ice margin zone, which acts as a nutrient filter, depleting their concentrations. The link between sea ice extension and phytoplankton distribution during spring and summer was proposed by Mayot et al. (2020), showing that in years with low export of sea ice, a late-spring/summer phytoplankton bloom develops close to the sea ice margin. These nutrient-depleted waters may follow the surface currents following the EGC, which could expand eastwards the area influenced by PSWw, initially enhancing P/R in a southern location (GSG) but have a low capacity to sustain high primary production in the study area (eastern Fram Strait). This is probably due to the stratification of fresher and colder waters at the surface with an unknown effect on the eddy-driven circulation and the upwelling of deeper N-rich waters.

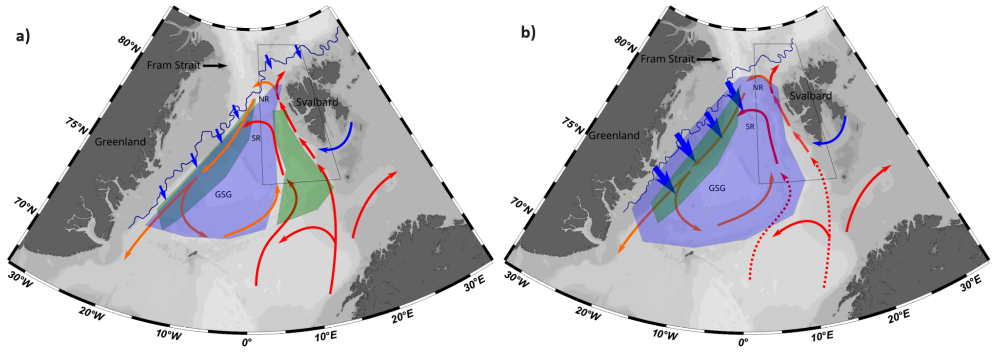

FIGURE 10
Theoretical concepts of the biological and physical situation in the area during: **(A)** narrower extension of warm Polar Surface Waters (PSWw) connected to a lower volume of sea ice meltwater (small blue arrows) in the surface layer and, **(B)** broader extension of PSWw as a consequence of a higher volume of sea ice meltwater in the surface layer. The blue area represents the zones of intense influence of PSWw, and the green area stands for the intense NPP zones developed during summer. The colour in the arrows represents a schematic view of the main water masses in the area and their transformations. Blue arrows represent the influence of Arctic waters, either as melted sea ice (small ones), or as Arctic waters carried by the South Cape Current (SCC), located south of the Svalbard Archipelago. The red arrows represent the Atlantic Water (AW), and the orange arrows are the Polar warm Surface Waters (PSWw). GSG, NR, and SR denote Greenland Sea Gyre, Northern Recirculation, and Southern Recirculation, respectively. The blue line represents the 10% sea ice coverage (SIC), northern of this line the SIC is higher than 10%.The black box delimits the study area.

Stratified waters with lower P/R would limit the capacity of the surface waters to capture atmospheric CO_2. This hypothesis implies that the influence of the sea ice meltwater within the Fram Strait is crucial for estimating and understanding the capacity of the region to absorb atmospheric CO_2. Future scenarios project a reduction in Arctic sea ice during summer. However, a better understanding of the relationship between the volume of melted sea ice and the biogeochemical processes in the surface waters is required, not only in the Fram Strait area but also in the Arctic Ocean in general.

4 Conclusions

This study investigated the distribution of the marine carbonate system parameters, as well as salinity and temperature in consecutive summers of 2019, 2020, and 2021 in the surface waters of the eastern part of the Fram Strait. This, together with analysis of the satellite-derived chlorophyll *a* distribution as well as sea ice extension in the region allowed us to draw the following conclusions:

- TA and DIC are mostly controlled by the mixing of Atlantic water and sea ice meltwater. The combined effect of organic matter production/remineralization, calcium carbonate precipitation/dissolution, and air/sea CO_2 gas exchange causes deviations from this salinity-related mixing, which are smaller and positive for TA (ΔTA_{bio} from 0.7 to 10.0 µmol kg^{-1}) and larger and negative for DIC (ΔDIC_{bio} from -42.9 to -73.4 µmol kg^{-1}).
- The ratios between ΔTA_{bio} and ΔDIC_{bio} suggest interannual shifts in P/R and dominant phytoplankton species in the area. The results indicated higher productivity (confirmed by satellite-derived chlorophyll *a* as well as pCO_2 and pH distribution) and a lower proportion of calcifying to non-calcifying species during 2019 and 2020 characterized by higher surface water temperatures compared to the colder year 2021.
- Net primary production is the main factor controlling the temporal and spatial variability of pH and pCO_2 in the study area followed by temperature (effects of seasonality and cooling as the Atlantic Waters propagate northward) and mixing of water masses expressed with salinity (seawater freshening).
- The patchiness in the latitudinal and longitudinal distributions of pCO_2 and O_2 saturation and their irregular relationship with salinity suggest that vertical mixing of the water column as an important process in shaping surface pCO_2 fields and P/R in the Fram Strait area.
- There is a need to better understand the role of sea ice extent and the associated spread of warm Polar Surface Waters (mixture of Polar Waters and Atlantic Waters) in controlling primary production in the region, which is crucial for predicting the capacity of Fram Strait waters for absorbing atmospheric CO_2 in the future with less sea ice. The smaller sea ice extent and greater spread of warm Polar Surface Waters observed in 2021 coincided with a westward shift of the chlorophyll *a* maximum towards the sea ice front. A reverse situation was observed in 2019 and 2020, when greater extension of Atlantic Waters in the eastern part, as well as sea ice in the western part of the Fram Strait area, were accompanied by chlorophyll *a* maximum in the Atlantic Waters.

Data availability statement

The datasets presented in this study can be found in online repositories. The names of the repository/repositories and accession number(s) can be found below: https://doi.org/10.48457/iopan-2024-159.

Author contributions

FG: Conceptualization, Writing – review & editing, Data curation, Formal analysis, Investigation, Methodology, Visualization, Writing – original draft. MS: Data curation, Methodology, Writing – review & editing. KK-M: Data curation, Writing – review & editing. PM: Data curation, Writing – review & editing. AB-M: Data curation, Writing – review & editing. PK: Conceptualization, Funding acquisition, Writing – review & editing. KK: Conceptualization, Funding acquisition, Project administration, Supervision, Validation, Writing – review & editing.

Funding

The author(s) declare financial support was received for the research, authorship, and/or publication of this article. Sampling, chemical analyses, and data interpretation related to the marine CO_2 system structure and variability were financially supported by the Polish National Science Center, grant no. 2019/34/E/ST10/00167, under the project PROSPECTOR. The analysis of the interrelationships between sea ice extent and chlorophyll *a* distribution was supported by the European Union within the Horizon Europe programme, project 101136480 — SEA-Quester. The interpretation of the seawater freshening was supported by the Norwegian Financial Mechanism 2014–2021 (85%) and National Science Centre (15%) within the GRIEG Programme, grants no. 2019/34/H/ST10/00504 and 2019/34/H/ST10/00645. Additionally, the contribution of PK to the study was supported by the Polish National Science Center, grant no. 2020/37/B/ST10/02905.

Acknowledgments

We would like to thank HEREON for allowing KK-M to measure DIC and TA samples collected in 2020 and also to OBPG/OB.DAAC for providing public access to Satellite Chlorophyll data included in this manuscript. We also would like to thank the captain and the crew of the R.V. Oceania for their enthusiasm and support during sampling.

Conflict of interest

The authors declare that the research was conducted in the absence of any commercial or financial relationships that could be construed as a potential conflict of interest.

Publisher's note

Supplementary material

The Supplementary Material for this article can be found online at: https://www.frontiersin.org/articles/10.3389/fmars.2024.1464653/full#supplementary-material

References

Ahmed, M. M., Else, B. G., Capelle, D., Miller, L. A., and Papakyriakou, T. (2020). Underestimation of surface pCO2 and air-sea CO2 fluxes due to freshwater stratification in an Arctic shelf sea, Hudson Bay. *Elementa* 8 (1), 084. doi: 10.1525/elementa.084

Arrigo, K. R., and van Dijken, G. L. (2015). Continued increases in Arctic Ocean primary production. *Prog. Oceanography* 136, 60–70. doi: 10.1016/j.pocean.2015.05.002

Arrigo, K. R., van Dijken, G. L., Castelao, R. M., Luo, H., Rennermalm, Å. K., Tedesco, M., et al. (2017). Melting glaciers stimulate large summer phytoplankton blooms in southwest Greenland waters. *Geophysical Res. Lett.* 44, 6278–6285. doi: 10.1002/2017GL073583

Athanase, M., Provost, C., Pérez-Hernández, M. D., Sennéchael, N., Bertosio, C., Artana, C., et al. (2020). Atlantic water modification North of svalbard in the mercator physical system from 2007 to 2020. *J. Geophysical Research: Oceans* 125, 1–26. doi: 10.1029/2020JC016463

Bashmachnikov, I. L. (2020). Eddies in the North Greenland sea and fram strait from satellite altimetry, SAR and high - resolution model data. *J. Geophysical Research : Oceans* 125 (7), e2019JC015832. doi: 10.1029/2019JC015832

Bashmachnikov, I. L., Raj, R. P., Golubkin, P., and Kozlov, I. E. (2023). Heat transport by mesoscale eddies in the Norwegian and Greenland seas. *J. Geophysical Research: Oceans* 128 (2). doi: 10.1029/2022JC018987

Bates, N. R., and Mathis, J. T. (2009). The Arctic Ocean marine carbon cycle: Evaluation of air-sea CO2 exchanges, ocean acidification impacts and potential feedbacks. *Biogeosciences* 6, 2433–2459. doi: 10.5194/bg-6-2433-2009

Bauerfeind, E., Nöthig, E. M., Beszczynska, A., Fahl, K., Kaleschke, L., Kreker, K., et al. (2009). Particle sedimentation patterns in the eastern Fram Strait during 2000–2005: Results from the Arctic long-term observatory HAUSGARTEN. *Deep Sea Res. Part I: Oceanographic Res. Papers* 56 (9). doi: 10.1016/j.dsr.2009.04.011

Beszczynska-Möller, A., Fahrbach, E., Schauer, U., and Hansen, E. (2012). Variability in Atlantic water temperature and transport at the entrance to the Arctic Ocean 1997–2010. *ICES J. Mar. Sci.* 69, 852–863. doi: 10.1093/icesjms/fss056

Brümmer, B., Müller, G., Affeld, B., Gerdes, R., Karcher, M., and Kauker, F. (2001). Cyclones over Fram Strait: impact on sea ice and variability. *Polar Res.* 20, 147–152. doi: 10.1111/j.1751-8369.2001.tb00050.x

Caldeira, K., and Wickett, M. E. (2003). Anthropogenic carbon and ocean pH. *Nature* 425, 365. doi: 10.1038/425365a

Capelle, D. W., Kuzyk, Z. Z. A., Papakyriakou, T., Guéguen, C., Miller, L. A., and Macdonald, R. W. (2020). Effect of terrestrial organic matter on ocean acidification and CO2 flux in an Arctic shelf sea. *Prog. Oceanography* 185, 102319. doi: 10.1016/j.pocean.2020.102319

Carmack, E. C., Yamamoto-Kawai, M., Haine, T. W., Bacon, S., Bluhm, B. A., Lique, C., et al. (2016). Freshwater and its role in the Arctic Marine System: Sources, disposition, storage, export, and physical and biogeochemical consequences in the Arctic and global oceans. *J. Geophysical Res. G: Biogeosciences* 121, 675–717. doi: 10.1002/2015JG003140

Chatterjee, S., Raj, R. P., Bertino, L., Skagseth, Ø., Ravichandran, M., and Johannessen, O. M. (2018). Role of Greenland sea gyre circulation on Atlantic water temperature variability in the fram strait. *Geophysical Res. Lett.* 45, 8399–8406. doi: 10.1029/2018GL079174

Chen, B., Cai, W. J., and Chen, L. (2015). The marine carbonate system of the Arctic Ocean: Assessment of internal consistency and sampling considerations, summer 2010. *Mar. Chem.* 176, 174–188. doi: 10.1016/j.marchem.2015.09.007

Chierici, M., Vernet, M., Fransson, A., and Børsheim, K. Y. (2019). Net community production and carbon exchange from winter to summer in the Atlantic water inflow to the arctic ocean. *Front. Mar. Sci.* 6. doi: 10.3389/fmars.2019.00528

Chierici, M., and Fransson, A. (2009). Calcium carbonate saturation in the surface water of the Arctic Ocean: Undersaturation in freshwater influenced shelves. *Biogeosciences* 6, 2421–2432. doi: 10.5194/bg-6-2421-2009

Cherkasheva, A., Bracher, A., Melsheimer, C., Köberle, C., Gerdes, R., Nöthig, E. M., et al. (2014). Influence of the physical environment on polar phytoplankton blooms: A case study in the Fram Strait. *J. Mar. Syst.* 132, 196–207. doi: 10.1016/j.jmarsys.2013.11.008

Comiso, J. C., Kwok, R., Martin, S., and Gordon, A. L. (2011). Variability and trends in sea ice extent and ice production in the Ross Sea. *J. Geophysical Research: Oceans* 116, 1–19. doi: 10.1029/2010JC006391

de Steur, L., Hansen, E., Mauritzen, C., Beszczynska-Möller, A., and Fahrbach, E. (2014). Impact of recirculation on the East Greenland Current in Fram Strait: Results from moored current meter measurements between 1997 and 2009. *Deep-Sea Res. Part I: Oceanographic Res. Papers* 92, 26–40. doi: 10.1016/j.dsr.2014.05.018

Devries, T. (2022). The ocean carbon cycle. *Annu. Rev. Environ. Resour.* 47, 317–341. doi: 10.1146/annurev-environ-120920-111307

Dickson, A. G., Wesolowski, D. J., Palmer, D. A., and Mesmer, R. E. (1990). Dissociation constant of bisulfate ion in aqueous sodium chloride solutions to 250° C. *J. Phys. Chem.* 94, 7978–7985. doi: 10.1021/j100383a042

Dickson, A. G., and Millero, F. J. (1987). A comparison of the equilibrium constants for the dissociation of carbonic acid in seawater media. *Deep Sea Res. Part A Oceanographic Res. Papers* 34, 1733–1743. doi: 10.1016/0198-0149(87)90021-5

Dickson, A. G., Sabine, C. L., and Christian, J. R. (Eds.) (2007). *Guide to Best Practices for Ocean CO2 Measurements*, Vol. 3 (PICES Special Publication), 191.

Forest, A., Wassmann, P., Slagstad, D., Bauerfeind, E., Nöthig, E. M., and Klages, M. (2010). Relationships between primary production and vertical particle export at the Atlantic-Arctic boundary (Fram Strait, HAUSGARTEN). *Polar Biol.* 33, 1733–1746. doi: 10.1007/s00300-010-0855-3

Fransson, A., Chierici, M., and Nojiri, Y. (2009). New insights into the spatial variability of the surface water carbon dioxide in varying sea ice conditions in the Arctic Ocean. *Cont. Shelf Res.* 29, 1317–1328. doi: 10.1016/j.csr.2009.03.008

Fransson, A., Chierici, M., Anderson, L. G., Bussmann, I., Kattner, G., Jones, E. P., et al. (2001). The importance of shelf processes for the modification of chemical constituents in the waters of the eastern Arctic Ocean. *Cont. Shelf Res.* 21, 225–242. doi: 10.1016/S0278-4343(00)00088-1

Fransson, A., Chierici, M., Skjelvan, I., Olsen, A., Assmy, P., Peterson, A. K., et al. (2017). Journal of Geophysical Research : Oceans high Arctic Ocean : Implications for sea-air CO 2 fluxes. *J. Geophysical Research: Oceans* 122 (7), 5566–5587. doi: 10.1002/2016JC012478

Ghaffari, P., Isachsen, P. E., Nøst, O. A., and Weber, J. E. (2018). The influence of topography on the stability of the Norwegian Atlantic Current off northern Norway. *J. Phys. Oceanography* 48 (11). doi: 10.1175/1520-0469

Graham, R. M., Itkin, P., Meyer, A., Sundfjord, A., Spreen, G., Smedsrud, L. H., et al. (2019). Winter storms accelerate the demise of sea ice in the Atlantic sector of the Arctic Ocean. *Sci. Rep.* 9, 9222. doi: 10.1038/s41598-019-45574-5

Haine, T. W., Curry, B., Gerdes, R., Hansen, E., Karcher, M., Lee, C., et al. (2015). Arctic freshwater export: Status, mechanisms, and prospects. *Global Planetary Change* 125, 13–35. doi: 10.1016/j.gloplacha.2014.11.013

Halvorsen, M. H., Smedsrud, L. H., Zhang, R., and Kloster, K. (2015). Fram Strait spring ice export and September Arctic sea ice. *Cryosphere Discussions* 9, 4205–4235. doi: 10.5194/tcd-9-4205-2015

Hattermann, T., Isachsen, P. E., von Appen, W. J., Albretsen, J., and Sundfjord, A. (2016). Eddy-driven recirculation of Atlantic water in Fram Strait. *Geophysical Res. Lett.* 43 (7). doi: 10.1002/2016GL068323

Håvik, L., Våge, K., Pickart, R. S., Harden, B., Appen, W. J. V., Jónsson, S., et al. (2017). Structure and variability of the shelfbreak East Greenland Current north of Denmark Strait. *J. Phys. Oceanography* 47 (10). doi: 10.1175/JPO-D-17-0062.1

Hofmann, Z., von Appen, W. J., and Wekerle, C. (2021). Seasonal and mesoscale variability of the two Atlantic water recirculation pathways in Fram Strait. *J. Geophysical Research: Oceans* 126 (7). doi: 10.1029/2020JC017057

Johnson, K. M., Wills, K. D., Butler, D. B., Johnson, W. K., and Wong, C. S. (2000). Coulometric total carbon dioxide analysis for marine studies: maximizing the performance of an automated gas extraction system and coulometric detector. *Mar. Chem.* 44, 1993, 167–187. doi: 10.1016/0304-4203(93)90201-X

Joli, N., Gosselin, M., Ardyna, M., Babin, M., Onda, D. F., Tremblay, J. É., et al. (2018). Need for focus on microbial species following ice melt and changing freshwater regimes in a Janus Arctic Gateway. *Sci. Rep.* 8, 1–11. doi: 10.1038/s41598-018-27705-6

Kahru, M., Brotas, V., Manzano-Sarabia, M., and Mitchell, B. G. (2011). Are phytoplankton blooms occurring earlier in the Arctic? *Global Change Biol.* 17, 1733–1739. doi: 10.1111/j.1365-2486.2010.02312.x

Karpouzoglou, T., de Steur, L., Smedsrud, L. H., and Sumata, H. (2022). Observed changes in the arctic freshwater outflow in fram strait. *J. Geophysical Research: Oceans* 127, 1–17. doi: 10.1029/2021JC018122

Kleypas, J. A. (2019). Impacts of ocean acidification on marine biodiversity. *Biodiversity Climate Change: Transforming Biosphere (Dic)*, 185–195. doi: 10.2307/j.ctv8jnzw1.25

Koziorowska-Makuch, K., Szymczycha, B., Thomas, H., and Kuliński, K. (2023). The marine carbonate system variability in high meltwater season (Spitsbergen Fjords, Svalbard). *Prog. Oceanography*, 211. doi: 10.1016/j.pocean.2023.102977

Krisch, S., Browning, T. J., Graeve, M., Ludwichowski, K. U., Lodeiro, P., Hopwood, M. J., et al. (2020). The influence of Arctic Fe and Atlantic fixed N on summertime primary production in Fram Strait, North Greenland Sea. *Sci. Rep.* 10, 1–13. doi: 10.1038/s41598-020-72100-9

Kuliński, K., Schneider, B., Szymczycha, B., and Stokowski, M. (2017). Structure and functioning of the acid-base system in the Baltic Sea. *Earth System Dynamics* 8, 1107–1120. doi: 10.5194/esd-8-1107-2017

Lalande, C., Bauerfeind, E., and Nöthig, E. M. (2011). Downward particulate organic carbon export at high temporal resolution in the eastern Fram Strait: influence of Atlantic Water on flux composition. *Mar. Ecol. Prog. Ser.*, 440. doi: 10.3354/meps09385

Lalande, C., Bauerfeind, E., Nöthig, E. M., and Beszczynska-Möller, A. (2013). Impact of a warm anomaly on export fluxes of biogenic matter in the eastern Fram Strait. *Prog. Oceanography* 109, 70–77. doi: 10.1016/j.pocean.2012.09.006

Lee, K., Kim, T. W., Byrne, R. H., Millero, F. J., Feely, R. A., and Liu, Y. M. (2010). The universal ratio of boron to chlorinity for the North Pacific and North Atlantic oceans. *Geochim. Cosmochim. Acta* 74, 1801–1811. doi: 10.1016/j.gca.2009.12.027

Lewis, K. M., Van Dijken, G. L., and Arrigo, K. R. (2020). Changes in phytoplankton concentration now drive increased Arctic Ocean primary production. *Science* 369, 198–202. doi: 10.1126/science.aay8380

Lewis, E., Wallace, D., and Allison, L. J. (1998). *Program developed for CO {sub 2} system calculations* (TN (United States: Brookhaven National Lab., Dept. of Applied Science, Upton, NY (United States); Oak Ridge National Lab., Carbon Dioxide Information Analysis Center). (No. ORNL/CDIAC-105).

Lueker, T. J., Dickson, A. G., and Keeling, C. D. (2000). Ocean pCO2 calculated from dissolved inorganic carbon, alkalinity, and equations for K1 and K2: validation based on laboratory measurements of CO2 in gas and seawater at equilibrium. *Mar. Chem.* 70 (1–3), 105–119.

MacGilchrist, G. A., Garabato, A. N., Tsubouchi, T., Bacon, S., Torres-Valdés, S., and Azetsu-Scott, K. (2014). The Arctic Ocean carbon sink. *Deep-Sea Res. Part I: Oceanographic Res. Papers* 86, 39–55. doi: 10.1016/j.dsr.2014.01.002

Manizza, M., Menemenlis, D., Zhang, H., and Miller, C. E. (2019). Modeling the recent changes in the arctic ocean CO2 sink, (2006–2013). *Global Biogeochemical Cycles* 33, 420–438. doi: 10.1029/2018GB006070

Marchese, C., de la Guardia, L. C., Myers, P. G., and Bélanger, S. (2019). Regional differences and inter-annual variability in the timing of surface phytoplankton blooms in the Labrador Sea. *Ecol. Indic.* 96, 81–90. doi: 10.1016/j.ecolind.2018.08.053

Marnela, M., Rudels, B., Houssais, M. N., Beszczynska-Möller, A., and Eriksson, P. B. (2013). Recirculation in the Fram Strait and transports of water in and north of the Fram Strait derived from CTD data. *Ocean Sci.* 9, 499–519. doi: 10.5194/os-9-499-2013

Mayot, N., Matrai, P. A., Arjona, A., Bélanger, S., Marchese, C., Jaegler, T., et al. (2020). Springtime export of arctic sea ice influences phytoplankton production in the Greenland sea. *J. Geophysical Research: Oceans* 125, 1–16. doi: 10.1029/2019JC015799

Mehrbach, C., Culberson, C. H., Hawley, J. E., and Pytkowicx, R. M. (1973). Measurement of the apparent dissociation constants of carbonic acid in seawater at atmospheric pressure 1. *Limnol. Oceanogr.* 18 (6). doi: 10.4319/lo.1973.18.6.0897

Meredith, M. P., Sommerkorn, M., Cassotta, S., Derksen, C., Ekaykin, A. A., Hollowed, A. B., et al. (2019). "Chapter 3: Polar Regions," in *The Ocean and Cryosphere in a Changing Climate: Summary for Policymakers*. Eds. O. Anisimov, G. Flato and C. Xiao (Monaco: Intergovernmental Panel on Climate Change), 3-1-3-173. Available online at: https://www.ipcc.ch/srocc/home/.

Middelburg, J. J., Soetaert, K., and Hagens, M. (2020). Ocean alkalinity, buffering and biogeochemical processes. *Rev. Geophysics* 58 (3), e2019RG000681. doi: 10.1029/2019RG000681

NASA Ocean Biology Processing Group (2023). *Moderate Resolution Imaging Spectroradiometer (Aqua-MODIS) Level-3 Monthly Chlorophyll concentration (4Km resolution).* Available online at: https://oceancolor.gsfc.nasa.gov/l3/ (Accessed 2023/02/29).

Nilsen, F., Skogseth, R., Vaardal-Lunde, J., and Inall, M. (2016). A simple shelf circulation model: intrusion of Atlantic Water on the West Spitsbergen Shelf. *J. Phys. Oceanography* 46 (4). doi: 10.1175/JPO-D-15-0058.1

Nilsen, F., Ersdal, E. A., and Skogseth, R. (2021). Wind-driven variability in the spitsbergen polar current and the svalbard branch across the yermak plateau. *J. Geophysical Research: Oceans* 126 (9), e2020JC016734. doi: 10.1029/2020JC016734

Nöthig, E. M., Bracher, A., Engel, A., Metfies, K., Niehoff, B., Peeken, I., et al. (2015). Summertime plankton ecology in fram strait-a compilation of long-and short-term observations. *Polar Res.* 34 (1), 23349. doi: 10.3402/polar.v34.23349

Orr, J. C., Epitalon, J. M., Dickson, A. G., and Gattuso, J. P. (2018). Routine uncertainty propagation for the marine carbon dioxide system. *Mar. Chem.* 207, 84–107. doi: 10.1016/j.marchem.2018.10.006

Pabi, S., van Dijken, G. L., and Arrigo, K. R. (2008). Primary production in the arctic ocean 1998-2006. *J. Geophysical Research: Oceans* 113, 1998–2006. doi: 10.1029/2007JC004578

Paulsen, M. L., Bratbak, G., Larsen, A., Seuthe, L., Egge, J. K., and Erga, S. R. (2017). *CarbonBridge 2014: Physical oceanography and microorganism composition during 5 cruises (Jan, March, May, August, Nov 2014) on and off the shelf northwest of Svalbard in 2014* (Center for Marine Environmental Sciences, University of Bremen (MARUM), Germany: PANGAEA). doi: 10.1594/PANGAEA.884255

Peng, G., Matthews, J. L., Wang, M., Vose, R., and Sun, L. (2020). What do global climate models tell us about future arctic sea ice coverage changes? *Climate* 8 (1), 15. doi: 10.3390/cli8010015

Perez, F. F., and Fraga, F. (1987). Association constant of fluoride and hydrogen ions in seawater. *Mar. Chem.* 21, 161–168. doi: 10.1016/0304-4203(87)90036-3

Polyakov, I. V., Timokhov, L. A., Alexeev, V. A., Bacon, S., Dmitrenko, I. A., Fortier, L., et al. (2010). Arctic Ocean warming contributes to reduced polar ice cap. *J. Phys. Oceanography* 40, 2743–2756. doi: 10.1175/2010JPO4339.1

Qi, D., Wu, Y., Chen, L., Cai, W. J., Ouyang, Z., Zhang, Y., et al. (2022). Rapid acidification of the arctic chukchi sea waters driven by anthropogenic forcing and biological carbon recycling. *Geophysical Res. Lett.* 49, 1–12. doi: 10.1029/2021GL097246

Raimondi, L., Matthews, J. B. R., Atamanchuk, D., Azetsu-Scott, K., and Wallace, D. W. (2019). The internal consistency of the marine carbon dioxide system for high latitude shipboard and *in situ* monitoring. *Mar. Chem.* 213, 49–70. doi: 10.1016/j.marchem.2019.03.001

Raj, R. P., Johannessen, J. A., Eldevik, T., Nilsen, J. Ø., and Halo, I. (2016). Quantifying mesoscale eddies in the Lofoten Basin. *J. Geophysical Research: Oceans* 121 (7). doi: 10.1080/01431161.2016.1201234

Richter, M. E., Von Appen, W. J., and Wekerle, C. (2018). Does the East Greenland Current exist in the northern Fram Strait? *Ocean Sci.* 14, 1147–1165. doi: 10.5194/os-14-1147-2018

Rippeth, T. P., Lincoln, B. J., Lenn, Y. D., Green, J. M., Sundfjord, A., and Bacon, S. (2015). Tide-mediated warming of Arctic halocline by Atlantic heat fluxes over rough topography. *Nat. Geosci.* 8, 191–194. doi: 10.1038/ngeo2350

Rudels, B., Björk, G., Nilsson, J., Winsor, P., Lake, I., and Nohr, C. (2005). The interaction between waters from the Arctic Ocean and the Nordic Seas north of Fram Strait and along the East Greenland Current: Results from the Arctic Ocean-02 Oden expedition. *J. Mar. Syst.* 55, 1–30. doi: 10.1016/j.jmarsys.2004.06.008

Rysgaard, S., Glud, R. N., Sejr, M. K., Bendtsen, J., and Christensen, P. B. (2007). Inorganic carbon transport during sea ice growth and decay: A carbon pump in polar seas. *J. Geophysical Research: Oceans* 112, 1–8. doi: 10.1029/2006JC003572

Saloranta, T. M., and Svendsen, H. (2001). Across the Arctic front west of Spitsbergen: high-resolution CTD sections from 1998–2000. *Polar Res.* 20, 177–184. doi: 10.3402/polar.v20i2.6515

Slagstad, D., Wassmann, P. F. J., and Ellingsen, I. (2015). Physical constrains and productivity in the future Arctic Ocean. *Front. Mar. Sci.* 2. doi: 10.3389/fmars.2015.00085

Schlitzer, R. (2023). *Ocean Data View, odv.awi.de.*

Spreen, G., Kaleschke, L., and Heygster, G. (2008). Sea ice remote sensing using AMSR-E 89-GHz channels. *J. Geophysical Research: Oceans* 113 (C2). doi: 10.1029/2005JC003384

Spreen, G., De Steur, L., and Divine, D. (2020). Arctic sea ice volume export through fram strait from 1992 to 2014. *J. Geophysical Research : Oceans*. 125 (6), e2019JC016039. doi: 10.1029/2019JC016039

Stokowski, M., Makuch, P., Rutkowski, K., Wichorowski, M., and Kuliński, K. (2021). A system for the determination of surface water pCO2 in a highly variable environment, exemplified in the southern Baltic Sea. *Oceanologia* 63 (2). doi: 10.1016/j.oceano.2021.01.001

Stroeve, J. C., Serreze, M. C., Holland, M. M., Kay, J. E., Malanik, J., and Barrett, A. P. (2012). The Arctic's rapidly shrinking sea ice cover: A research synthesis. *Climatic Change* 110, 1005–1027. doi: 10.1007/s10584-011-0101-1

Stroeve, J., and Notz, D. (2018). Changing state of Arctic sea ice across all seasons. *Environ. Res. Lett.* 13 (10), 103001. doi: 10.1088/1748-9326/aade56

Takahashi, T., Olafsson, J., Goddard, J. G., Chipman, D. W., and Sutherland, S. C. (1993). Seasonal variation of CO2 and nutrients in the high-latitude oceans: A comparative study. *Global Biogeochemical Cycles* 7, 843–878. doi: 10.1029/93GB02263

Takahashi, T., Sutherland, S. C., Sweeney, C., Poisson, A., Metzl, N., Tilbrook, B., et al. (2002). Global sea–air CO2 flux based on climatological surface ocean pCO2, and seasonal biological and temperature effects. *Deep Sea Res. Part II: Topical Stud. Oceanography* 49 (9-10). doi: 10.1016/S0967-0645(02)00003-6

Tremblay, J. É., Anderson, L. G., Matrai, P., Coupel, P., Bélanger, S., Michel, C., et al. (2015). Global and regional drivers of nutrient supply, primary production and CO2 drawdown in the changing Arctic Ocean. *Prog. Oceanography*. doi: 10.1016/j.pocean.2015.08.009

Trodahl, M., and Isachsen, P. E. (2018). Topographic influence on baroclinic instability and the mesoscale eddy field in the northern North Atlantic Ocean and the Nordic Seas. *J. Phys. Oceanography* 48 (11). doi: 10.1175/JPO-D-17-0220.1

Tsukernik, M., Deser, C., Alexander, M., and Tomas, R. (2010). Atmospheric forcing of Fram Strait sea ice export: A closer look. *Climate Dynamics* 35, 1349–1360. doi: 10.1007/s00382-009-0647-z

Tuerena, R. E., Hopkins, J., Buchanan, P. J., Ganeshram, R. S., Norman, L., von Appen, W. J., et al. (2021). An arctic strait of two halves: the changing dynamics of nutrient uptake and limitation across the fram strait. *Global Biogeochemical Cycles* 35, 1–20. doi: 10.1029/2021GB006961

Tynan, E., Clarke, J. S., Humphreys, M. P., Ribas-Ribas, M., Esposito, M., Rérolle, V. M., et al. (2016). Physical and biogeochemical controls on the variability in surface pH and calcium carbonate saturation states in the Atlantic sectors of the Arctic and Southern Oceans. *Deep-Sea Res. Part II: Topical Stud. Oceanography* 127, 7–27. doi: 10.1016/j.dsr2.2016.01.001

Vihma, T., Screen, J., Tjernström, M., Newton, B., Zhang, X., Popova, V., et al. (2016). The atmospheric role in the Arctic water cycle: A review on processes, past and future changes, and their impacts. *J. Geophysical Research: Biogeosciences* 121, 586–620. doi: 10.1002/2015JG003132

Wittmann, A. C., and Pörtner, H. O. (2013). Sensitivities of extant animal taxa to ocean acidification. *Nat. Climate Change* 3, 995–1001. doi: 10.1038/nclimate1982

Wolf-Gladrow, D. A., Zeebe, R. E., Klaas, C., Körtzinger, A., and Dickson, A. G. (2007). Total alkalinity: The explicit conservative expression and its application to biogeochemical processes. *Mar. Chem.* 106, 287–300. doi: 10.1016/j.marchem.2007.01.006

Woosley, R. J., and Millero, F. J. (2020). Freshening of the western Arctic negates anthropogenic carbon uptake potential. *Limnology Oceanography* 65, 1834–1846. doi: 10.1002/lno.11421

Woosley, R. J., Millero, F. J., and Takahashi, T. (2017). Internal consistency of the inorganic carbon system in the Arctic Ocean. *Limnology Oceanography: Methods* 15, 887–896. doi: 10.1002/lom3.10208

Yasunaka, S., Murata, A., Watanabe, E., Chierici, M., Fransson, A., van Heuven, S., et al. (2016). Mapping of the air–sea CO2 flux in the Arctic Ocean and its adjacent seas: Basin-wide distribution and seasonal to interannual variability. *Polar Sci.* 10, 323–334. doi: 10.1016/j.polar.2016.03.006

Yasunaka, S., Siswanto, E., Olsen, A., Hoppema, M., Watanabe, E., Fransson, A., et al. (2018). Arctic Ocean CO 2 uptake : an improved multiyear estimate of the air – sea CO 2 flux incorporating chlorophyll a concentrations. *Biogeosciences* 15 (6), 1643–1661. doi: 10.5194/bg-15-1643-2018

Yasunaka, S., Manizza, M., Terhaar, J., Olsen, A., Yamaguchi, R., Landschützer, P., et al. (2023). An assessment of CO2 uptake in the arctic ocean from 1985 to 2018. *Global Biogeochemical Cycles* 37, 1–27. doi: 10.1029/2023GB007806

Zhang, Y., Yamamoto-Kawai, M., and Williams, W. J. (2020). Two decades of ocean acidification in the surface waters of the beaufort gyre, arctic ocean: effects of sea ice melt and retreat from 1997–2016. *Geophysical Res. Lett.* 47, 1–11. doi: 10.1029/2019GL086421

Supplementary Material

1 Supplementary Figures.

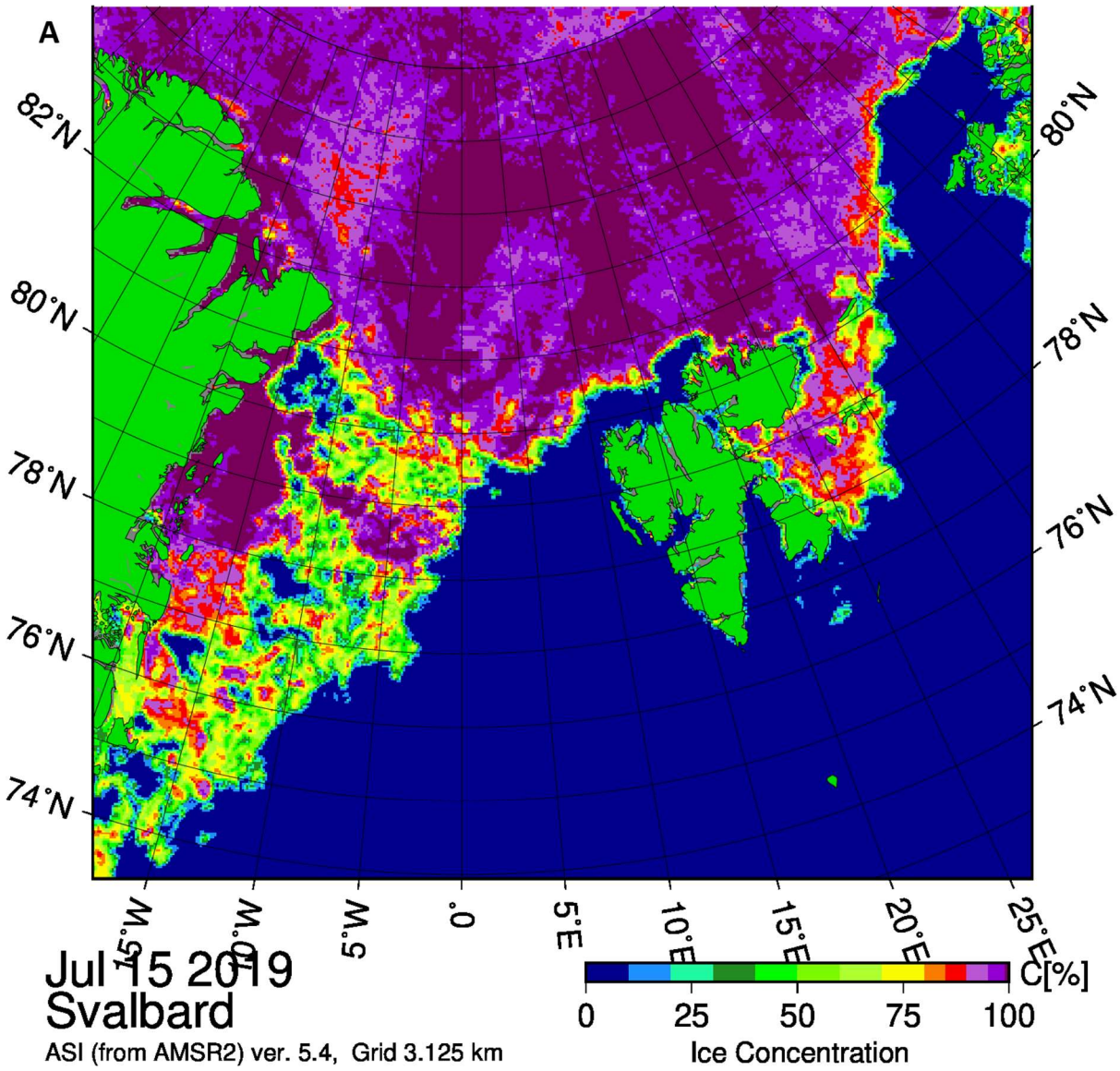

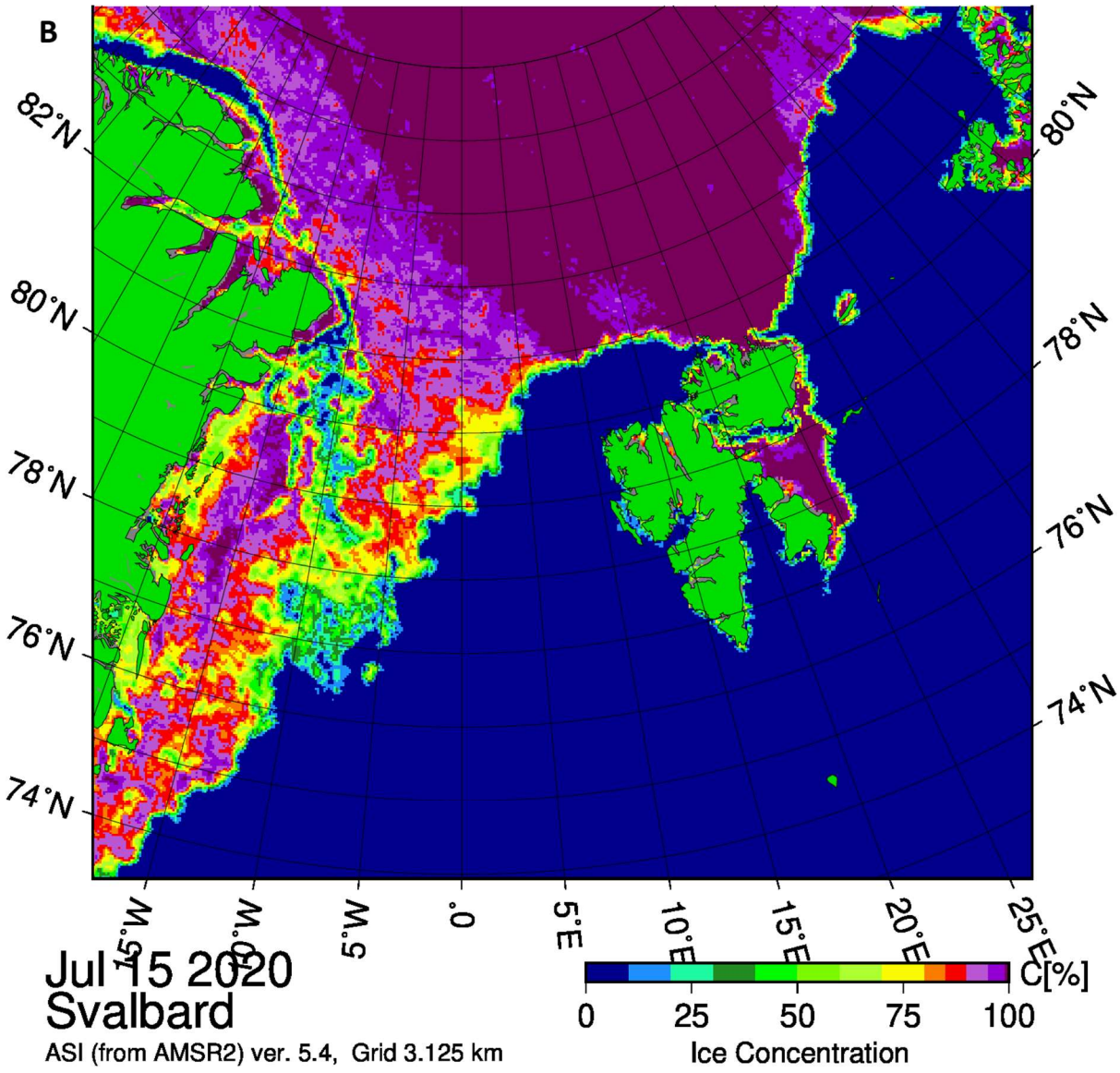
B
82°N
80°N
78°N
76°N
74°N
80°N
78°N
76°N
74°N
15°W
10°W
5°W
0°
5°E
10°E
15°E
20°E
25°E
Jul 15 2020
Svalbard
ASI (from AMSR2) ver. 5.4, Grid 3.125 km
C[%]
0
25
50
75
100
Ice Concentration

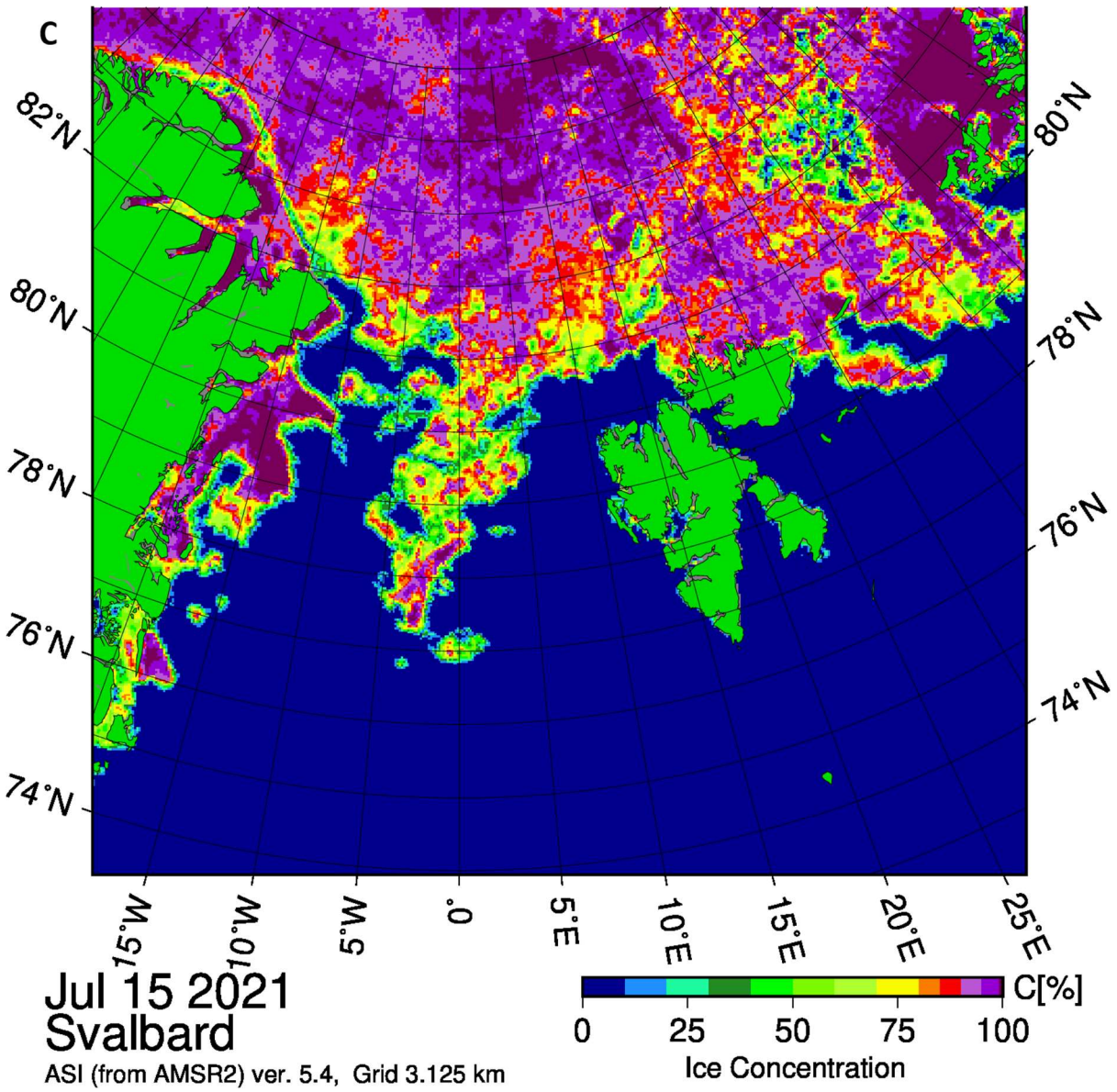

Figure S1: Maps of sea ice concentrations, as derived from satellite passive-microwave observations from the Advance Microwave Scanning Radiometer 2 (AMSR-2), University of Bremen (seaice.uni-bremen.de, Spreen et al., 2008). Sea ice concentration on July 15th in **(a)** 2019, **(b)** 2020 and **(c)** 2021.

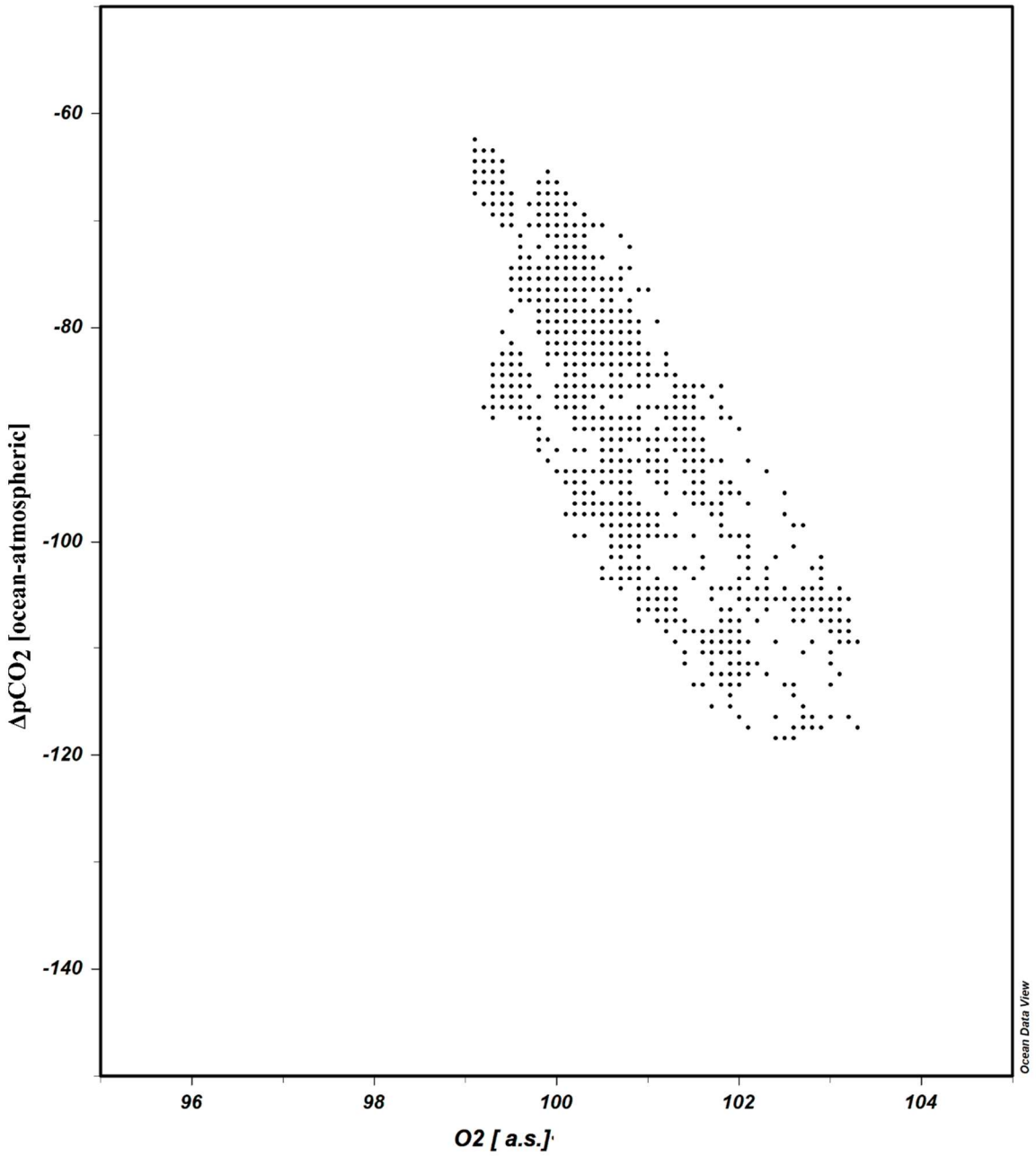

Figure S2: Correlation between ΔpCO_2 and O_2 saturation [a.s.] for the transect b) in figure 7 between 7.5°E and 11.5°E. The strong correlation ($y = -8.9427x + 815.28$, $R^2 = 0.809$) indicates that P/R is the main process triggering changes in surface pCO_2.

2 Supplementary Table.

Table S1: Data collected during summer 2021 in the water column between 100 and 500m water depth at different stations.

STATION	LAT	LONG	DATE	SAMPLING DEPTH[m]	DIC [µmol/kg]	TA [µmol/kg]	SALINITY	TEMP (℃)
N-5	76 30.062' N	07 29.789' E	7/4/21	500	2166	2300	34.97	1.85
N-5	76 30.062' N	07 29.789' E	7/4/21	200	2153	2304	35.01	3.33
N-5	76 30.062' N	07 29.789' E	7/4/21	100	2158	2329	35.00	3.53
K12	75 00.040' N	08 29.753' E	7/7/21	500	2178	2288	34.91	0.19
K12	75 00.040' N	08 29.753' E	7/7/21	200	2168	2296	34.98	2.77
K12	75 00.040' N	08 29.753' E	7/7/21	100	2166	2299	35.03	3.88
Z8	78 08.209' N	07 29.006' E	7/15/21	500	2183	2302	34.92	0.39
Z8	78 08.209' N	07 29.006' E	7/15/21	200	2169	2313	34.97	1.93
EX9	79 24.994' N	04 31.130' E	7/17/21	500	2177	2294	34.94	1.34
EX9	79 24.994' N	04 31.130' E	7/17/21	200	2167	2297	34.99	2.85
EX9	79 24.994' N	04 31.130' E	7/17/21	100	2164	2300	34.96	3.07
WB14	80 34.794' N	12 02.792' E	7/20/21	400	2168	2297	34.96	1.94
WB14	80 34.794' N	12 02.792' E	7/20/21	200	2163	2301	34.96	2.59
Y8	79 52.794' N	09 02.572' E	7/21/21	450	2170	2296	34.96	2.04
Y8	79 52.794' N	09 02.572' E	7/21/21	400	2168	2303	34.98	2.88
Y8	79 52.794' N	09 02.572' E	7/21/21	200	2166	2302	34.99	3.29

Statement of co-authors

Sopot, 18/03/2026

MSc Fernando Aguado Gonzalo

Institute of Oceanology of the Polish Academy of Sciences

Laboratory of marine biogeochemistry

Author contribution statement

I declare that my contribution to the publication:

Aguado Gonzalo, F., Stokowski, M., Koziorowska-Makuch, K., Makuch, P., Beszczyńska-Möller, A., Kukliński, P., & Kuliński, K. (2024). Key processes controlling the variability of the summer marine CO2 system in Fram Strait surface waters. Frontiers in Marine Science, 11, 1464653.

Involved: Conceptualization, Writing– review & editing, Data curation, Formal analysis, Investigation, Methodology, Visualization, Writing– original draft.

and accounted for 60% of the total work needed for the realization of this publication.

Sopot, 18/03/2026

Dr. Marcin Stokowski

Institute of Oceanology of the Polish Academy of Sciences

Laboratory of physiology of marine organisms

Author contribution statement

I declare that my contribution to the publication:

Aguado Gonzalo, F., Stokowski, M., Koziorowska-Makuch, K., Makuch, P., Beszczyńska-Möller, A., Kukliński, P., & Kuliński, K. (2024). Key processes controlling the variability of the summer marine CO2 system in Fram Strait surface waters. Frontiers in Marine Science, 11, 1464653.

Involved: Data curation, Methodology, Writing– review & editing.

and accounted for 7% of the total work needed for the realization of this publication.

Sopot, 19/03/2026

Dr. Katarzyna Koziorowska

Institute of Oceanology of the Polish Academy of Sciences

Laboratory of Marine Biogeochemistry

Author contribution statement

I declare that my contribution to the publication:

Aguado Gonzalo, F., Stokowski, M., Koziorowska-Makuch, K., Makuch, P., Beszczyńska-Möller, A., Kukliński, P., & Kuliński, K. (2024). Key processes controlling the variability of the summer marine CO2 system in Fram Strait surface waters. Frontiers in Marine Science, 11, 1464653.

Involved: Data curation, Writing– review & editing.

and accounted for 5% of the total work needed for the realization of this publication.

Katarzyna Koziorowska

Sopot, 18/03/2026

Dr. Przemysław Makuch

Institute of Oceanology of the Polish Academy of Sciences

Laboratory of sea-atmosphere interactions

Author contribution statement

I declare that my contribution to the publication:

Aguado Gonzalo, F., Stokowski, M., Koziorowska-Makuch, K., Makuch, P., Beszczyńska-Möller, A., Kukliński, P., & Kuliński, K. (2024). Key processes controlling the variability of the summer marine CO2 system in Fram Strait surface waters. Frontiers in Marine Science, 11, 1464653.

Involved: Data curation, Writing– review & editing.

and accounted for 5% of the total work needed for the realization of this publication.

Sopot, 18/03/2026

Dr. Agnieszka Beszczyńska-Möller

Institute of Oceanology of the Polish Academy of Sciences

Laboratory of observational oceanography

Authorcontribution statement

I declare that my contribution to the publication:

Aguado Gonzalo, F., Stokowski, M., Koziorowska-Makuch, K., Makuch, P., Beszczyńska-Möller, A., Kukliński, P., & Kuliński, K. (2024). Key processes controlling the variability of the summer marine CO2 system in Fram Strait surface waters. Frontiers in Marine Science, 11, 1464653.

Involved: Data curation, Writing– review & editing.

and accounted for 8% of the total work needed for the realization of this publication.

Sopot, 23/03/2026

Prof. Piotr Kukliński

Institute of Oceanology of the Polish Academy of Sciences

Laboratory of biodiversity and scientific diving research

Author contribution statement

I declare that my contribution to the publication:

Aguado Gonzalo, F., Stokowski, M., Koziorowska-Makuch, K., Makuch, P., Beszczyńska-Möller, A., Kukliński, P., & Kuliński, K. (2024). Key processes controlling the variability of the summer marine CO2 system in Fram Strait surface waters. Frontiers in Marine Science, 11, 1464653.

Involved: Data curation, Writing– review & editing.

and accounted for 5% of the total work needed for the realization of this publication.

PIOTR KUKLIŃSKI

Elektronicznie podpisany przez PIOTR KUKLIŃSKI
Data: 2026.03.23 21:35:49 +01'00'

Sopot, 18/03/2026

Dr. hab. Karol Kuliński

Institute of Oceanology of the Polish Academy of Sciences

Laboratory of marine biogeochemistry

Author contribution statement

I declare that my contribution to the publication:

Aguado Gonzalo, F., Stokowski, M., Koziorowska-Makuch, K., Makuch, P., Beszczyńska-Möller, A., Kukliński, P., & Kuliński, K. (2024). Key processes controlling the variability of the summer marine CO2 system in Fram Strait surface waters. Frontiers in Marine Science, 11, 1464653.

Involved: Conceptualization, Funding acquisition, Project administration, Supervision, Validation, Writing– review & editing

and accounted for 10% of the total work needed for the realization of this publication.

Karol Kuliński

Publication 2

Aguado Gonzalo, F., Koziorowska, K., Szymczycha, B. and Kuliński, K., 2026. The internal consistency between calculated and measured variables of the marine carbonate system in Arctic open and coastal waters, case study: Atlantic Arctic. *Marine Chemistry*, p.104604. doi.org/10.1016/j.marchem.2026.104604.

Marine Chemistry 274 (2026) 104604

Contents lists available at ScienceDirect

Marine Chemistry

journal homepage: www.elsevier.com/locate/marchem

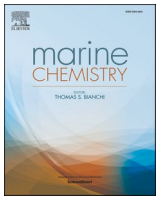

The internal consistency between calculated and measured variables of the marine carbonate system in Arctic open and coastal waters, case study: Atlantic Arctic

Fernando Aguado Gonzalo *, Katarzyna Koziorowska, Beata Szymczycha, Karol Kuliński

Department of Marine Chemistry and Biochemistry, Institute of Oceanology of the Polish Academy of Sciences, Sopot 81-712, Poland

ARTICLE INFO

Keywords:
Arctic region
Marine carbonate system
Inorganic carbon
Marine chemistry

ABSTRACT

The Arctic Ocean plays a crucial role in anthropogenic carbon sequestration, while also being among the regions most susceptible to Ocean Acidification (OA). To understand, quantify, and monitor the rapid biogeochemical changes in the Arctic shelves and coastal waters, it is necessary to accurately determine the complete marine carbonate system. However, the uncertainty range in the calculated values is still unclear, fogging our ability to properly estimate carbon inventory and OA. In this study, we collected samples in the Arctic open and coastal waters to estimate the internal consistency of total alkalinity (TA), pH, partial pressure of CO_2 (pCO_2) and dissolved inorganic carbon (DIC) when only two of them are measured and the other two calculated. In open ocean waters, calculated values generally show good consistency with observations, whereas in coastal areas, it was only possible to accurately calculate two variables: 1) pH using as input parameters pCO_2 together with either TA or DIC, and 2) pCO_2 using DIC and pH. Furthermore, we found that, in this dataset, using the TA estimated from its correlation with salinity together with pCO_2 also allowed obtaining accurate pH values in both coastal and ocean waters. This opens a new possibility of monitoring changes in the carbon cycle by measuring only salinity and pCO_2 in areas where its consistency has been evaluated. Finally, in this study, we provide guidelines for obtaining and reporting good-quality carbonate system data in Arctic coastal areas.

1. Introduction

Due to its low temperature, the Arctic Ocean has a large capacity to absorb atmospheric CO_2 (Bates and Mathis, 2009; Friedlingstein et al., 2022). The constant uptake of anthropogenic CO_2 decreases seawater's pH and lowers the carbonate saturation state, which is the principle of a mechanism called Ocean Acidification (OA). OA is especially important in Arctic continental shelf areas (Cross et al., 2018; Qi et al., 2022; Qi et al., 2017; Robbins et al., 2013; Terhaar et al., 2020), where the increasing freshwater discharge together with the remineralization of terrestrial and in-situ-produced organic matter lowers the concentrations of carbonate ion (CO_3^{2-}) (Capelle et al., 2020; Qi et al., 2022; Semiletov et al., 2016). Even though the Arctic shelves represent only 1% of the global ocean volume, they receive around 11% of the global river discharge (Dai and Trenberth, 2002; Feng et al., 2021) and contribute to as much as 5%–15% of the total carbon uptake (Bates and Mathis, 2009; MacGilchrist et al., 2014; Manizza et al., 2019) representing a disproportionate role in the global coastal ocean carbon budget (Dai et al., 2022). Due to its vast influence on the global carbon cycle, it is crucial to obtain accurate, year-round data on the marine carbonate system variables in order to understand and monitor ongoing changes. Unfortunately, as a result of the harsh Arctic conditions, measurements are scarce and most studies report only some variables, while others have to be calculated using thermodynamic ion-pairing models (Bates et al., 2009; Jones et al., 2021; Qi et al., 2020). This deficit of direct in situ observations makes our ability to accurately calculate different variables of the marine carbonate system crucial to assessing and understanding the key drivers for ocean acidification and carbon sequestration in the Arctic region.

The marine carbonate system consists of four measurable variables: total alkalinity (TA), dissolved inorganic carbon (DIC), partial pressure of carbon dioxide (pCO_2), and pH. Commonly available mass balance models make it possible to calculate two variables when the other two are known (e.g. Lewis et al., 1998), as well as some other variables related to the marine carbonate system such as aragonite and calcite saturation states (Ω_{Ar}, Ω_{Ca}), concentration of carbonate ion (CO_3^{2-}) or

* Corresponding author at: Institute of Oceanology of the Polish Academy of Sciences, Powstańców Warszawy 55, Sopot 81-712, Poland.
E-mail address: aguadof@iopan.pl (F. Aguado Gonzalo).

https://doi.org/10.1016/j.marchem.2026.104604
Received 24 March 2025; Received in revised form 7 January 2026; Accepted 8 January 2026
Available online 9 January 2026

fugacity of CO_2 (fCO_2), which are the backbone for studies on OA and carbon sequestration.

When different variables are calculated using mass balance models, the accuracy of the computed parameters is directly influenced by 1) the accuracy and precision of the measured initial input variables, 2) the estimated uncertainties for the dissociation constants, and 3) the contribution of non-parameterized seawater constituents like, for example, organic alkalinity, NH_3, or HS^- (Kerr et al., 2023; Lee and Millero, 1995; Orr et al., 2018).

Orr et al. (2018) introduced an add-on for CO2SYSto compute the estimated uncertainty for the calculated variables based on the uncertainties of the input variables, providing the community with a tool to report the propagated total uncertainty of the calculated values used in their scientific studies. Furthermore, Carter et al. (2024) used discrete open-ocean carbonate chemistry measurements collected within the Global Ocean Data Analysis Project (GLODAPv2.2022) to calculate the difference between the measured and calculated variables. Their work shows that this difference was 1.7 times greater than the computed estimated uncertainty, which questions our ability to produce calculated data within the initial estimated uncertainties in open-ocean areas.

The structure and interconnections of the marine carbonate system are even more complex in coastal areas, where the non-parameterized components can be an important part of the carbonate system (Cai et al., 2010; Kerr et al., 2021; Kuliński et al., 2014) and thus a considerable source of errors (Patsavas et al., 2015; Sharp and Byrne, 2020). Since the Arctic shelf areas are heavily influenced by inputs of fresh water (e.g., Solomon et al., 2021), terrigenous organic matter (e.g., Capelle et al., 2020), and freshly produced organic matter (e.g., Qi et al., 2022), all of which could be a source of unquantified contributions to the carbonate equilibria, it is expected that the same type of intercomparison as presented by Carter et al. (2024) can produce there even larger errors than in open-ocean areas. However, until today, there have not been reported dedicated assessments of the marine carbonate system consistency in Arctic coastal waters, providing an initial guide on the quality of the calculated essential variables for OA and carbon inventory in these regions.

Furthermore, the relationship between TA and salinity can be considered conservative in oceanic waters (Lee et al., 2006), making it possible to approximate TA from routinely measured salinity. Having TA estimated in this way, the entire marine carbonate system can be described by measuring only one of the remaining three variables: DIC, pH, or pCO_2. The calculations also require an input of other ancillary data, such as temperature (also routinely measured) and concentrations of DSi (dissolved silicate) and PO_3^{4-} (phosphate), the latter two being often neglected due to their low contribution in oceanic waters. In recent years, significant developments have also been made to measure pH and pCO_2 using autonomous underwater sensors (e.g. Branham et al., 2016; Nehir et al., 2022), providing high-resolution spatial and temporal measurements in the entire water column. This approach has been successfully used in open seas and coastal studies (Cullison Gray et al., 2011; Jones et al., 2016), showing that salinity-derived TA can be combined with accurate pH measurements to calculate different variables of the marine carbonate system. Applying a similar, simplified approach to Arctic shelf areas could open new opportunities for monitoring these key regions for carbon sequestration, which are also highly vulnerable to climate change. Before this can be done, however, it is necessary to demonstrate that it is possible to calculate good-quality data when only salinity (and salinity-derived TA), temperature, and pH (or pCO_2) are known and when some ancillary data that would increase the accuracy of calculations are missing (e.g. DSi and PO_4^{3-}).

The insufficient knowledge about the internal consistency of the carbonate system in Arctic coastal waters and thus about the quality of calculated marine carbonate system parameters was the overarching motivation for the present study. The basis for conducting this research was a high-quality dataset including the full set of measurable variables describing the structure of the carbonate system in coastal and open Arctic waters. This allowed us to define three research goals, which were: (i) to understand how accurately TA, DIC, pH, and pCO_2 can be calculated in Arctic waters by comparing calculated values with measured ones; (ii) to assess the quality of marine carbonate system parameters calculated out of salinity-derived TA and measured pH or pCO_2; (iii) to estimate the errors in calculated marine carbonate system variables resulting from omitting DSi and PO_4^{3-} as input parameters.

The findings of this study provide a general guideline on the quality of previously and future reported calculated values of the marine carbonate system within the Arctic region.

2. Materials and methods

2.1. Sampling strategy

In the summer of 2021, within the frame of the annual Arctic expedition on the RV Oceania (AREX21), 110 stations in the Atlantic sector of the Arctic region were sampled to collect a complete set of parameters to characterize the marine carbonate system (see below for further description of the data collected). Samples were obtained from the open ocean waters of the Fram Strait (between 74°N – 81°N and 0° - 20°E) and in the coastal waters of the western Svalbard Archipelago covering the continental shelf and three fjords: Kongsfjorden, Isfjorden, and Hornsund (Fig. 1). The data has been grouped into two sets: (i) 'oceanic samples' covering the Fram Strait waters and the open waters of continental shelf, and (ii) 'coastal samples' representing the Svalbard fjords, all of them within the Arctic region. A detailed representation of the sampling locations is presented in the supplementary material (Fig. S1). At all stations, samples were collected at a depth of 2.5 m, representing the surface data. Additionally, at 18 selected stations in fjords, samples were also taken at different depths in the water column. In total, 28 sets of oceanic samples and 146 sets of coastal samples (80 surface and 66 water column) were collected during the cruise and used for further research.

The set of parameters to characterize the marine carbonate system comprised temperature, salinity, DIC, TA, pH, phosphate (PO_4^{3-}), and dissolved silicate (DSi). All of these variables were measured in both, water column and surface samples. Additionally, pCO_2 was measured in the surface layer (2.5 m water depth). All the water column and surface water samples for pH, DIC, TA, pCO_2, phosphate, and silicate followed the same state-of-the-art sampling and storage procedures as described by Dickson (2007) and Grasshoff et al. (2009). A detailed description of the methods and accuracy/precision of the measurements is provided in Appendix A.

DIC, DSi, and PO_4^{3-} data from the water column in fjords were previously compiled and published by Saghravani et al. (2024). The oceanic data were taken from Aguado Gonzalo et al. (2024). The rest of the water column data and all the surface data from the fjords are unique and original products of this study and can be downloaded from Aguado Gonzalo et al. (2024). Since the database was compiled from different sources, all data used in this study have also been collected and attached to this manuscript as supplementary material (Table S1).

2.2. Calculations of the marine carbonate system parameters and its propagated total uncertainty

The carbonate system parameters (DIC, TA, pCO_2, and pH) were calculated using all possible combinations of input pairs. For instance, in the surface waters, calculated DIC (DIC_{calc}) was obtained using TA&pH, TA&pCO_2, and pCO_2&pH. In the case of the water column data, pCO_2 was not collected; therefore, only one calculation for each variable was done, e.g., DIC_{calc} using TA&pH. This results in 12 calculated variables in each set of surface samples (4 parameters × 3 combinations of input parameters) and 3 in each set of water column samples (3 parameters × 1 combination). For each calculation, DSi and PO_4^{3-} were included as ancillary data.

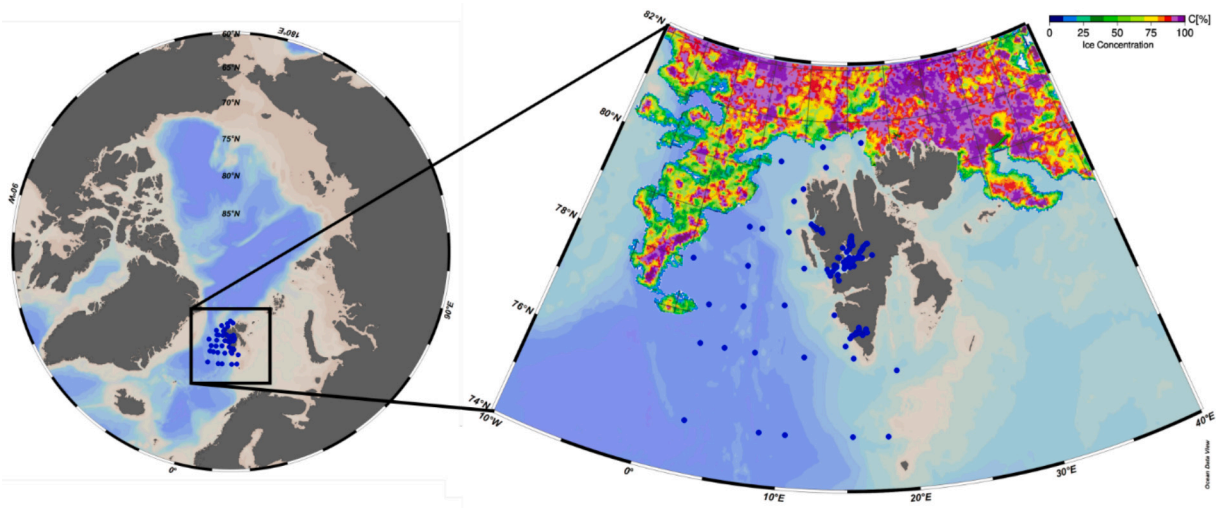

Fig. 1. Map of the sampling locations (blue dots) in the Fram Strait and western fjords of the Svalbard Archipelago. Colored area represents zones covered with sea ice. Sea ice has been calculated from AMSR2 data using the ARTIST sea ice algorithm (ASI 5) (Spreen et al., 2008). A more detailed view of the surface and water column stations is presented in the supplementary material (Fig. S1).

Hereafter, computed values will be noted as X(Y,Z), similar to the notation proposed by Patsavas et al. (2015), where X is the parameter calculated as a function of the input parameters Y and Z. The subscript "no nu", $X(Y,Z)_{no\ nu}$, was added for specific cases where measured DSi and PO_4^{3-} were not used as input ancillary data to test the influence of ignoring nutrient data on the quality of marine carbonate system calculations (see section 2.4.).

Calculations of the marine carbonate system parameters were carried out using the EXCEL version of the CO2sys program (Lewis et al., 1998) updated by Orr et al. (2018) (https://github.com/jamesorr/CO2SYS-Excel). The selection of dissociation constants has been preceded by a thorough literature review. Several authors have evaluated the consistency of the calculations in Arctic waters when using different dissociation constants of carbonic acid (Chen et al., 2015; Chierici and Fransson, 2009; Raimondi et al., 2019; Woosley et al., 2017; Woosley and Moon, 2023; Anderson et al., 1998). They suggested that the set of constants (K_1 and K_2) proposed by both Lueker et al. (2000) and Mehrbach et al. (1973), refitted by Dickson and Millero (1987), produces the lowest bias between calculated and measured values of the carbonate system parameters. Since the set of constants from Lueker et al. (2000) was determined on the total pH scale, similarly to our measurements, it better fits into our study. Moreover, Woosley and Moon (2023) evaluated the sets of constants across a wide range of temperatures and salinities, which includes the ones reported in this study. Based on their findings and previous studies in the other Arctic regions, the set of constants from Lueker et al. (2000) was used together with the $KHSO_4$ from Dickson et al. (1990), the fluoride dissociation constant of Perez and Fraga (1987), and the borate dissociation constants of Lee et al. (2010). An independent evaluation of the influence of the different dissociation constants on the internal consistency of our dataset was not possible because of the biogeochemical complexity of the samples, which covers not only a wide range of salinities and temperatures but also depths, and biogeochemical gradients (e.g. proximity to sea ice and glaciers, mixed influence of river runoff from geologically different catchment areas and thus of mixed chemical composition of seawater, influence of sediments). Unravelling the relationship between the dissociation constants and the complex biogeochemical gradients is beyond the scope of this study. Still, we tested the sensitivity of the calculations based on the choice of the dissociation constants and added a rationale in Appendix C.

The pressure used for all calculations was 1 atm, meaning that the results are not compared at "in situ" conditions but rather at laboratory conditions, reducing the errors associated with re-calculations to in situ pressure. Since pH was measured at 25 °C and pCO_2 at in situ temperature, calculations using the pair of pH and pCO_2 were first normalized to the same temperature. This was done by recalculating pH data to in situ temperature.

The add-on to the CO_2sys provided by Orr et al. (2018) allowed us to estimate the uncertainties of all final calculated results. These uncertainties, defined in our study as "expected uncertainties", are related to the propagation of the initial uncertainties of all the individual components used in the calculations. In this study, we use as initial uncertainties (i) the input parameters measured and (ii) the dissociation and solubility constants applied in the calculations. No more initial uncertainties were taken into account, like for example, the effect of organic-acid alkalinity, the concentration of NH_3 or HS^-, therefore, the term expected uncertainties was used rather than the propagated total uncertainties. The summary of uncertainties of both these groups is compiled in the supplementary material (Table S2). The uncertainties of the measured parameters have been determined in this study and correspond to the precision/accuracy of the measurements (see supplementary material Text S1), while the uncertainties of dissociation and solubility constants are presented after Orr et al. (2018), who collected them from previously published data. Following the procedure from Orr et al. (2018), the expected uncertainties have been determined for every single calculation performed in this study, X(Y,Z). Afterwards, the expected uncertainties were grouped according to the calculated variables (X) and the applied combination of the input parameters (Y,Z) and, finally, averaged for the coastal and oceanic subgroups. For instance, 30 different oceanic data sets were collected and used to calculate 30 different TA(DIC,pH), together with their expected uncertainties. The average of the corresponding 30 expected uncertainties of TA was estimated and denoted as the expected uncertainty for the oceanic TA(DIC,pH).

2.3. Consistency between measured and calculated variables, the real errors

All the marine carbonate system parameters, X(Y,Z), calculated as described in section 2.2., were then compared with the corresponding measured values, X^{meas}. The differences between both measured and calculated values represent the dispersion of the calculated results with respect to the measured ones, ΔX(Y,Z), Eq. (3). Assuming that the measured values are the "true values", the difference represents the real

error derived from the calculations, hereinafter referred to as the "real errors".

$$\Delta X(Y,Z) = X^{meas} - X(Y,Z) \quad (3)$$

To understand the scale of the dispersion of all the ΔX(Y,Z) calculated in each of the two subgroups (oceanic and coastal samples) three statistical approaches were used: a) the average of ΔX(Y,Z) together with its SD ($\bar{x}$ΔX(Y,Z) ± SD), b) the 68 percentile (68%ile) of all the absolute values of ΔX(Y,Z) (68%ileΔ|X(Y,Z)|), and c) the 95 percentile (95%ile) of all the absolute values of ΔX(Y,Z) (95%ileΔ|X(Y,Z)|).

The $\bar{x}$ΔX(Y,Z) is computed as the mean of all the ΔX(Y,Z) determined separately for each subgroup (oceanic or coastal samples), and it only represents their apparent offset from X^{meas}, which could be an indication of a systematic deviation in the dataset or a systematic error. Importantly, the SD is, in this case, a measure of the spread of the data around the mean absolute uncertainty $\bar{x}$ΔX(Y,Z), and it is not a representation of the spread of the data around the measured value X^{meas}. Since the ΔX(Y,Z) values are not normally distributed in our dataset, the dispersion of the data around the real value (ΔX(Y,Z) = 0) was calculated using the 68th and the 95th percentile of the absolute values of ΔX(Y,Z), providing a tool to estimate the uncertainty of the calculated dataset, hereinafter referred to as the "absolute uncertainty". A brief justification for this choice is addressed later on in the discussion section.

The 68%ile and the 95%ile were initially determined using the absolute values of Δ|X(Y,Z)|. Further in the process, the absolute value sign was removed, and the corresponding absolute uncertainty was presented as:

68%ileΔX(Y,Z) = ±68%ileΔ|X(Y,Z)|.

The same procedure was applied to 95%ile, defined as:

95%ileΔX(Y,Z) = ±95%ileΔ|X(Y,Z)|.

2.4. The effect of omitting phosphate and silicate in the calculations

When calculating different variables of the marine carbonate system, DSi and PO_4^{3-} can be added as ancillary parameters to reduce the uncertainty and improve the accuracy of X(Y,Z). In case DSi and PO_4^{3-} are not provided as input data, the CO2sys program assumes that both values are 0, which consequently adds new uncertainties to the calculated values. To estimate the contribution of not including nutrient data to the real errors ΔX(Y,Z), we calculated the absolute difference between each of the computed parameters with and without the input of measured DSi and PO_4^{3-}:

$$\Delta NuX(Y,Z) = |X(Y,Z) - X(Y,Z)_{no\ nu}| \quad (4)$$

Then, similarly to ΔX(Y,Z), the 68%ile was also determined for ΔNuX(Y,Z), and denoted as 68%ileNuX(Y,Z). The contribution of nutrients to the absolute uncertainty was expressed as the 68%NuX(Y,Z)/68%ileΔX(Y,Z), and further in the text its notation is simplified to %ΔNu. Similar to other uncertainty estimations, ΔNuX(Y,Z) and %ΔNu were quantified for all the oceanic and coastal samples. For samples in which DSi and PO_4^{3-} were below the detection limit of the instrument (0.3 μmol L^{-1} and 0.1 μmol L^{-1}, respectively), the concentrations equal to 50% of the detection limit were applied in the calculations due to the mathematical constraints, which is equivalent to 0.15 μmol L^{-1} for DSi and 0.05 μmol L^{-1} of PO_4^{3-}, respectively.

2.5. Using TA as a function of salinity

To estimate the accuracy of the marine carbonate system calculations when salinity-derived TA is used as the input parameter, we first determined the linear regression between all the TA data collected in this study and the corresponding salinities. Afterwards, the absolute differences between the TA measured and the TA estimated from this linear regression were calculated. The 10% of the data with the highest absolute differences was excluded (only during this exercise, but not from the main dataset) to prevent big deviations in the relationship due to exceptionally high/low values. Finally, based on the remaining 90% of the data, a new linear regression equation (The graphical projection is presented in Appendix B as Fig. B1) was determined (Eq. 5) from which the salinity-derived TA (TA_S) was quantified for further numerical tests. TA_S was calculated for all the samples, including the ones not taken into account to estimate TA_S. Furthermore, we used TA_S to compare the absolute uncertainties in calculated pCO_2 and pH when TA_S was used as the input parameter. Quantitatively, the effects of substituting measured TA with TA_S on the quality of calculated pCO_2 and pH were assessed by comparing the 68%ile of $\Delta pCO_2(TA_S,pH)$ with the 68%ile of $\Delta pCO_2(TA, pH)$ and the 68%ile of $\Delta pH(TA_S,pCO_2)$ with the 68%ile of $\Delta pH(TA, pCO_2)$, respectively.

$$TA_S = 43.426^{*}(S) + 782.18; R^2 = 0.9579 \quad (5)$$

2.6. Establishing a threshold for data quality

To understand the quality of marine carbonate system calculations in Arctic waters, we compared the 68%iles of different combinations of ΔX(Y,Z) obtained in our study with thresholds defined by Newton et al. (2014) for weather-quality measurements, i.e. those that allow for resolving the regional and short-term variability of the marine carbonate system. According to Newton et al. (2014), the relative standard uncertainties should be less than 10 μmol kg^{-1} for DIC and TA, 0.020 for pH, and 2.5% for pCO_2. In this study, the mean measured pCO_2 was 294 μatm, therefore, we proposed a limit of 7 μatm (2.5%) for pCO_2 uncertainty, which, together with the above-mentioned thresholds for DIC, TA, and pH, allowed us to segregate the ΔX(Y,Z) between "good quality" data and "bad quality" data.

3. Results and discussion

3.1. Variability of the collected data

The mean, maximum, and minimum values of DIC, TA, PO_4^{3-}, DSi, salinity, temperature, pH, and pCO_2 characterizing oceanic and coastal samples are presented in Table 1.

Due to the interaction between melted sea ice water and Atlantic water at the surface in the Fram Strait (Aguado Gonzalo et al., 2024), the oceanic samples covered a wide range of salinities from a minimum of 31.77 to a maximum of 35.01, with an average of 34.23. Samples collected in fjords had, on average, lower salinities (32.52) due to the overall high influence of continental runoff and glacial melting water, with a maximum salinity of 34.85 and a minimum of 27.97. The water temperature in both datasets had a similar variability, with an average of 4.09 °C and 4.44 °C for the open ocean and coastal areas, respectively.

Please note that for the range of salinities and temperatures presented in this dataset, the assessment of the internal consistency associated with the different dissociation constants was rigorously evaluated by Woosley and Moon (2023). The uncertainty related to the choice of dissociation constants was used in this study to estimate the expected errors (together with the other input parameters, see Table S2).

The concentrations of TA ranged from 1970 μmol kg^{-1} to 2343 μmol kg^{-1}; both the highest and the lowest values were found in fjord waters, while the oceanic samples showed a lower variability, from 2128 μmol kg^{-1} to 2333 μmol kg^{-1}. On average, oceanic samples had a higher TA (2270 μmol kg^{-1}) than the fjord samples (2194 μmol kg^{-1}). A similar distribution was found for DIC samples, where the highest (2283 μmol kg^{-1}) and lowest (1835 μmol kg^{-1}) concentrations were sampled in the fjords. On average, DIC concentration in the fjord samples (2028 μmol kg^{-1}) was lower than in the open ocean (2071 μmol kg^{-1}).

The surface waters in the entire region were undersaturated in CO_2 with respect to the atmospheric levels. The lowest pCO_2, with a value of 202 μatm, was measured in the oceanic area close to the sea ice. The

Table 1
Average, maximum, and minimum of all the parameters measured in this study (28 oceanic samples and 146 coastal samples). pH data is reported at 25 °C on the total scale. Values of PO_4^{3-} and DSi marked with a star mean half of the detection limits.

		DIC [μmol kg^{-1}]	TA [μmol kg^{-1}]	PO_4^{3-} [μmol L^{-1}]	DSi [μmol L^{-1}]	Salinity	T [°C]	pH	pCO_2 [μatm]
Ocean	Average	2071	2270	0.60	1.70	34.23	4.09	7.853	280
	Max	2135	2333	8.00	4.12	35.01	6.81	7.925	352
	Min	1923	2128	0.05*	0.15*	31.77	−0.74	7.749	202
Coastal	Average	2028	2194	0.16	1.47	32.52	4.44	7.812	299
	Max	2283	2343	1.03	7.94	34.85	7.74	7.878	333
	Min	1835	1970	0.05*	0.15*	27.97	−1.69	7.478	245

highest values (352 μatm) were also observed in the open ocean, but in the waters of Atlantic origin located in the southern part of the study area.

The pH in all the samples was measured at 25 °C; therefore, the discussed pH variability does not reflect the in situ conditions. On average, the pH in the fjords was lower (7.812) than in the oceanic part (7.853), which reflects, on average, lower TA and higher pCO_2 measured in the fjords (Table 1). The larger spread of the pH data, as reflected by minimum and maximum values, was observed in the fjords (from 7.478 to 7.878) than in the open ocean (from 7.749 to 7.925).

The distribution of the concentrations of the two nutrient species included in our dataset (PO_4^{3-} and DSi) shows patterns opposite to each other. While the maximum of DSi (7.94 μmol L^{-1}) was measured in fjord waters, the maximum of PO_4^{3-} (8.00 μmol L^{-1}) was in the oceanic samples (Table 1). The average concentration of DSi was very similar in the fjords and the ocean, with 1.47 and 1.70 μmol L^{-1}, respectively. On the other hand, the average concentration of PO_4^{3-} in the ocean (0.60 μmol L^{-1}) was about 4 times higher than in the fjords (0.16 μmol L^{-1}). Approximately 40% of all the PO_4^{3-} samples and 5% of the DSi samples had concentrations below the instrument's detection limit.

3.2. Statistical analysis to present the absolute uncertainty

The datasets containing results of at least 3 measurable parameters of the marine carbonate system (TA, DIC, pCO_2, and pH) give a unique opportunity to investigate the consistency between the variables and determine the absolute uncertainty (or real errors). This is done by quantification of the differences between measured and calculated parameters, ΔX(Y,Z). The dispersion of the obtained ΔX(Y,Z) in the dataset is the most commonly presented with an average, $\bar{x}$ΔX(Y,Z), and its SD (e.g., Chen et al., 2015; Patsavas et al., 2015; Raimondi et al., 2019). However, as reported by Carter et al. (2024), the $\bar{x}$ΔX(Y,Z) only represents a bias of the data with respect to ΔX(Y,Z) = 0, and its SD shows the spread of the data around $\bar{x}$ΔX(Y,Z), which makes difficult to compare the SD of different studies unless the $\bar{x}$ΔX(Y,Z) bias is corrected in all of them.

In this study, in addition to the commonly used approach referring to the arithmetic average, we also estimated the absolute uncertainty as the spread of the data around the value of 0 error, or ΔX(Y,Z) = 0. For this, we determined the 95% and 68% confidence intervals (95%ile and 68% ile, respectively) around the true value (ΔX(Y,Z) = 0), which correspond approximately to two standard deviations and one standard deviation, respectively, describing the spread of the results around the median value in the dataset. Although ΔX(Y,Z) = 0 is usually not a median in our datasets, applying 95%ile and 68%ile allowed us to estimate the absolute uncertainties (or real errors) of the calculations as a spread around the true/measured results, which may be useful information for those who conduct CO_2 system studies in Arctic waters. Another approach to calculating SD around ΔX(Y,Z) = 0 would be to correct the dataset first for the bias represented by $\bar{x}$ΔX(Y,Z). However, most of the studies about the carbonate chemistry in Arctic waters are based on measurements of two variables only and the calculation of the other two (e.g. Capelle et al., 2020; Cross et al., 2018; Qi et al., 2020). Thus, it is impossible to correct the $\bar{x}$ΔX(Y,Z) bias, as this requires at least three measured variables. Since this study aimed to present the real errors without any correction for bias (systematic uncertainty) to understand our overall ability to estimate the marine carbonate system structure when only two variables are measured/known (as in most of the studies in Arctic waters), we decided to use the 68%ileΔX(Y,Z) as the main tool further in the discussion to understand the absolute uncertainty associated to our results.

3.3. Calculated TA and DIC data quality in oceanic and fjord waters

The expected uncertainties and the absolute uncertainties for each TA(Y,Z) and DIC(Y,Z) are graphically presented in Figs. 2 and 3, while their averages are collected in Table 2. Please note that the expected uncertainties are solely related to the propagation of errors of the input parameters through the calculations (uncertainties related to the selection of dissociation and solubility constants and measured variables).

The results of both expected uncertainty and absolute uncertainty clearly show that the accuracy of the calculated DIC and TA highly depends on the combinations of the input variables (Table 2). Calculations of DIC and TA that use pH and pCO_2 together provide the worst results, with an absolute uncertainty, as expressed with 68%iles of ΔTA and ΔDIC, between 2.5 and 6 times larger than the weather-quality limit of 10 μmol kg^{-1}. The poor agreement between measured TA and DIC and calculated as TA(pH,pCO_2) and DIC(pH,pCO_2) is a well-known principle, already documented in copious studies (e.g. Carter et al., 2024; Millero, 2007; Orr et al., 2018). Our results support previous findings and clearly show that TA and DIC can not be calculated within the weather-quality goal out of pCO_2 and pH, neither in oceanic nor coastal samples. Due to the low quality, the results of TA(pH,pCO_2) and DIC(pH, pCO_2) will not be further discussed in the text.

Other combinations to calculate TA and DIC require whichever pH or pCO_2 and DIC (to calculate TA) or TA (to calculate DIC). For all of them, the 68%ile of ΔTA and ΔDIC range between ±5 and ± 8 μmol kg^{-1} for open ocean waters, which is below the weather-quality threshold (Table 2, Fig. 2 and 3) and comparable to previously published values for high latitudes. Woosley et al. (2017) reported the SD for the $\bar{x}$ΔTA ranging from ±4.8 to ±5.8 μmol kg^{-1} and between ±4.8 and ± 5.2 μmol kg^{-1} for $\bar{x}$DIC in the Arctic Ocean. Similar results were found by Raimondi et al. (2019) in the Labrador Sea, who computed an SD between ±4.2 and ± 7.9 μmol kg^{-1} for $\bar{x}$ΔTA and between ±4.8 and ± 8.2 μmol kg^{-1} for $\bar{x}$DIC. In all these studies (including our), the weather-quality threshold was achieved.

Importantly, the absolute uncertainty of all calculated TA and DIC in the oceanic samples was between 1.6 and 2 times higher than the expected uncertainty (see Table 3 and Figs. 2 and 3). This suggests that other components influencing the structure of marine carbonate chemistry, which are not accounted for in the uncertainty propagation in the thermodynamic model, may have been present in the seawater at the time of sampling. Looking at the oceanic data in our study (Table 2, Fig. 2) a little bit more in detail, it is possible to identify a positive bias in ΔTA, which is expressed with the average values of $\bar{x}$ΔTA(DIC,pH) = 4 μmol kg^{-1} and $\bar{x}$ΔTA(DIC,pCO_2) = 3 μmol kg^{-1}. This is the effect of an

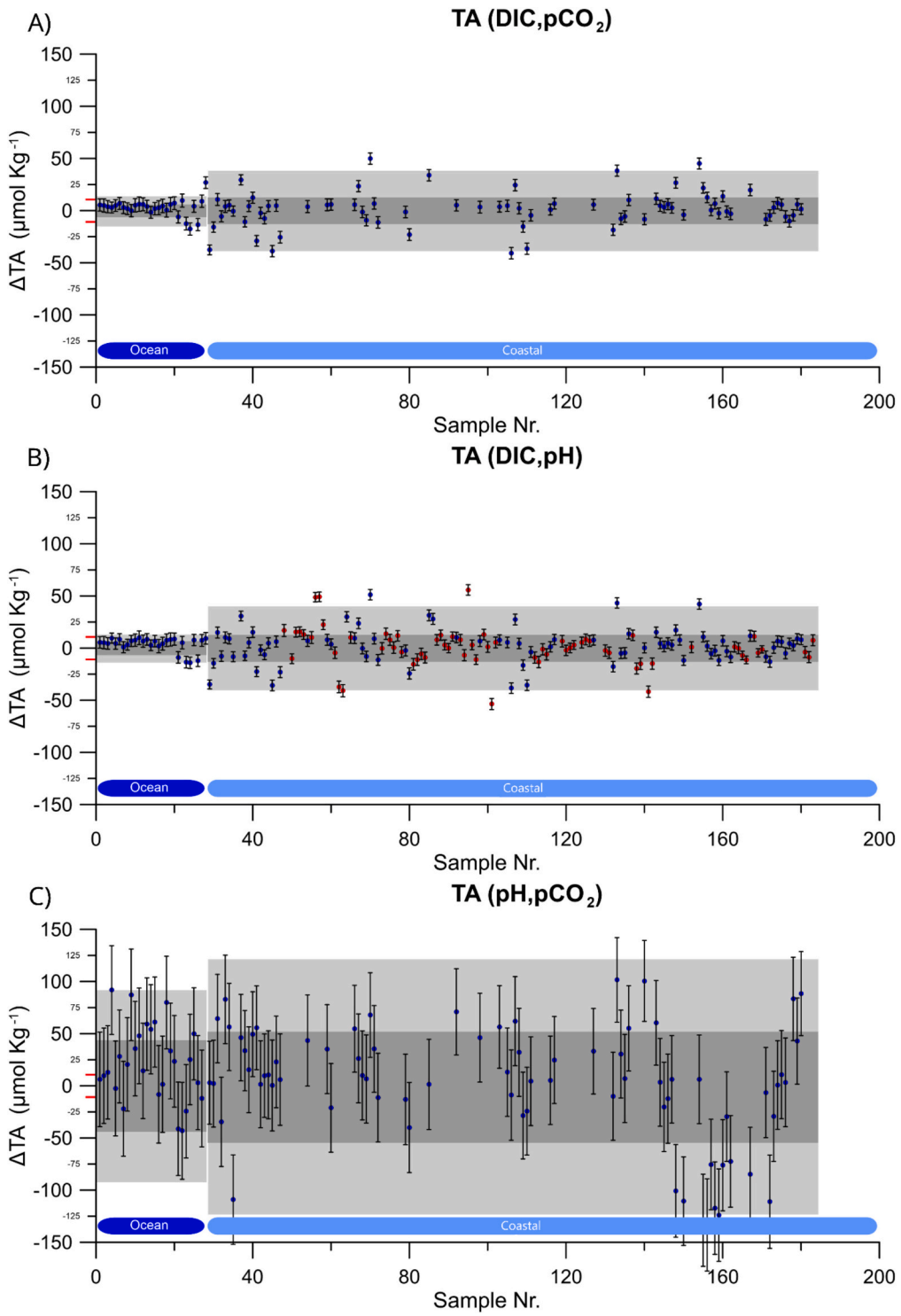

Fig. 2. Graphic representation of the ΔTA for all the samples collected in this study. The blue dots represent samples collected in the surface waters, and the red dots in the water column. The error bars indicate the range of the expected uncertainty. The weather quality threshold is graphically marked as two red lines on the Y axis; results with larger ΔTA could be considered as of bad quality, while those with smaller ΔTA as of good quality. The dark grey area covers 68% of the results with the ΔTA closer to the true value (ΔTA = 0). When the dark grey area does not extend beyond the red lines, the calculations are within the weather-quality threshold. The light grey area covers 95% of the results closer to ΔTA = 0 and represents the maximum variability of the dataset.

overall predominance of positive ΔTA results in this dataset, which includes only four results of negative ΔTA lower than −5 µmol kg^{-1} The positive ΔTA as generated by higher TA measured than TA calculated (Eq. 3) is often interpreted as an excessive TA caused by organic substances (e.g. Kuliński et al., 2014). Fram Strait waters are characterized by high productivity during summer (Cherkasheva et al., 2014). Therefore, a small amount of excess alkalinity is expected there due to the influence of non-parameterized organic alkalinity freshly produced by the phytoplankton (Ko et al., 2016). As presented before, to calculate ΔTA, it is necessary to use DIC as an input parameter and vice versa. Thus, non-parameterized organic alkalinity that generates a positive ΔTA bias should also be reflected as a negative bias in ΔDIC (excess of

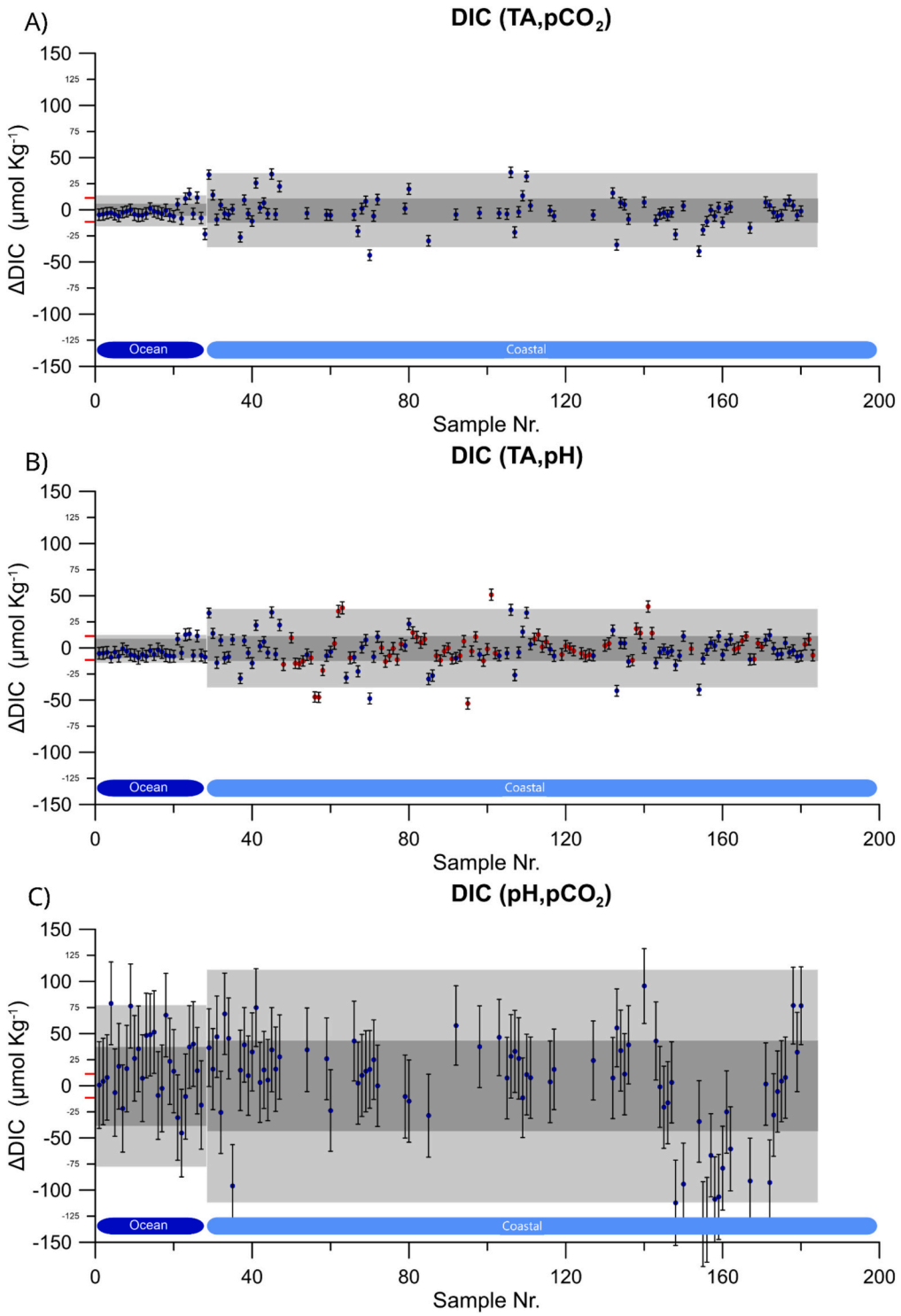

Fig. 3. Graphic representation of the ΔDIC for all the samples collected in this study. The blue dots represent samples collected in the surface waters, and the red dots in the water column. The error bars indicate the range of the expected uncertainty. The weather quality threshold is graphically marked as two red lines on the Y axis; results with larger ΔDIC could be considered as of bad quality, while those with smaller ΔDIC as of good quality. The dark grey area covers 68% of the results with the ΔDIC closer to the true value (ΔDIC = 0). When the dark grey area does not extend beyond the red lines, the calculations are within the weather-quality threshold. The light grey area covers 95% of the results closer to ΔDIC = 0 and represents the maximum variability of the dataset.

calculated DIC). This is because the excess TA is not included in the thermodynamic model as organic alkalinity, but instead, it is interpreted in the model as carbonate alkalinity, producing artificially high calculated DIC. This situation was observed in our data, where the $\bar{x}$ΔDIC (TA,pH) is equal to −3 µmol kg^{-1}. On the other hand, the negative ΔTA values in the oceanic waters were found close to the sea ice. Although there is no clear explanation for this phenomenon, it may be related to the presence of ikaites (a form of carbonates) in seawater, which have been documented to cause inconsistencies in non-filtered samples (Chen et al., 2015).

For coastal waters, the quality of the calculated TA and DIC was lower compared to the open ocean, and the associated absolute

Table 2
Averages of the expected uncertainties for all the ΔX(Y,Z) calculated in this study and the absolute uncertainty expressed with $\bar{x}$ΔX(SD), 68%ile and 95%ile for the oceanic and coastal samples.

Variable	Expected uncertainty	$\bar{x}$ΔX(SD) Ocean	$\bar{x}$ΔX(SD) Coastal	68%ileΔX(Y,Z) Ocean	68%ileΔX(Y,Z) Coastal	95%ileΔX(Y,Z) Ocean	95%ileΔX(Y,Z) Coastal
ΔTA(DIC,pCO_2)	±3	3 ± 8	1 ± 17	±6	±11	± 16	± 38
ΔTA(DIC,pH)	±5	4 ± 7	2 ± 17	±8	±12	± 13	± 42
ΔTA(pH,pCO_2)	±26	14 ± 54	4 ± 59	±45	±56	± 90	± 119
ΔDIC(TA,pCO_2)	±3	−2 ± 7	−1 ± 15	±5	±10	± 14	± 34
ΔDIC(TA,pH)	±5	−3 ± 6	−2 ± 16	±8	±11	± 12	± 39
ΔDIC(pH, pCO_2)	±25	10 ± 50	2 ± 53	±38	±42	± 78	± 110
ΔpH(TA,DIC)	±0.010	−0.007 ± 0.014	−0.003 ± 0.039	±0.017	±0.027	± 0.027	± 0.093
ΔpH(TA,pCO2)	±0.004	−0.002 ± 0.009	−0.001 ± 0.010	±0.007	±0.010	± 0.015	± 0.02
ΔpH(DIC,pCO_2)	±0.005	−0.002 ± 0.010	−0.001 ± 0.010	±0.007	±0.009	± 0.015	± 0.021
ΔpCO_2(TA,DIC)	±11	3 ± 10	0 ± 31	±9	±19	± 23	± 71
ΔpCO_2(TA,pH)	±11	−2 ± 6	−1 ± 9	±5	±9	± 14	± 18
ΔpCO_2(DIC,pH)	±11	−2 ± 6	0 ± 8	±5	±6	± 13	± 17

Table 3
Increase of the real error, with 68% confidence intervals (68%ile ΔNu), when the values of PO_4^{3-} and DSi are not used as input data in the calculations, in oceanic and coastal samples. The %ΔNu indicates the increment of the absolute uncertainty in %.

Variable	68%ile ΔNuX(Y,Z) Oceanic	68%ile ΔNuX(Y,Z) Coastal	%ΔNu Oceanic	%ΔNu Coastal
TA(DIC,pCO_2)	±0.39	±0.03	6.5%	0.3%
TA(DIC,pH)	±0.41	±0.22	5.1%	1.8%
TA(pH,pCO_2)	±0.39	±0.03	0.9%	0.1%
DIC(TA,pCO_2)	±0.34	±0.03	6.8%	0.3%
DIC(TA,pH)	±0.39	±0.21	4.9%	1.9%
DIC(pH, pCO_2)	±0.00	±0.00	0.0%	0.0%
pH(TA,DIC)	±0.001	±0.000	5.9%	0.0%
pH(TA,pCO2)	±0.000	±0.000	0.0%	0.0%
pH(DIC,pCO_2)	±0.000	±0.000	0.0%	0.0%
pCO_2(TA,DIC)	±0.65	±0.34	7.2%	1.8%
pCO_2(TA,pH)	±0.09	±0.04	1.8%	0.4%
pCO_2(DIC,pH)	±0.03	±0.02	0.6%	0.3%

uncertainties were between 1.7 and 3.7 times higher than the expected uncertainties. In this case, the 68%ileΔTA and the 68%ileΔDIC were equal or slightly worse (from ±10 μmol kg^{-1} to ±12 μmol kg^{-1}) than the weather-quality goal (±10 μmol kg^{-1}) (Table 2). Importantly, the results of this study are, until today, the only ones describing the real errors of the marine carbonate system calculations for Arctic coastal areas. Although this fact makes it impossible to directly compare our findings with other similar studies from high latitudes, the obtained results contribute to the global efforts aiming at quantifying the quality of the calculated marine carbonate system variables in coastal regions. Our absolute uncertainties for TA and DIC are slightly higher than those by Patsavas et al. (2015), who reported SD for $\bar{x}$ΔTA from two U.S. coastal cruises with values between ±4.2 and ± 7.4 μmol kg^{-1}. However, their TA range, with minimum values of 2100 μmol kg^{-1}, was rather more similar to our oceanic TA variability (min. TA of 2128 μmol kg^{-1}) than to conditions we observed in coastal waters (min. TA of 1970 μmol kg^{-1}). On the other hand, Salt et al. (2016) reported higher values of SD for $\bar{x}$ΔTA and $\bar{x}$ΔDIC (between ±7 and ± 29 μmol Kg^{-1}) for the North Sea, claiming that they are due to the influence of organic compounds.

To attribute the absolute uncertainty in the calculated TA and DIC that we found in the coastal samples to organic alkalinity, it would be expected a correspondingly high positive bias in the ΔTA. This was, however, not the case. Instead, there was a strong variability around the 0 value, without any recognizable positive $\bar{x}$ΔTA, and also with no clear differences between the surface water layer and water column. Still, it was possible to find some high positive values of ΔTA >30 μmol kg^{-1} close to river mouths and strong negative ΔDIC near glacial fronts (only in some cases and near the bottom waters). However, a detailed interpretation of each positive and negative ΔTA or ΔDIC was not the main objective of our study, which aimed to investigate for the first time the overall consistency of the marine carbonate system in Arctic coastal waters. Nevertheless, with our results, we would like to transmit the conclusion that calculating TA or DIC in coastal Arctic waters produces data of lower quality. Thus, the computed DIC and TA for high-latitude coastal regions should be interpreted with caution and preferably also supported by in situ measurements.

3.4. pH calculated vs measured in oceanic and fjord waters

The expected uncertainties and the absolute uncertainties for each pH(Y,Z) are graphically presented in Fig. 4, while their averages are collected in Table 2.

The absolute uncertainty (or real errors) for calculated pH was larger than the estimated one for both oceanic (1.7 times larger) and coastal (between 2.7 and 3.8 times larger) Arctic waters. The magnitude of the discrepancy we identified for the open ocean is comparable to findings by Carter et al. (2024), who assessed the consistency of the carbonate system using oceanic data from the Global Ocean Data Analysis Project (GLODAP) and reported between 1.5 and 1.8 times larger absolute uncertainty (denoted as combined standard uncertainty) than the expected one. Interestingly, the 68%ile of ΔpH reported in this study for oceanic waters is exactly the same as the SD of the $\bar{x}$ΔpH reported by Woosley et al. (2017), which solidifies our knowledge about the observed consistency of the marine carbonate system in the region.

The quality of the calculated pH clearly depends on the pair of variables used to calculate it (Table 2). In this study, all the absolute uncertainty (68%ilesΔpH) determined for oceanic samples were below the weather-quality threshold of ±0.020. The worst quality of the pH results was calculated out of TA and DIC, for coastal waters, where the absolute uncertainty was larger (±0.027) than the weather-quality limit. Similar observations were made by Raimondi et al. (2019), who calculated the SD of the $\bar{x}$ΔpH data collected during several cruises in the North Sea, and in some of them, the SD of $\bar{x}$ΔpH(TA,DIC) was ±0.021. This confirms that calculations of pH using TA and DIC as input variables should be avoided in coastal waters, including Arctic regions. On the other hand, when pH in fjords was calculated using pCO_2 and either TA or DIC, their quality was high and only slightly worse than for the open ocean (Table 2). All these findings entail that pCO_2 has to be measured to obtain an accurately calculated pH. In this study, we only evaluated ΔpH(TA,pCO_2) and ΔpH(DIC,pCO_2) in surface waters due to the pCO_2 sampling limitations. However, it would be interesting to check in future studies the quality of pH calculations also in the water column, exploiting data generated by pCO_2 profilers.

3.5. pCO2 calculated vs measured in oceanic and coastal waters

The expected uncertainties and the absolute uncertainties for each pCO_2(Y,Z) are graphically presented in Fig. 5, while their averages are

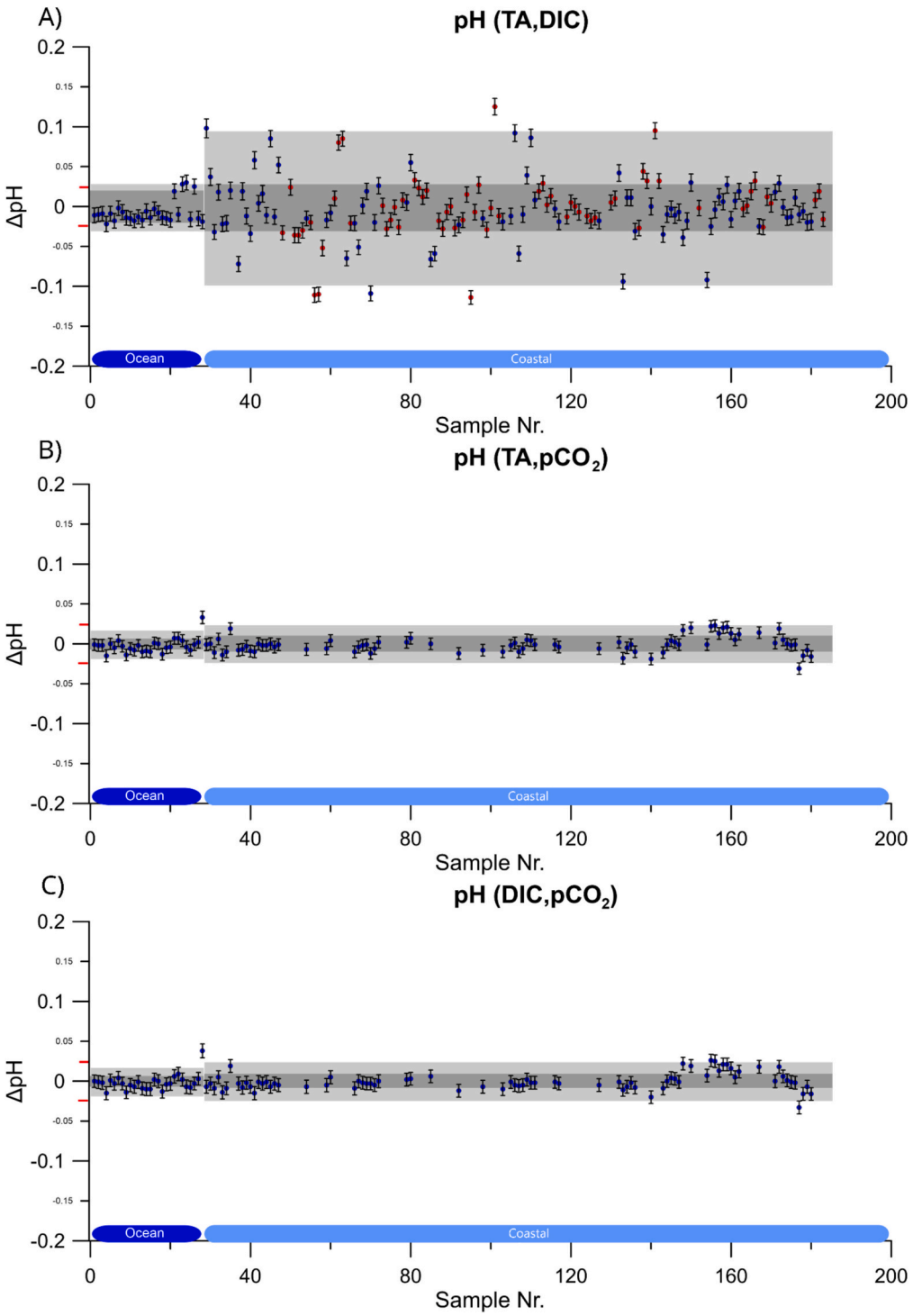

Fig. 4. Graphic representation of the ΔpH for all the samples collected in this study. The blue dots represent samples collected in the surface waters, and the red dots in the water column. The error bars indicate the range of the expected uncertainty. The weather quality threshold is graphically marked as two red lines on the Y axis; results with larger ΔpH could be considered as of bad quality, while those with smaller ΔpH as of good quality. The dark grey area covers 68% of the results with the ΔpH closer to the true value (ΔpH = 0). When the dark grey area does not extend beyond the red lines, the calculations are within the weather-quality threshold. The light grey covers 95% of the results closer to ΔpH = 0 and represents the maximum variability of the dataset.

collected in Table 2.

In contrast to all other variables, the expected uncertainty for all the pCO_2 results calculated with different pairs was the same (±11 μatm), and it was larger than any of the absolute uncertainties (68%ile of ΔpCO_2) determined for oceanic waters. While generally pCO_2(TA,DIC) is expected to produce larger expected uncertainties than pCO_2 (TA,pH) or pCO_2(DIC,pH) (e.g., Carter et al., 2024), the recalculation of pH to situ temperature from the measured value at 25 °C entails extra uncertainties. The CO_2sys used for the calculations (Orr et al., 2018) estimates an extra 0.01 uncertainty for this step. Indeed, larger uncertainties are expected due to the temperature-related conversion. However, the 68%iles of ΔpCO_2(TA,pH) and ΔpCO2(DIC,pH) obtained in this study demonstrate that it is possible to calculate high-quality pCO_2 even if the whole procedure requires an additional step in

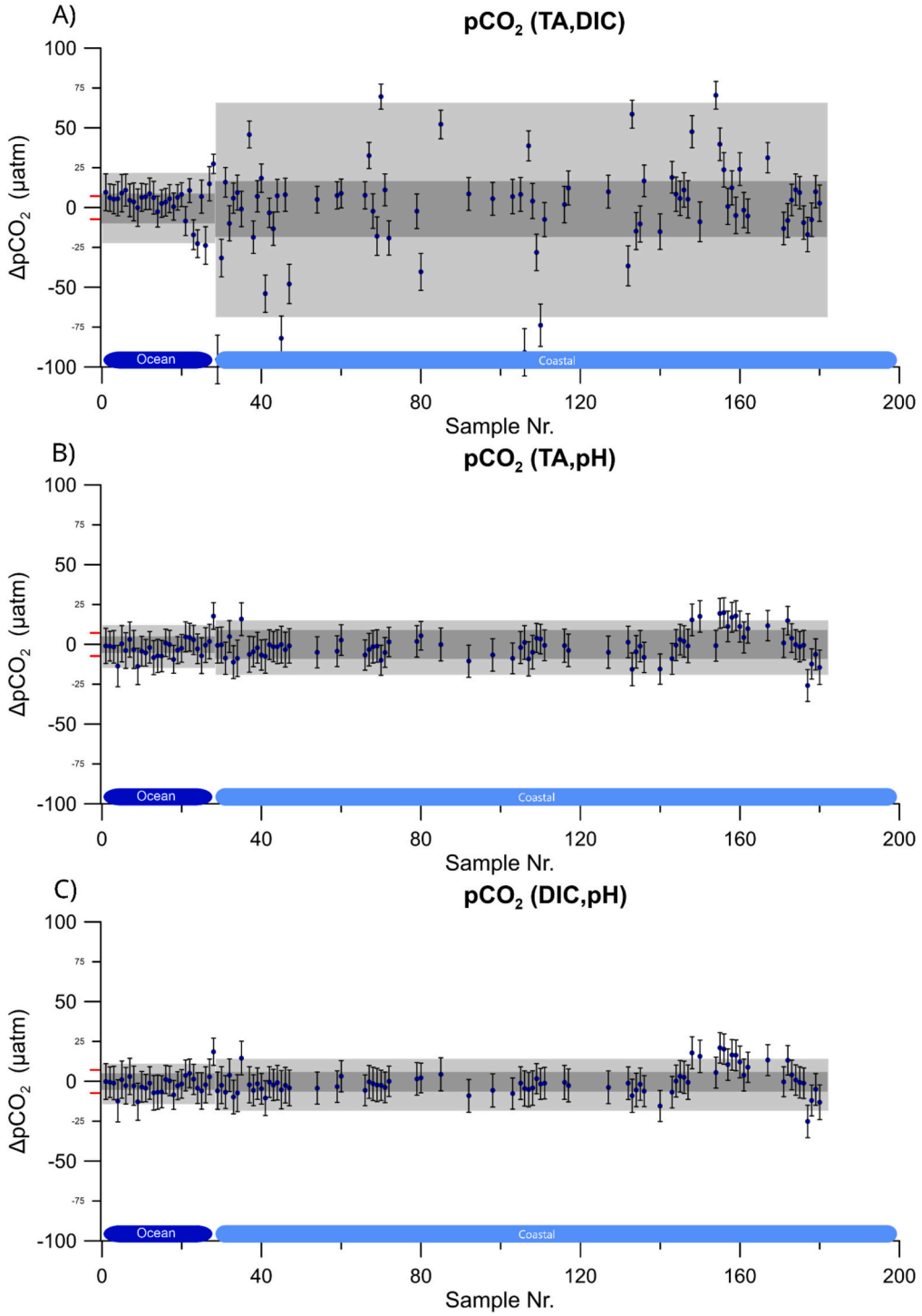

Fig. 5. Graphic representation of the ΔpCO_2 for all the samples collected in this study. The blue dots represent samples collected in the surface waters, and the red dots in the water column. The error bars indicate the range of the expected uncertainty. The weather quality threshold is graphically marked as two red lines in the Y axis; results with larger ΔpCO_2 could be considered as of bad quality, while those with smaller ΔpCO_2 as of good quality. The dark grey area covers 68% of the results with the ΔpCO_2 closer to the true value ($\Delta pCO_2 = 0$). When the dark grey area does not extend beyond the red lines, the calculations are within the weather-quality threshold. The light grey covers 95% of the results closer to $\Delta pCO_2 = 0$ and represents the maximum variability of the dataset.

computation. In fact, the real errors of pCO_2 calculated with the use of pH measured at 25 °C as an input parameter were low and within the weather-quality threshold (2.5% of the measured pCO_2, equivalent to ±7 µatm in our study) for oceanic samples and only slightly higher for coastal waters, but still for ΔpCO2(DIC,pH) the 68%ile was lower than ±7 µatm (Table 2).

Previously published studies evaluating the quality of calculated pCO_2 in oceanic waters are not always conclusive (reference in the next lines). While all of them reported smaller absolute uncertainties for ΔpCO_2(TA,pH) and ΔpCO2(DIC,pH) than the weather quality threshold, there is no clear agreement for ΔpCO_2(TA,DIC). Some studies indicated smaller real errors than the 2.5% threshold (Chen et al., 2015; Patsavas et al., 2015), while others have shown larger ones (Carter et al., 2024; Raimondi et al., 2019; Woosley et al., 2017). The findings of the latter

group are also supported by our observations (Table 2), which suggest an overall low quality of pCO_2(TA,DIC) and a necessity to supplement such calculations with pCO_2 measurements, especially in Arctic coastal waters.

3.6. The influence of nutrients in the calculations

The nutrient concentrations (PO_4^{3-} and DSi) are a part of the marine carbonate system as a component of TA (Wolf-Gladrow et al., 2007). Therefore, it is expected that calculations of the marine carbonate variables without including nutrients may have lower quality. Our results (Table 3) from coastal samples show that omitting nutrients increases only slightly the absolute uncertainty (from 1.9% to 0.0%). The effect is even smaller (max. 0.6% increase) if we take into account only these calculations, which give the results of quality better than the weather threshold, namely pH(TA,pCO_2), pH(DIC,pCO_2), pCO_2(TA,pH), and pCO_2(DIC,pH). This contribution can be considered negligible. Still, the results we present refer to the time of sampling in the middle of the polar day when the nutrient concentrations were low in fjords, and their contribution to the total absolute uncertainty may change in different seasons depending on the concentration of PO_4^{3-} and DSi in coastal waters.

On the other hand, a substantial contribution to the errors resulting from omitting PO_4^{3-} and DSi (an increase up to 7.2% of the real errors) was found for oceanic samples, especially in cases when TA was either calculated or used as an input variable (Table 3). To some extent, the higher percentage contributions (compared to coastal samples) are an effect of higher nutrient concentration in samples with lower absolute uncertainties. Thus, the contribution of nutrients to the absolute uncertainty becomes more prominent (Table 3). Looking at the oceanic dataset a bit more in detail, it is possible to observe that a particularly high contribution of nutrients to the absolute uncertainty was measured in samples collected close to the sea ice. The Fram Strait area is known for productive waters supplied with nutrients also from sea ice melting (e.g. Mayot et al., 2020). It is well known that there is a natural accumulation of PO_4^{3-} and DSi associated with the precipitation of ikaites during sea ice formation and their subsequent release into the surrounding waters during the melting season (Hu and Wang, 2020; Nedashkovskii et al., 2008), thus, the exceptionally high errors were a consequence of this process. Overall, the errors generated by not including nutrients in marine carbonate system calculations are not critically high in our dataset. Still, taking them into account may considerably improve the quality of the calculations in which TA is either calculated or used as an input variable, especially in areas influenced by sea ice melt waters.

3.7. Estimating TA from salinity and its consequences on the quality of calculations

Total alkalinity derived from the salinity, TA_S was used as the input parameter in the calculations of ΔpH(TA_S,pCO_2) and ΔpCO_2(TA_S,pH). The 68%ile of ΔpH(TA_S,pCO_2) was ±0.007 for oceanic samples and ± 0.012 for coastal samples. The corresponding values of the 68%ile for calculations with measured TA, ΔpH(TA,pCO_2), were ± 0.007 and ± 0.010, respectively (Table 2). This shows that the absolute uncertainty was exactly the same in oceanic waters, and only ±0.002 larger in coastal waters when TA_S was used in calculations instead of TA. In the case of ΔpCO_2(TA_S,pH) the 68%ile amounted to ±6 µatm for oceanic samples and ± 10 µatm for coastal samples, which for both was only ±1 µatm more than the 68%iles obtained from calculations using measured TA, ΔpCO_2(TA,pH) (Table 2).

When estimating pH(TA_S,pCO_2) or pCO_2(TA_S,pH), most of the errors in calculated pH (or in calculated pCO_2) are related to our ability to accurately measure pCO_2 (or pH). This is related to the strong correlation between [CO_2*] and [H^+] (Millero, 2007; Orr et al., 2018) and the low sensitivity of the calculations to changes in TA (Orr et al., 2018). Our results (Table 4) showed that, in both oceanic and coastal waters, the real errors of pCO_2 calculated from TA_S and pH are only 1µatm larger than those using measured TA, and it does not change the fact that pCO_2 determined from this pair can be obtained with weather quality only in oceanic waters. In the case of pH, our results revealed that using pCO_2 and TA_S instead of measured TA produced the same absolute uncertainty for oceanic samples and only ±0.002 larger for coastal waters. Nevertheless, for both regions, the absolute uncertainty of pH calculated with the use of TA_S (±0.007 and ± 0.010) was lower than the weather-quality threshold. This demonstrates that the correlation between TA and salinity is not the key factor to calculate pH and pCO_2, opening new opportunities for coastal monitoring in areas where the relationship between TA and salinity may not be perfectly linear (Koziorowska-Makuch et al., 2023) due to the wide range of freshwater TA end members. On the other hand, similar studies in different coastal areas show generally good consistency between calculated and measured pH and pCO_2 when TA approximated from salinity is used as an input parameter (Cullison Gray et al., 2011; Jones et al., 2016), even when a generalized (and not locally specific) TA to salinity ratio is used – an effect of overall low sensitivity of calculations to the TA variability. The TA_S function determined in our study covered the salinity range from 28 to 31 (Fig. S2). Thus, the accuracy of TA_S may decrease at lower salinities and generate more significant errors in the marine carbonate system calculations. However, for calculating pH and/or pCO_2, large errors are not expected since most of the uncertainty is related to the variability of the pCO_2/pH measurements.

All these findings bring new opportunities for monitoring the carbonate chemistry and ocean acidification in coastal environments. However, it is still necessary to confirm if the same accuracy in

Table 4
Synthesis of the quality assessment made for different combinations of calculated variables from the oceanic and coastal Arctic waters. The green colour indicates that the calculated data has an absolute uncertainty below 10 µmol kg^{-1} for DIC and TA, 0.020 for pH, and 7 µatm for pCO_2 (weather-goal quality data). The red colour shows combinations of variables which produce bad-quality data (individual values within the cells).

Variable	Oceanic	Coastal
TA(DIC,pCO_2)	±6	±11
TA(DIC,pH)	±8	±12
TA(pH,pCO_2)	±45	±56
DIC(TA,pCO_2)	±5	±10
DIC(TA,pH)	±8	±11
DIC(pH, pCO_2)	±38	±42
pH(TA,DIC)	±0.017	±0.027
pH(TA,pCO_2)	±0.007	±0.010
pH(DIC,pCO_2)	±0.007	±0.009
pCO_2(TA,DIC)	±9	±19
pCO_2(TA,pH)	±5	±9
pCO_2(DIC,pH)	±5	±6
pH(TA_S,pCO_2)	±0.007	±0.012
pCO_2(TA_S,pH)	±6	±10

calculations can be achieved in the water column. In that case, monitoring the water column pH within the weather goal in Arctic coastal environments could be possible in areas where its consistency has been evaluated by using local and/or regional TA_S and continuous underwater measurements of pCO_2. In this case, the uncertainties in calculated pH will be directly affected by the quality of the sensor-based pCO_2 measurements.

4. Synthesis and conclusions

Most of the studies about the consistency of the marine carbonate system present the real errors of the calculated values as the averages, $\bar{x}\Delta X(Y,Z)$, together with their SD. Although it is a fairly extended method, SD shows the dispersion of the differences between measured and calculated data around the average and not the absolute value ($\Delta X(Y,Z) = 0$). Thus, in addition to $\bar{x}\Delta X(Y,Z)$ and SD, we proposed to use the 68% confidence interval (presented as the 68%ile) to quantify the absolute uncertainty and the spread of the $\Delta X(Y,Z)$ results around $\Delta X(Y,Z) = 0$. The assessment of the results obtained in this study for both oceanic and coastal waters of the European Arctic allowed us to draw the following conclusions, which can be considered as a reference for future ocean acidification and marine carbonate system studies in this key region:

1) The determined absolute uncertainty for almost all combinations of $\Delta X(Y,Z)$ was slightly larger than the initially estimated uncertainties expected from the propagation of the individual uncertainties related to both the accuracy of the measurements and the uncertainties of the solubility and dissociation constants (except for pCO_2). This may be an effect of the presence of non-parameterized substances in seawater (e.g. organic alkalinity) and/or ion anomalies in the region influenced by both sea ice/glacier meltwater (oceanic and coastal samples) and freshwater inputs (coastal samples).
2) The direct comparison between the absolute uncertainty and the weather-quality thresholds (10 μmol kg^{-1} for DIC and TA, 0.020 for pH, and 7 μatm for pCO_2), summarized in Table 4, suggests generally high-quality calculated values for samples collected in Arctic oceanic waters.
3) Due to overall relatively high errors, calculations of the marine carbonate system in the Arctic coastal waters should be applied with great caution and awareness of the potential uncertainties behind them (as documented in this study), and should preferably be supported by direct observations of relevant parameters. The calculations that guarantee good quality of the final results are only those of pH exploiting pCO_2 and either TA or DIC as input parameters, and of pCO_2 based on DIC and pH (Table 4).
4) The results confirm previous findings that combining pH and pCO_2 as input parameters should be strictly avoided in calculations, while the one based on TA and DIC should be used cautiously, as, according to our assessment (Table 4), using this pair only works for determining pH in Arctic open waters, and for other combinations generates data of poor quality.
5) Not including measured PO_4^{3-} and DSi as ancillary input data in the calculations generates additional, rather small, errors, especially in cases when TA is either calculated or used as an input parameter. The relative contribution to the absolute uncertainty caused by omitting nutrient data was relatively low (up to 1.9%) for coastal waters where nutrient concentrations were low and absolute uncertainties were high. The contributions were somewhat higher (up to 7.2%) in the open ocean waters, where there was a reversed situation – nutrient concentrations were high and absolute uncertainties low. These conclusions are based on observations taken in the middle of the polar day, and the contribution of PO_4^{3-} and DSi to calculations may be different in different seasons, along with changes in nutrient availability.
6) The linear relationship between TA and salinity determined in this study ($TA = 43.426 \cdot S + 782.18$) has been proven to be a useful tool to estimate TA_S from salinity measurements, which is accurate enough to be used as an input parameter in the marine carbonate system calculations. In combination with pCO_2, TA_S guarantees high-quality calculations of pH both in the open ocean but also in coastal waters, at least for the European sector of the Arctic. Additionally, when applied together with pH, it allows for estimating high-quality pCO_2 in ocean waters and only slightly worse in coastal samples. These findings may open a new perspective and simplify the research and monitoring of marine carbonate system variability and issues like ocean acidification in harsh conditions of the European Arctic.

CRediT authorship contribution statement

Fernando Aguado Gonzalo: Writing – review & editing, Writing – original draft, Visualization, Methodology, Investigation, Formal analysis, Data curation, Conceptualization. **Katarzyna Koziorowska:** Writing – review & editing, Data curation. **Beata Szymczycha:** Writing – review & editing, Project administration, Methodology, Funding acquisition, Data curation. **Karol Kuliński:** Writing – review & editing, Validation, Supervision, Project administration, Funding acquisition, Conceptualization.

Funding sources

The author(s) declare that financial support was received for the research, authorship, and/or publication of this article. The study was performed within the framework of grant no. 2019/34/E/ST10/00167 financed by the Polish National Science Center. In addition, some sampling and chemical analyses were financially supported by the Norwegian Financial Mechanism 2014–2021 (85%) and National Science Centre (15%) within the GRIEG Programme, grants no. 2019/34/H/ST10/00504 and 2019/34/H/ST10/00645. The interpretation of the results in terms of their contextualization was supported by the European Union's Horizon Europe research and innovation programme under Grant Agreement No. 101136480 (SEA-Quester)

Declaration of competing interest

The authors declare that the research was conducted in the absence of any commercial or financial relationships that could be construed as a potential conflict of interest.

Acknowledgements

We would like to thank the captain and the crew of the R.V. Oceania for their enthusiasm and support during sampling. We also would like to thank Diak, M.; Prusiński, P.; Saghravany, R.; Makuch, P., and Stokowski, M. for their support during laboratory measurements.

Appendix A

A.1. Sampling design and chemical analyses

Surface water samples were collected via the ship's underway pumping system, which had the inlet at a depth of 2.5 m. The water was delivered at a

rate of 20 L min^{-1} to the ship's laboratories equipped with several outlets, allowing us to collect in parallel discrete samples for pH, TA, DIC, DSi, and PO_4^{3-}, and to conduct continuous measurements of pCO_2, temperature, and salinity. The latter two were measured with an SBE 21 SeaCAT thermosalinograph and an additional temperature probe SBE 38 located at the water inlet and measuring in situ temperature (Sea-Bird Scientific). Both temperature and salinity were measured continuously every 10 s and later on averaged to a one-minute resolution. The accuracy for temperature was ±0.01 °C (for both sensors) and for conductivity ±0.001 S/m, respectively.

The pCO_2 measurements were carried out using a cavity ring-down spectroscope (CRDS) G2101-i (Picarro) directly from the headspace of a bubble-type equilibrator equipped with an additional spray-type water diffuser. The quality of the CRDS measurements was regularly monitored, measuring three gases with different CO_2 concentrations, namely pure nitrogen (Linde 5.0), as well as artificial air with 205 and 507 ppm of CO_2, providing a precision and an accuracy of ±1.3 μatm. A detailed description of this pCO_2 system performance, including its accuracy/precision and the response time, was provided by Stokowski et al. (2021). The pCO_2 readings were averaged to a one-minute resolution. The effect of the temperature changes between the water inlet (in situ) and the equilibrator (lab) was corrected using the formula proposed by Takahashi et al. (1993):

$$pCO_2(\text{in situ}) = pCO_2(\text{lab})^{*} \exp.\left(0.0423^{*}\left(t_{(\text{in situ})} - t_{(\text{lab})}\right)\right) \quad \text{(A1)}$$

To standardize all the pCO_2 measurements and calculations, all the pCO_2 data were corrected to 1 atm. Atmospheric pressure (P) changes were measured in the laboratory using a Fibox 4 (PreSens GmbH, Germany). Normalization of the data to 1 atm was done using Eq. (A2):

$$pCO_2\ (1\ \text{atm}) = pCO_2(\text{in situ})^{*}\ 1013.25/P \quad \text{(A2)}$$

where pCO_2(in situ) is the pCO_2 obtained after temperature correction in Eq. (A1).

The water column sampling was performed at selected stations using the CTD-rosette (SBE9/11, Sea-Bird Scientific) system equipped with a carousel with twelve 10 L Niskin bottles. The accuracy for temperature was ±0.01 °C and for conductivity ±0.001 S/m. At a selected depth, the CTD-rosette was stopped for at least 20 s to provide stable readings of temperature and salinity, followed by closing Niskin bottles.

All the water column and surface water samples for pH, DIC, TA, phosphate, and silicate followed the same state-of-the-art sampling and storage procedures as described by Dickson et al. (2007) and Grasshoff et al. (2009). The samples for pH were collected in borosilicate bottles and sealed with ground-glass stoppers. They were measured right after sampling. If several samples were collected in a short period, they were stored in a fridge, maintaining the samples at temperatures similar to in situ conditions. All the samples for pH were measured within max. 2 h after collection. The pH was measured at 25 °C on a HydroFIA flow-through spectrophotometric system (CONTROS, 4H-JENA engineering GmbH), using mCresolPurple as an indicator agent (Carter et al., 2013; Clayton and Byrne, 1993; Liu et al., 2015; Mosley et al., 2004) and the parametrization of the second dissociation constant proposed by Müller and Rehder (2018). The system had a precision of 0.002 and an accuracy of 0.003, both being quantified after repeated measurements of the certified TRIS buffer (TRIS-CRM-T37) provided by A.G. Dickson (Scripps Institution of Oceanography/UCSD, USA).

TA and DIC samples were collected in 270 mL borosilicate glass bottles, first overflowing the bottles for at least 10 s. Afterwards, 1 mL of the sample was removed to allow thermal expansion, and 100 μL of saturated $HgCl_2$ was added to stop the biological activity. The bottles were then closed with greased ground glass stoppers and stored in the dark, as described by Huang et al. (2012). TA and DIC samples were measured in the laboratories of the Institute of Oceanology of the Polish Academy of Sciences (IOPAN) in Poland within max. Eight weeks after collection. The TA was measured using a custom-designed open-cell potentiometric titrator developed by Andrew Dickson (Scripps Institution of Oceanography/UCSD, USA), following the analytical method described by Dickson et al. (2003). The system yielded an accuracy/precision of ±3 μmol Kg^{-1} as derived from regular measurements of certified reference materials (CRMs), batch no. #190 and #195 provided by A.G. Dickson (Marine Physical Laboratory, Scripps Institution of Oceanography/UCSD, USA). The concentration of DIC was determined using an automated DIC analyzer (Apollo SciTech Inc.), equipped with Li7815 CO_2 detector and following the methods described by Chen et al. (2015). The instrument conducted repeated measurements (at least three measurements) of the same sample and CRMs (the same batches as for TA) until ±1.5 μmol Kg^{-1} precision was achieved, assuring that all the samples were measured with an accuracy/precision better than ±1.5 μmol Kg^{-1}.

Water samples for PO_4^{3-} and DSi were filtered using cellulose acetate filters with a pore size of 0.45 μm. A volume of 10 mL was collected in a 15 mL pre-cleaned high-density polyethylene vial to allow expansion after freezing. Samples were stored at −20 °C for further nutrient analysis performed at IOPAN laboratories within eight weeks after collection. The concentrations of DSi and PO_4^{3-} were determined using a SEAL AA500 AutoAnalyzer (Seal Analytical), applying standard photometric methods (Grasshoff et al., 2009). Quality control consisted of repeated measurements of two different CRMs (QC3179, Sigma Aldrich, and HAMIL, Environment Canada). The method detection limits were 0.1 μmol L^{-1} for PO_4^{3-} and 0.3 μmol L^{-1} for DSi. The accuracy of PO_4^{3-} and DSi measurements was 99.0% and 100.1%, respectively, while the precision was 0.01 μmol L^{-1} and 0.03 μmol L^{-1}, respectively.

Appendix B

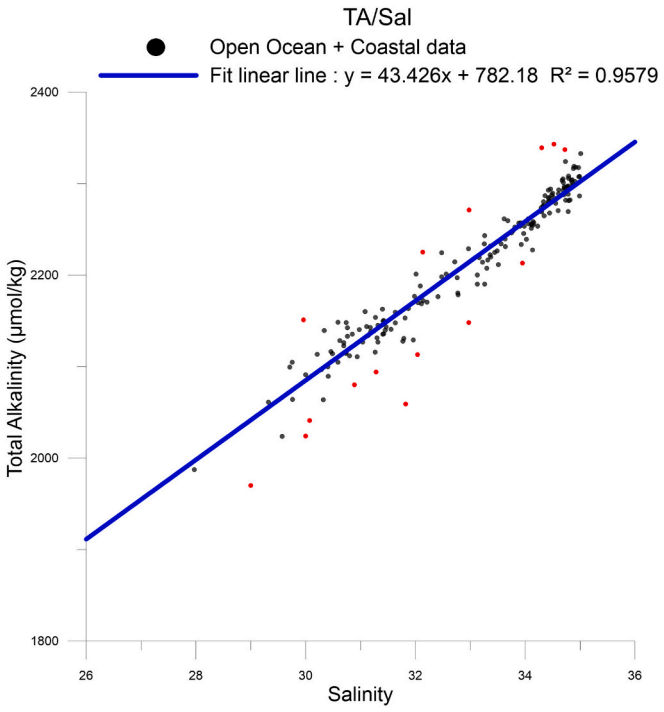

Fig. B1. Linear correlation between total alkalinity (TA) and salinity (S) for 90% of the total number of collected samples, guaranteeing the best linearity. The remaining 10% has been marked as red dots in the graph. (For interpretation of the references to colour in this figure legend, the reader is referred to the web version of this article.)

Appendix C

As shown in this study, the inconsistencies in the Arctic coastal waters are significantly larger than in the open ocean (Table 2 and Figs. 2–5). These regional differences can be observed independently of the choice of dissociation constants used in the calculations (Table C1 and C2). Although the choice of dissociation constants produces some differences in the calculated values, these differences are less pronounced in the coastal samples. Results presented in Tables C1 and C2 indicate that the choice of dissociation constants have a larger influence in the variability of the results in oceanic waters, while in coastal areas, the higher uncertainty of the results due to the influence of unparametrized substances and processes masks the effect of the dissociation constants. Although the choice of dissociation constants generates some differences in the absolute uncertainties, the main conclusions of this study are independent of the choosen ones. The absolute uncertainties of the calculated variables are larger in coastal samples than in oceanic ones and only two variables can be estimated within the weather-goal quality threshold in coastal waters, pH and pCO_2. Furthermore, there is no one set of dissociation constants which is clearly better than others, although some of them produce results slighly more consistent with the observations (Table C1 and C2)

Table C1

Absolute uncertainty in oceanic samples, expressed as the 68%ile, of the calculated variables using different set of dissociation constants. Abreviations for the constants are L00 (Lueker et al., 2000), DM87 (Dickson and Millero, 1987), MPM02 (Mojica Prieto et al. 2002), M02 (Millero et al., 2002), M06 (Millero et al., 2006), and M10 (Millero, 2010). The green colour indicates that the calculated data has an absolute uncertainty below 10 µmol kg^{-1} for DIC and TA, 0.020 for pH, and 7 µatm for pCO_2 (weather-goal quality data). The red colour shows combinations of variables which produce bad-quality data (individual values within the cells).

Oceanic	L00 Dataset	DM87 Dataset	MPM02 Dataset	M02 Dataset	M06 Dataset	M10 Dataset
$\Delta TA(DIC,pCO_2)$	±6	±8	±4	±6	±5	±4
$\Delta TA(DIC,pH)$	±8	±5	±4	±4	±7	±7
$\Delta TA(pH,pCO_2)$	±45	±49	±61	±113	±39	±40
$\Delta DIC(TA,pCO_2)$	±5	±7	±3	±5	±4	±4
$\Delta DIC(TA,pH)$	±8	±4	±3	±3	±7	±6
$\Delta DIC(pH,pCO_2)$	±38	±49	±54	±92	±34	±35
$\Delta pH(TA,DIC)$	±0.017	±0.010	±0.007	±0.007	±0.015	±0.013
$\Delta pH(TA,pCO2)$	±0.007	±0.008	±0.010	±0.019	±0.007	±0.007
$\Delta pH(DIC,pCO_2)$	±0.007	±0.009	±0.010	±0.019	±0.007	±0.007
$\Delta pCO_2(TA,DIC)$	±9	±11	±6	±9	±8	±6
$\Delta pCO_2(TA,pH)$	±5	±7	±8	±13	±5	±5
$\Delta pCO_2(DIC,pH)$	±5	±6	±7	±12	±5	±5

Table C2
Absolute uncertainty in coastal samples, expressed as the 68%ile, of the calculated variables using different set of dissociation constants. Abreviations for the constants are L00 (Lueker et al., 2000), DM87 (Dickson and Millero, 1987), MPM02 (Mojica Prieto et al. 2002), M02 (Millero et al., 2002), M06 (Millero et al., 2006), and M10 (Millero, 2010). The green colour indicates that the calculated data has an absolute uncertainty below 10 μmol kg^{-1} for DIC and TA, 0.020 for pH, and 7 μatm for pCO_2 (weather-goal quality data). The red colour shows combinations of variables which produce bad-quality data (individual values within the cells).

Variable	L00 Coastal	DM87 Coastal	MPM02 Coastal	M02 Coastal	M06 Coastal	M10 Coastal
$\Delta TA(DIC,pCO_2)$	±11	±12	±12	±12	±11	±11
$\Delta TA(DIC,pH)$	±12	±12	±12	±12	±12	±12
$\Delta TA(pH,pCO_2)$	±56	±57	±69	±134	±48	±46
$\Delta DIC(TA,pCO_2)$	±10	±10	±10	±10	±9	±9
$\Delta DIC(TA,pH)$	±11	±12	±11	±12	±11	±11
$\Delta DIC(pH,pCO_2)$	±42	±49	±53	±115	±40	±36
$\Delta pH(TA,DIC)$	±0.027	±0.027	±0.029	±0.029	±0.027	±0.027
$\Delta pH(TA,pCO2)$	±0.010	±0.010	±0.012	±0.025	±0.009	±0.008
$\Delta pH(DIC,pCO_2)$	±0.009	±0.010	±0.011	±0.024	±0.008	±0.008
$\Delta pCO_2(TA,DIC)$	±19	±19	±21	±21	±20	±20
$\Delta pCO_2(TA,pH)$	±9	±8	±10	±20	±7	±7
$\Delta pCO_2(DIC,pH)$	±6	±7	±8	±18	±6	±5

Appendix D. Supplementary data

Supplementary data to this article can be found online at https://doi.org/10.1016/j.marchem.2026.104604.

Data availability

The datasets presented in this study can be found in online repositories. The names of the repository/repositories and accession number(s) can be found in Saghravani et al. (2024), Aguado Gonzalo et al. (2024) and Aguado Gonzalo et al. (2025).

References

Aguado Gonzalo, F., Stokowski, M., Koziorowska-Makuch, K., Makuch, P., Beszczyńska-Möller, A., Kukliński, P., Kuliński, K., 2024. Key processes controlling the variability of the summer marine CO2 system in Fram Strait surface waters. Front. Mar. Sci. 11, 1–19. https://doi.org/10.3389/fmars.2024.1464653.

Aguado Gonzalo, F., Koziorowska, K., Szymczycha, B., Kulinski, K., 2025. Surface carbonate chemistry in high Arctic fjords (Svalbard Archipelago) during summer 2021. Geonetwork. https://doi.org/10.48457/IOPAN.2025.534.

Anderson, L.G., Olsson, K., Chierici, M., 1998. A carbon budget for the Arctic Ocean. Glob. Biogeochem. Cycles 12, 455–465. https://doi.org/10.1029/98GB01372.

Bates, N.R., Mathis, J.T., 2009. The Arctic Ocean marine carbon cycle: evaluation of air-sea CO2 exchanges, ocean acidification impacts and potential feedbacks. Biogeosciences 6, 2433–2459. https://doi.org/10.5194/bg-6-2433-2009.

Bates, N.R., Mathis, J.T., Cooper, L.W., 2009. Ocean acidification and biologically induced seasonality of carbonate mineral saturation states in the western Arctic Ocean. J. Geophys. Res. Ocean. 114, 1–21. https://doi.org/10.1029/2008JC004862.

Branham, C.W., Murphy, D., Johnson, K., Jannasch, H., 2016. Optimization of a robust and reliable ISFET sensor for measuring pH in the deep ocean. Ocean. 2016 MTS/IEEE Monterey. OCE. https://doi.org/10.1109/OCEANS.2016.7761357.

Cai, W.J., Hu, X., Huang, W.J., Jiang, L.Q., Wang, Y., Peng, T.H., Zhang, X., 2010. Alkalinity distribution in the western North Atlantic Ocean margins. J. Geophys. Res. Ocean. 115, 1–15. https://doi.org/10.1029/2009JC005482.

Capelle, D.W., Kuzyk, Z.Z.A., Papakyriakou, T., Guéguen, C., Miller, L.A., Macdonald, R. W., 2020. Effect of terrestrial organic matter on ocean acidification and CO2 flux in an Arctic shelf sea. Prog. Oceanogr. 185. https://doi.org/10.1016/j.pocean.2020.102319.

Carter, B.R., Radich, J.A., Doyle, H.L., Dickson, A.G., 2013. An automated system for spectrophotometric seawater pH measurements. Limnol. Oceanogr. Methods 11, 16–27. https://doi.org/10.4319/lom.2013.11.16.

Carter, B.R., Sharp, J.D., García-ib, M.I., Woosley, R.J., Fong, M.B., Alvarez, M., Barbero, L., Clegg, S.L., Easley, R., Fassbender, A.J., Li, X., Schockman, K.M., Wang, Z.A., 2024. Review Random and Systematic Uncertainty in Ship-Based Seawater Carbonate Chemistry Observations 1–16. https://doi.org/10.1002/lno.12674.

Chen, B., Cai, W.J., Chen, L., 2015. The marine carbonate system of the Arctic Ocean: assessment of internal consistency and sampling considerations, summer 2010. Mar. Chem. 176, 174–188. https://doi.org/10.1016/j.marchem.2015.09.007.

Cherkasheva, A., Bracher, A., Melsheimer, C., Köberle, C., Gerdes, R., Nöthig, E.M., Bauerfeind, E., Boetius, A., 2014. Influence of the physical environment on polar phytoplankton blooms: a case study in the Fram Strait. J. Mar. Syst. 132, 196–207. https://doi.org/10.1016/j.jmarsys.2013.11.008.

Chierici, M., Fransson, A., 2009. Calcium carbonate saturation in the surface water of the Arctic Ocean: Undersaturation in freshwater influenced shelves. Biogeosciences 6, 2421–2432. https://doi.org/10.5194/bg-6-2421-2009.

Clayton, T.D., Byrne, R.H., 1993. Spectrophotometric seawater pH measurements: total hydrogen ion concentration scale calibration of m-cresol purple and at-sea results. Deep. Res. Part I 40, 2115–2129. https://doi.org/10.1016/0967-0637(93)90048-8.

Cross, J.N., Mathis, J.T., Pickart, R.S., Bates, N.R., 2018. Formation and transport of corrosive water in the Pacific Arctic region. Deep Res. Part II Top. Stud. Oceanogr. 152, 67–81. https://doi.org/10.1016/j.dsr2.2018.05.020.

Cullison Gray, S.E., DeGrandpre, M.D., Moore, T.S., Martz, T.R., Friederich, G.E., Johnson, K.S., 2011. Applications of in situ pH measurements for inorganic carbon calculations. Mar. Chem. 125, 82–90. https://doi.org/10.1016/j.marchem.2011.02.005.

Dai, A., Trenberth, K.E., 2002. Estimates of freshwater discharge from continents: latitudinal and seasonal variations. J. Hydrometeorol. 3, 660–687. https://doi.org/10.1175/1525-7541(2002)003<0660:EOFDFC>2.0.CO;2.

Dai, M., Su, J., Zhao, Y., Hofmann, E.E., Cao, Z., Cai, W.J., Gan, J., Lacroix, F., Laruelle, G.G., Meng, F., Mudieller, J.D., Regnier, P.A.G., Wang, G., Wang, Z., 2022. Carbon fluxes in the Coastal Ocean: synthesis, boundary processes, and future trends.

Annu. Rev. Earth Planet. Sci. 50, 593–626. https://doi.org/10.1146/annurev-earth-032320-090746.
Dickson, A.G., 2007. Guide to best practices for ocean CO2 measurements. PICES Spec. Publ. 191.
Dickson, A.G., Millero, F.J., 1987. A comparison of the equilibrium constants for the dissociation of carbonic acid in seawater media. Deep Sea Res. Part Oceanogr. Res. Pap. 34, 1733–1743. https://doi.org/10.1016/0198-0149(87)90021-5.
Dickson, A.G., Wesolowski, D.J., Palmer, D.A., Mesmer, R.E., 1990. Dissociation constant of bisulfate ion in aqueous sodium chloride solutions to 250°C. J. Phys. Chem. 94, 7978–7985. https://doi.org/10.1021/j100383a042.
Dickson, A.G., Afghan, J.D., Anderson, G.C., 2003. Reference materials for oceanic CO2 analysis: a method for the certification of total alkalinity. Mar. Chem. 80, 185–197. https://doi.org/10.1016/S0304-4203(02)00133-0.
Feng, D., Gleason, C.J., Lin, P., Yang, X., Pan, M., Ishitsuka, Y., 2021. Recent changes to Arctic river discharge. Nat. Commun. 12, 1–9. https://doi.org/10.1038/s41467-021-27228-1.
Friedlingstein, P., Jones, M.W., O'Sullivan, M., Andrew, R.M., Bakker, D.C., Hauck, J., Le Quéré, C., Peters, G.P., Peters, W., Pongratz, J., Sitch, S., 2022. Global carbon budget 2021. Earth Syst. Sci. Data 14 (4), 1917–2005.
Grasshoff, K., Kremling, K., Ehrhardt, M., 2009. 2009: Methods of Seawater Analysis. John Wiley & Sons. ISBN 3–527–29589-5.
Hu, Y., Wang, F., 2020. Effect of ikaite precipitation on phosphate removal in sea ice, 1, pp. 2–6.
Jones, J.M., Sweet, J., Brzezinski, M.A., McNair, H.M., Passow, U., 2016. Evaluating carbonate system algorithms in a nearshore system: does total alkalinity matter? PLoS One 11, 1–12. https://doi.org/10.1371/journal.pone.0165191.
Jones, E.M., Chierici, M., Menze, S., Fransson, A., Ingvaldsen, R.B., Lødemel, H.H., 2021. Ocean acidification state variability of the Atlantic Arctic Ocean around northern Svalbard. Prog. Oceanogr. 199. https://doi.org/10.1016/j.pocean.2021.102708.
Kerr, D.E., Brown, P.J., Grey, A., Kelleher, B.P., 2021. The influence of organic alkalinity on the carbonate system in coastal waters. Mar. Chem. 237, 104050. https://doi.org/10.1016/j.marchem.2021.104050.
Kerr, D.E., Turner, C., Grey, A., Keogh, J., Brown, P.J., Kelleher, B.P., 2023. OrgAlkCalc: estimation of organic alkalinity quantities and acid-base properties with proof of concept in Dublin Bay. Mar. Chem. 251, 104234. https://doi.org/10.1016/j.marchem.2023.104234.
Ko, Y.H., Lee, K., Eom, K.H., Han, I.S., 2016. Organic alkalinity produced by phytoplankton and its effect on the computation of ocean carbon parameters. Limnol. Oceanogr. 61, 1462–1471. https://doi.org/10.1002/lno.10309.
Koziorowska-Makuch, K., Szymczycha, B., Thomas, H., Kuliński, K., 2023. The marine carbonate system variability in high meltwater season (Spitsbergen fjords, Svalbard). Prog. Oceanogr. 211. https://doi.org/10.1016/j.pocean.2023.102977.
Kuliński, K., Schneider, B., Hammer, K., Machulik, U., Schulz-Bull, D., 2014. The influence of dissolved organic matter on the acid-base system of the Baltic Sea. J. Mar. Syst. 132, 106–115. https://doi.org/10.1016/j.jmarsys.2014.01.011.
Lee, K., Millero, F.J., 1995. Thermodynamic studies of the carbonate system in seawater. Deep. Res. Part I 42, 2035–2061. https://doi.org/10.1016/0967-0637(95)00077-1.
Lee, K., Tong, L.T., Millero, F.J., Sabine, C.L., Dickson, A.G., Goyet, C., Park, G.H., Wanninkhof, R., Feely, R.A., Key, R.M., 2006. Global relationships of total alkalinity with salinity and temperature in surface waters of the world's oceans. Geophys. Res. Lett. 33, 1–5. https://doi.org/10.1029/2006GL027207.
Lee, K., Kim, T.W., Byrne, R.H., Millero, F.J., Feely, R.A., Liu, Y.M., 2010. The universal ratio of boron to chlorinity for the North Pacific and North Atlantic oceans. Geochim. Cosmochim. Acta 74, 1801–1811. https://doi.org/10.1016/j.gca.2009.12.027.
Lewis, E., Wallace, D., Allison, L.J., 1998. *Program developed for CO2 system calculations* (No. ORNL/CDIAC-105). Brookhaven National Lab., Dept. of Applied Science, Upton, NY (United States); Oak Ridge National Lab.. Carbon Dioxide Information Analysis Center, TN (United States).
Liu, P., He, S., Wei, H., Wang, J., Sun, C., 2015. Characterization of α-Fe2O3/γ-Al2O3 catalysts for catalytic wet peroxide oxidation of m-cresol. Ind. Eng. Chem. Res. 54, 130–136. https://doi.org/10.1021/ie5037897.
Lueker, T.J., Dickson, A.G., Keeling, C.D., 2000. Ocean pCO2 calculated from dissolved inorganic carbon, alkalinity, and equations for K1 and K2: validation based on laboratory measurements of CO2 in gas and seawater at equilibrium. Mar. Chem. 70 (1–3), 105–119.
MacGilchrist, G.A., Naveira Garabato, A.C., Tsubouchi, T., Bacon, S., Torres-Valdés, S., Azetsu-Scott, K., 2014. The Arctic Ocean carbon sink. Deep Res. Part I Oceanogr. Res. Pap. 86, 39–55. https://doi.org/10.1016/j.dsr.2014.01.002.
Manizza, M., Menemenlis, D., Zhang, H., Miller, C.E., 2019. Modeling the recent changes in the Arctic Ocean CO2 sink (2006–2013). Glob. Biogeochem. Cycles 33, 420–438. https://doi.org/10.1029/2018GB006070.
Mayot, N., Matrai, P.A., Arjona, A., Bélanger, S., Marchese, C., Jaegler, T., Ardyna, M., Steele, M., 2020. Springtime export of Arctic Sea ice influences phytoplankton production in the Greenland Sea. J. Geophys. Res. Ocean. 125, 1–16. https://doi.org/10.1029/2019JC015799.
Mehrbach, C., Culberson, C.H., Hawley, J.E., Pytkowicx, R.M., 1973. Measurement of the apparent dissociation constants of carbonic acid in seawater at atmospheric pressure. Limnol. Oceanogr. 18, 897–907. https://doi.org/10.4319/lo.1973.18.6.0897.
Millero, F.J., 2007. The marine inorganic carbon cycle. Chem. Rev. 107 (2), 308–341.
Millero, F.J., 2010. Carbonate constants for estuarine waters. Marine and freshwater research, 61(2), pp.139-142.Millero, F.J., 2007. The marine inorganic carbon cycle. Chem. Rev. 107, 308–341. https://doi.org/10.1021/cr0503557.
Millero, F.J., Pierrot, D., Lee, K., Wanninkhof, R., Feely, R., Sabine, C.L., Key, R.M., Takahashi, T., 2002. Dissociation constants for carbonic acid determined from field measurements. Deep-Sea Res. I Oceanogr. Res. Pap. 49 (10), 1705–1723.
Millero, F.J., Graham, T.B., Huang, F., Bustos-Serrano, H., Pierrot, D., 2006. Dissociation constants of carbonic acid in seawater as a function of salinity and temperature. Mar. Chem. 100 (1–2), 80–94.
Mosley, L.M., Husheer, S.L.G., Hunter, K.A., 2004. Spectrophotometric pH measurement in estuaries using thymol blue and m-cresol purple. Mar. Chem. 91, 175–186. https://doi.org/10.1016/j.marchem.2004.06.008.
Müller, J.D., Rehder, G., 2018. Metrology of pH measurements in brackish waters-part 2: experimental characterization of purified meta-cresol purple for spectrophotometric pHT measurements. Front. Mar. Sci. 5, 1–9. https://doi.org/10.3389/fmars.2018.00177.
Nedashkovskii, A.P., Khvedynich, S.V., Petrovskii, T.V., 2008. Phosphates and silicates in sea ice of the high-latitudinal Arctic: data of the north Pole-34 drifting ice station. Oceanology 48, 646–655. https://doi.org/10.1134/S0001437008050044.
Nehir, M., Esposito, M., Loucaides, S., Achterberg, E.P., 2022. Field application of automated spectrophotometric analyzer for high-resolution in situ monitoring of pH in dynamic estuarine and coastal waters. Front. Mar. Sci. 9, 1–14. https://doi.org/10.3389/fmars.2022.891876.
Newton, J.A., Feely, R.A., Jewett, E.B., Williamson, P., Mathis, J., 2014. Global Ocean acidification observing network: requirements and governance plan. Glob. Ocean Acidif. Obs. Netw. 5–28.
Orr, J.C., Epitalon, J.M., Dickson, A.G., Gattuso, J.P., 2018. Routine uncertainty propagation for the marine carbon dioxide system. Mar. Chem. 207, 84–107. https://doi.org/10.1016/j.marchem.2018.10.006.
Patsavas, M.C., Byrne, R.H., Wanninkhof, R., Feely, R.A., Cai, W.J., 2015. Internal consistency of marine carbonate system measurements and assessments of aragonite saturation state: insights from two U.S. coastal cruises. Mar. Chem. 176, 9–20. https://doi.org/10.1016/j.marchem.2015.06.022.
Perez, F.F., Fraga, F., 1987. Association constant of fluoride and hydrogen ions in seawater. Mar. Chem. 21, 161–168. https://doi.org/10.1016/0304-4203(87)90036-3.
Qi, D., Chen, L., Chen, B., Gao, Z., Zhong, W., Feely, R.A., Anderson, L.G., Sun, H., Chen, J., Chen, M., Zhan, L., Zhang, Y., Cai, W.J., 2017. Increase in acidifying water in the western Arctic Ocean. Nat. Clim. Chang. 7, 195–199. https://doi.org/10.1038/nclimate3228.
Qi, D., Chen, B., Chen, L., Lin, H., Gao, Z., Sun, H., Zhang, Y., Sun, X., Cai, W., 2020. Coastal acidification induced by biogeochemical processes driven by sea-ice melt in the western Arctic Ocean. Polar Sci. 23. https://doi.org/10.1016/j.polar.2020.100504.
Qi, D., Wu, Y., Chen, L., Cai, W.J., Ouyang, Z., Zhang, Y., Anderson, L.G., Feely, R.A., Zhuang, Y., Lin, H., Lei, R., Bi, H., 2022. Rapid acidification of the Arctic Chukchi Sea waters driven by anthropogenic forcing and biological carbon recycling. Geophys. Res. Lett. 49, 1–12. https://doi.org/10.1029/2021GL097246.
Raimondi, L., Matthews, J.B.R., Atamanchuk, D., Azetsu-Scott, K., Wallace, D.W.R., 2019. The internal consistency of the marine carbon dioxide system for high latitude shipboard and in situ monitoring. Mar. Chem. 213, 49–70. https://doi.org/10.1016/j.marchem.2019.03.001.
Robbins, L.L., Wynn, J.G., Lisle, J.T., Yates, K.K., Knorr, P.O., Byrne, R.H., Liu, X., Patsavas, M.C., Azetsu-Scott, K., Takahashi, T., 2013. Baseline monitoring of the western Arctic Ocean estimates 20% of Canadian basin surface waters are undersaturated with respect to aragonite. PLoS One 8. https://doi.org/10.1371/journal.pone.0073796.
Saghravani, S.R., Böttcher, M.E., Hong, W.-L., Kuliński, K., Lepland, A., Sen, A., Szymczycha, B., 2024. In-situ parameters, nutrients and dissolved carbon distribution in the water column and pore waters of Arctic fjords (Western Spitsbergen) during a melting season. Earth Syst. Sci. Data Discuss. 2024, 1–19.
Salt, L.A., Thomas, H., Bozec, Y., Borges, A.V., de Baar, H.J.W., 2016. The internal consistency of the North Sea carbonate system. J. Mar. Syst. 157, 52–64. https://doi.org/10.1016/j.jmarsys.2015.11.008.
Semiletov, I., Pipko, I., Gustafsson, Ö., Anderson, L.G., Sergienko, V., Pugach, S., Dudarev, O., Charkin, A., Gukov, A., Bröder, L., Andersson, A., Spivak, E., Shakhova, N., 2016. Acidification of east Siberian Arctic shelf waters through addition of freshwater and terrestrial carbon. Nat. Geosci. 9, 361–365. https://doi.org/10.1038/ngeo2695.
Sharp, J.D., Byrne, R.H., 2020. Interpreting measurements of total alkalinity in marine and estuarine waters in the presence of proton-binding organic matter. Deep. Res. Part I Oceanogr. Res. Pap. 165, 103338. https://doi.org/10.1016/j.dsr.2020.103338.
Solomon, A., Heuzé, C., Rabe, B., Bacon, S., Bertino, L., Heimbach, P., Inoue, J., Iovino, D., Mottram, R., Zhang, X., Aksenov, Y., McAdam, R., Nguyen, A., Raj, R.P., Tang, H., 2021. Freshwater in the Arctic Ocean 2010-2019. Ocean Sci. 17, 1081–1102. https://doi.org/10.5194/os-17-1081-2021.
Spreen, G., Kaleschke, L., Heygster, G., 2008. Sea ice remote sensing using AMSR-E 89 GHz channels. J. Geophys. Res. 113, C02S03. https://doi.org/10.1029/2005JC003384.
Stokowski, M., Makuch, P., Rutkowski, K., Wichorowski, M., Kuliński, K., 2021. A system for the determination of surface water pCO2 in a highly variable environment, exemplified in the southern Baltic Sea. Oceanologia 63 (2), 276–282. https://doi.org/10.1016/j.oceano.2021.01.001.
Takahashi, T., Olafsson, J., Goddard, J.G., Chipman, D.W., Sutherland, S.C., 1993. Seasonal variation of CO_2 and nutrients in the high-latitude oceans: a comparative study. Glob. Biogeochem. Cycles 7, 843–878.
Terhaar, J., Kwiatkowski, L., Bopp, L., 2020. Emergent constraint on Arctic Ocean acidification in the twenty-first century. Nature 582, 379–383. https://doi.org/10.1038/s41586-020-2360-3.
Wolf-Gladrow, D.A., Zeebe, R.E., Klaas, C., Körtzinger, A., Dickson, A.G., 2007. Total alkalinity: the explicit conservative expression and its application to biogeochemical

processes. Mar. Chem. 106, 287–300. https://doi.org/10.1016/j.marchem.2007.01.006.
Woosley, R.J., Moon, J.Y., 2023. Re-evaluation of carbonic acid dissociation constants across conditions and the implications for ocean acidification. Mar. Chem. 250, 104247. https://doi.org/10.1016/j.marchem.2023.104247.
Woosley, R.J., Millero, F.J., Takahashi, T., 2017. Internal consistency of the inorganic carbon system in the Arctic Ocean. Limnol. Oceanogr. Methods 15, 887–896. https://doi.org/10.1002/lom3.10208.

Statement of co-authors

Sopot, 18/03/2026

MSc Fernando Aguado Gonzalo

Institute of Oceanology of the Polish Academy of Sciences

Laboratory of marine biogeochemistry

Author contribution statement

I declare that my contribution to the publication:

Gonzalo, F. A., Koziorowska, K., Szymczycha, B., & Kuliński, K. (2026). The internal consistency between calculated and measured variables of the marine carbonate system in Arctic open and coastal waters, case study: Atlantic Arctic. *Marine Chemistry*, 104604.

Involved: Writing – review & editing, Writing – original draft, Visualization, Methodology, Investigation, Formal anal ysis, Data curation, Conceptualization.

and accounted for 75% of the total work needed for the realization of this publication.

Sopot, 19/03/2026

Dr Katarzyna Koziorowska

Institute of Oceanology of the Polish Academy of Sciences

Laboratory of marine biogeochemistry

Author contribution statement

I declare that my contribution to the publication:

Gonzalo, F. A., Koziorowska, K., Szymczycha, B., & Kuliński, K. (2026). The internal consistency between calculated and measured variables of the marine carbonate system in Arctic open and coastal waters, case study: Atlantic Arctic. *Marine Chemistry*, 104604.

Involved: Writing – review & editing, Data curation.

and accounted for 5% of the total work needed for the realization of this publication.

Katarzyna Koziorowska

Sopot, 18/03/2026

Dr. hab. Beata Szymczycha

Institute of Oceanology of the Polish Academy of Sciences

Department of marine chemistry and biochemistry

Author contribution statement

I declare that my contribution to the publication:

Gonzalo, F. A., Koziorowska, K., Szymczycha, B., & Kuliński, K. (2026). The internal consistency between calculated and measured variables of the marine carbonate system in Arctic open and coastal waters, case study: Atlantic Arctic. *Marine Chemistry*, 104604.

Involved: Writing – review & editing, Project administration, Methodology, Funding acquisition, Data curation.

and accounted for 5% of the total work needed for the realization of this publication.

Sopot, 18/03/2026

Dr. hab. Karol Kuliński

Institute of Oceanology of the Polish Academy of Sciences

Laboratory of marine biogeochemistry

Author contribution statement

I declare that my contribution to the publication:

Gonzalo, F. A., Koziorowska, K., Szymczycha, B., & Kuliński, K. (2026). The internal consistency between calculated and measured variables of the marine carbonate system in Arctic open and coastal waters, case study: Atlantic Arctic. *Marine Chemistry*, 104604.

Involved: Writing – review & editing, Validation, Supervision, Project administration, Funding acquisition, Conceptualization.

and accounted for 15% of the total work needed for the realization of this publication.

Karol Kuliński

Publication 3

Aguado Gonzalo, F., Koziorowska, K., Bromboszcz-Szczypior, L., Loginova, A., and Kuliński, K., 2026. High vertical resolution measurements of pH, pCO 2, Total Alkalinity and Dissolved Inorganic Carbon using a new approach: the carbonate profile. *Oceanologia*, 68(1), 68101. doi.org/10.5697/VMDA8631.

Oceanologia, 68 (1)/2026, 68101
Polish Academy of Sciences
Institute of Oceanology

https://doi.org/10.5697/VMDA8631

High vertical resolution measurements of pH, pCO_2, total alkalinity, and dissolved inorganic carbon using a new approach: the carbonate profiler

Fernando Aguado Gonzalo*, Katarzyna Koziorowska, Laura Bromboszcz-Szczypior, Alexandra Loginova, Karol Kuliński

Abstract
The equilibrium between the different parameters of the marine carbonate system – dissolved inorganic carbon (DIC), total alkalinity (TA), partial pressure of CO_2, and pH – is the core of ocean acidification studies, evaluation of inorganic carbon inventory, and air-sea CO_2 fluxes. To date, it has been challenging to simultaneously measure all those components in the water column due to different sampling methodologies, and especially in stratified waters, where sharp vertical biogeochemical gradients may occur. In this study, we designed a low-cost and easy-to-assemble pumping system, which, combined with a CTD profiler, makes a PUMP-CTD system that can efficiently serve as a precise water column sampler, allowing for simultaneous measurements and sampling of dissolved inorganic carbon, total alkalinity, partial pressure of CO_2, and pH with high vertical resolution. Importantly, this water sampler (denoted as the carbonate profiler) can be easily integrated with equilibrator-based continuous pCO_2 measurement systems, which are routinely used for underway data acquisition, making them suitable for water column sampling as well. We tested the carbonate profiler in the open ocean water column, where we obtained excellent consistency between measured pCO_2 and calculated values based on pH and DIC. Afterwards, we tested the operability of the system by measuring the vertical variability of all the components of the marine carbonate system in the Vistula River estuarine waters (southern Baltic Sea) and within the Arctic fjords affected by continental freshwater runoff. Overall, this system performed outstandingly, with a vertical resolution of half a meter, proving its utility in accurately measuring steep biogeochemical changes in the water column regardless of the analytical method used.

Keywords
Ocean acidification; pH; Total alkalinity; pCO2; Land ocean continuum; Arctic; Baltic Sea

Institute of Oceanology, Polish Academy of Sciences, Powstańców Warszawy 55, 81–712 Sopot, Poland
***Correspondence**: aguadof@iopan.pl (F. Aguado Gonzalo)

Received: 26 June 2025; **revised:** 4 November 2025; **accepted**: 12 November 2025

1. Introduction

The Oceans are key components for mitigating climate change due to their capacity to absorb atmospheric carbon dioxide (CO_2) at the surface and export it to the deeper water layers and sediments (Friedlingstein et al., 2025). Among oceanic regions, coastal areas, which often have very high carbon fixation rates, are key contributors to carbon export driven by intense primary production (Cai, 2011). As such, they are vital components of the global carbon cycling (Bauer et al., 2013; Dai et al., 2022; Regnier et al., 2022). However, the total contribution of these regions to the global carbon budget remains uncertain due to high spatiotemporal biogeochemical variability (Cai, 2011; Resplandy et al., 2018).

Within the coastal areas, estuaries represent complex biogeochemical environments where particulate and dissolved organic and inorganic carbon compounds of both autochthonous and allochthonous origin undergo rapid transformations (Mosley and Liss, 2020). In addition to commonly investigated processes related to organic matter production and remineralization (sink and source of CO_2, respectively), including respiration of terrigenous organic matter (Cross et al., 2018; Kuliński et al., 2016), carbon transformations are also driven here by significant shifts in pH and ionic composition resulting from the mixing of freshwater and seawater. In turn, pH, or concentration of protons ($pH = -\log[H]$), is mainly controlled

by the excess of proton acceptors over proton donors in water, defined as total alkalinity (TA) (Dickson, 1981). In the compounds that make up TA, the largest share comes from two inorganic carbon species, namely bicarbonate (HCO_3^-) and carbonate (CO_3^{2-}) ions, which together with dissolved CO_2 (or H_2CO_3) constitute dissolved inorganic carbon (DIC). Therefore, there is an intricate balance between pH, TA, and DIC, which ultimately determines dissolved CO_2 concentrations expressed most often as CO_2 partial pressure (pCO_2) (e.g., Millero, 2007). These four measurable parameters and their chemical interactions are often referred to as the marine carbonate system. Biological, physical and chemical processes continuously alter the delicate equilibrium between these parameters, initiating cascade changes in all of them. Therefore, to estimate the effect of biogeochemical processes and air-sea CO_2 exchange on the carbon inventory and fluxes in the coastal areas, it is necessary to characterize the complex horizontal and vertical distribution of all the marine carbonate system parameters.

While the variables of the marine carbonate system are interrelated, their measurement approaches differ. Generally, pCO_2 is obtained using the well-established underway systems, in which continuously flowing water is equilibrated with a closed air loop where pCO_2 is measured. These systems can provide highly accurate data with uncertainties lower than 2 µatm or 0.5% of the measured values (e.g., Arruda et al., 2020; Stokowski et al., 2021a). However, they are designed and installed on research vessels and ships of opportunity to obtain measurements at a fixed depth corresponding to the water inlet depth of the vessel's pumping system (typically between 2 and 10 m water depth). This setup makes them suitable for studying the horizontal distribution of pCO_2 but inappropriate for resolving vertical gradients in the water column. Although they are being used to estimate air-sea CO_2 fluxes in areas where sharp vertical gradients of CO_2 are expected, it has been demonstrated that differences in the sampling depth can introduce significant errors in the results (e.g., Ahmed et al., 2020; Azevedo et al., 2024). Thus, capturing the vertical distribution of pCO_2 in the water column is essential for precise flux calculations in stratified waters. Recent advances in underwater CO_2 sensors enable in situ measurements of CO_2 in the entire water column (when mounted on CTD profilers) or at a fixed depth for extended monitoring (when deployed in mooring systems). However, they often have lower accuracy and longer response times (between 5 and 20 minutes) than underway systems (Arruda et al., 2020; Clarke et al., 2017; Schar et al., 2010b).

Similarly, high vertical resolution TA, DIC, and pH measurements are challenging due to sampling limitations. Water for these analyses is commonly collected using bathometers, typically mounted in sampling carousels with a vertical resolution not better than 2–3 m, which is often insufficient to study rapid biogeochemical gradients in the water column. Moreover, the number of samples collected in the profile is directly correlated with the number of Niskin bottles mounted in the sampling carousel, which significantly limits the resolution of the sampling. For pH, direct measurements in the water column are also possible using submersible sensors. Several can perform spectrophotometric measurements directly in the water column, providing high-quality data (Bresnahan et al., 2014; Johengen et al., 2015). However, their response time (5–15 minutes) is usually too slow to obtain water column pH profiles with high vertical resolution.

In addition to direct measurements, each of the two marine carbonate variables can be calculated from the other two, which are known from direct measurements or modelling. This requires the use of thermodynamic ion-pairing models describing the carbonate system (Lewis et al., 1998). However, these models are primarily dedicated to open ocean waters where the marine carbonate system is well characterized. Their application in coastal areas remains challenging (Aguado Gonzalo et al., 2025a) due to anomalies in seawater composition and the influence of non-parameterized seawater constituents, leading to significant errors in calculations (Kerr et al., 2023; Kuliński et al., 2017; Ulfsbo et al., 2015). Thus, to characterize the marine carbonate system in coastal regions, it is often necessary to measure the complete set of variables (pCO_2, TA, DIC, and pH). This approach can be considered excessive or redundant in ocean waters. Such comprehensive sampling, especially in stratified waters, requires careful planning, standardization of the vertical resolution, and unification of the sampling technique for all parameters, regardless of the analytical methods used later. This is particularly important for combining state-of-the-art high-quality methods based on collecting discrete samples (TA, DIC, pH) with pCO_2 measurements, which require continuous water flow through the equilibrator (Dickson et al., 2007).

These challenges were the motivation to undertake this study, the aim of which was to design a sampling system that: (i) is capable of simultaneous discrete sampling of TA, DIC and pH and continuous equilibrator-based pCO_2 measurements in a vertical profile, (ii) allows easy switching in water supply between on-station vertical profiling and underway mode, (iii) inexpensive and easy to implement on a variety of vessels, including small ones, and (iv) provides high-quality results describing the marine carbonate system. The latter has been proven by tests made in the open waters of the Greenland Sea, while the operability of the system has been tested in two different coastal environments: the turbid freshwater plumes in the high Arctic fjords and the mid-latitude estuarine system of the Vistula River in the Baltic Sea.

2. Material and methods

2.1 The carbonate profiler

The inspiration for the system setup was a PUMP-CTD concept as reported, for instance, by Strady et al. (2008). However, the PUMP-CTD we designed was coupled with an equilibrator-based pCO_2 measurement system typically used for underway sampling. Thus, this carbonate profiler follows a similar principle as any underway system for pCO_2 measurements: a pump carries water along a pipeline to the ship's laboratory, where it flows continuously through the equilibrator whose headspace is connected by a closed air loop to a CO_2 analyser, while an additional water bypass allows for discrete sampling for TA, DIC, pH or any other parameter. The sole distinction of the carbonate profiler is the water supply, which is a submersible pump attached to the CTD profiler and deployed together with it by a winch. The pump provides water from a desired depth in the water column using a flexible and retractable plumbing system, which is deployed simultaneously with the CTD cable. In this study, we developed a system capable of sampling water from a maximum depth of 60 m, which is generally sufficient to investigate the variability of the carbonate system in both the mixing zone and the photic zone. A simplified scheme of the system installed in r/v *Oceania* is presented in Figure 1.

Our ambition was to develop a system that is inexpensive, transportable, and easy to implement on a variety of vessels, including smaller ones. The latter requires that the system can interoperate with any CTD profiler the vessel is equipped with. In our case, it was a Sea-Bird 19plus (Sea-Bird Electronics, Inc., Bellevue, Washington, USA) to which the submersible pump was attached, ensuring that the water inlets to both units were at the same depth to unify CTD readings with carbonate chemistry measurements. The submersible pump used in this prototype was a Pedrollo 3SR2/28 (www.pedrollo.com, San Bonitacio, Italy), with a deployment depth of approximately 60 m and an adjustable flow rate (through the power controller) between 10–50 L min^{-1} that may further depend on how high the water needs to be pumped above the ocean surface. This high water flow minimized the transport time to the laboratories and greatly exceeded the flow required for continuous pCO_2 measurements (approximately 0.8 L min^{-1}); therefore, excess water was bypassed, allowing for sampling of TA, DIC, and pH, as well as additional in-lab CTD measurements. All the pipes in the system had the same diameter, and narrow pipe connectors were avoided to elude overpressure. The flexible pipe system consisted of a commercially available Gardena Classic ¾" PVC cross-woven fabric hose (Gardena, www.gardena.com, Ulm, Germany), directly connecting the submersible pump to the ship's laboratories. The delay time, which is necessary for sampled water to be transported to laboratories, depends on the length of the hose deployed and the water flow. In our case, it was 19.5 seconds, calculated for a pipe length of 120 m and a water flow rate of 40 L min^{-1}. To minimise temperature changes during sampling, the hose system was not placed under direct sunlight or on warm surfaces. In the laboratories, four T-connectors equipped with flow regulators were installed to split the water flow to: (i) the equilibrator-based continuously measuring pCO_2 sys-

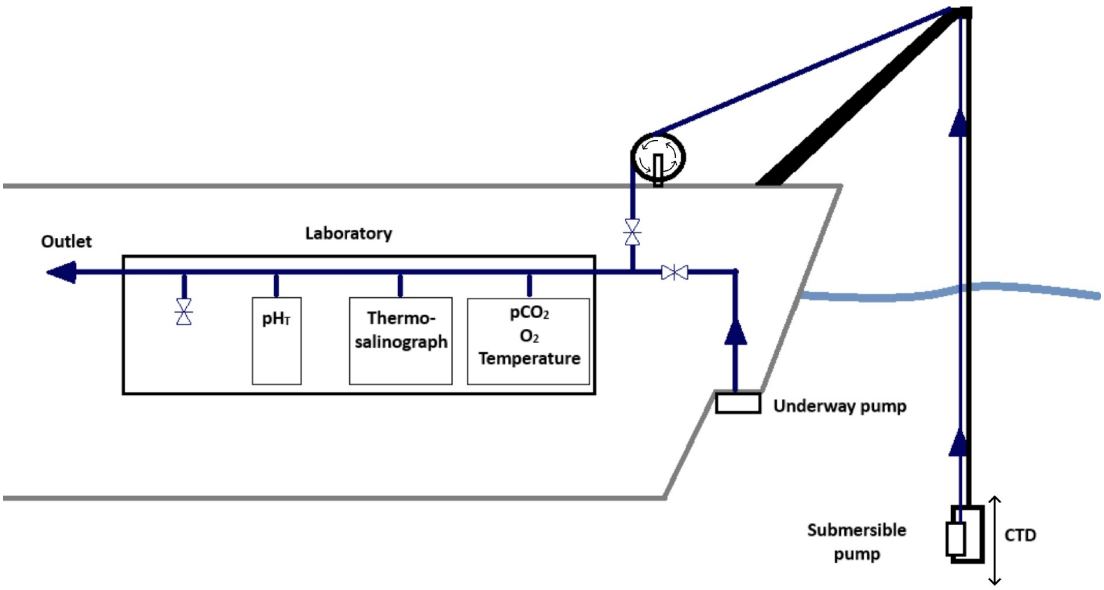

Figure 1. Simplified schematic representation of the carbonate profiler for a semi-continuous, precise sampling of the marine carbonate parameters in the water column.

tem, (ii) the flow-through thermosalinograph, (iii) the pH-spectrophotometer unit, and (iv) free-flowing water for collecting discrete samples for different analyses, in our case, DIC, TA, and in some cases also pH. Furthermore, additional valves enable immediate switching of the water source between the submersible PUMP-CTD and the ship's underway pumping system (having a water inlet at a fixed depth, 2.5 m on r/v *Oceania*), allowing the same laboratory equipment to be used for horizontal and vertical measurements (Figure 1). Importantly, the entire system consists of only quick connectors, making it easy to install, uninstall, and transport.

2.2 The laboratory instrumentation and analytical techniques

Measurements of pCO_2 were carried out using the system described in detail by Stokowski et al. (2021a). The system consists of a bubble-type equilibrator where the seawater flowing in is additionally sprayed using a shower diffuser. The air from the headspace flows along a closed loop through a cavity ring-down spectroscope (CRDS) G2101-I (Picarro). The quality of the measurements was regularly monitored using three gases with different CO_2 concentrations: 0, 205, and 507 ppm, which enabled achieving an accuracy and precision of $\pm$ 1.3 µatm. The effect of temperature changes during water transport from the PUMP-CTD to the laboratory has been corrected using the function proposed by Takahashi et al. (1993) (Eq. 1), so that the pCO_2 measured in the equilibrator, pCO_2(lab), was recalculated to the in situ temperature, pCO_2(in situ).

$$pCO_2(\text{in situ}) = pCO_2(\text{lab}) \times \exp(0.0423 \times (t_{(\text{in situ})} - t_{(\text{lab})})) \quad (1)$$

All pCO_2 measurements were also standardized to 1 atmosphere of pressure to remove the effect of atmospheric pressure changes in the final results, using Equation 2.

$$pCO_2(1\,\text{atm}) = pCO_2(\text{in situ}) \times 1012.25/P \quad (2)$$

The pH measurements were carried out on board using a HydroFIA flow-through spectrophotometric system (CONTROS, 4H-JENA engineering GmbH), directly connected to the carbonate profiler plumbing system. The pH was estimated spectrophotometrically using mCresolPurple as an indicator agent (Carter et al., 2013; Clayton and Byrne, 1993; Liu et al., 2015; Mosley et al., 2004). The accuracy of the pH measurements was ensured by routine measurements of TRIS-buffer (TRIS-CRM-T37) provided by A.G. Dickson (Scripps Institution of Oceanography, USA), which showed an accuracy/precision better than $\pm$ 0.003. All pH measurements were performed at 25°C, and the results were reported on the total scale.

The discrete water samples for analysis of TA and DIC were collected in 270 mL borosilicate glass bottles using the free-flowing bypassed water from the carbonate profiler. Samples were carefully poured from the bottom of the bottle to avoid air bubbles and left overflowing for at least 10 seconds. Next, 1 mL of the sample was removed to allow thermal expansion, and 100 µL of saturated $HgCl_2$ was added to inhibit/prevent biological activity. All the bottles were closed with greased ground-glass stoppers and stored in the dark at +4°C until analysis.

The TA was estimated using the methodology described in Dickson et al. (2003). Open cell titrations were carried out using a Methrom 888 Titrando, equipped with a 1mL burette. Total alkalinity was calculated from the potentiometric titration curves using version V23 of the Python package "Calkulate" (Humphreys and Matthews, 2024). The accuracy of the measurements was estimated by repeated measurements of Certified Reference Material (CRM) batch #CRM-209, provided by A.G. Dickson (Scripps Institution of Oceanography, USA). At least three measurements of CRM were done before and after the batch of samples until a precision better than $\pm$ 2 µmol kg^{-1} was achieved. Any deviation from the CRM values was corrected accordingly, and the accuracy correction was applied to a batch of samples. Each sample was measured in triplicate with a precision always better than $\pm$ 3 µmol kg^{-1}. The same methodology was applied to all samples. However, some were analyzed on board and others in the laboratories of the Institute of Oceanology, Polish Academy of Sciences (IO PAN), within a maximum time of four weeks.

The concentration of DIC was determined using an automated DIC analyzer (Apollo SciTech Inc.), equipped with a Li7815 CO_2 detector and following the methods described by Chen et al. (2015). All the measured samples were cross-calibrated with measurements of the CRMs (same as for TA), assuring an accuracy of $\pm$ 2 µmol kg^{-1} during the sample measurements. Each sample and CRM was measured at least three times until a precision better than $\pm$ 1.5 µmol kg^{-1} was achieved. All the measurements were carried out in the IO PAN laboratories within a maximum of four weeks after collection.

2.3 Calculations of the carbonate system parameters

Calculations of pCO_2 and estimations of the uncertainties related to the calculated values were carried out using the Excel version of the CO_2sys program (Pierrot et al., 2006), as published by Orr et al. (2018). For the calculations, the carbonic acid dissociation constants (K1 and K2) from Lueker et al. (2000) were used together with the $KHSO_4$ from Dickson et al. (1990), the fluoride dissociation constant of Perez and Fraga (1987), and the boron to chlorinity ratio of Lee et al. (2010). All calculations were reported to 1 atmosphere to minimize errors due to recalculations to in situ pressure. The uncertainties related to the dissocia-

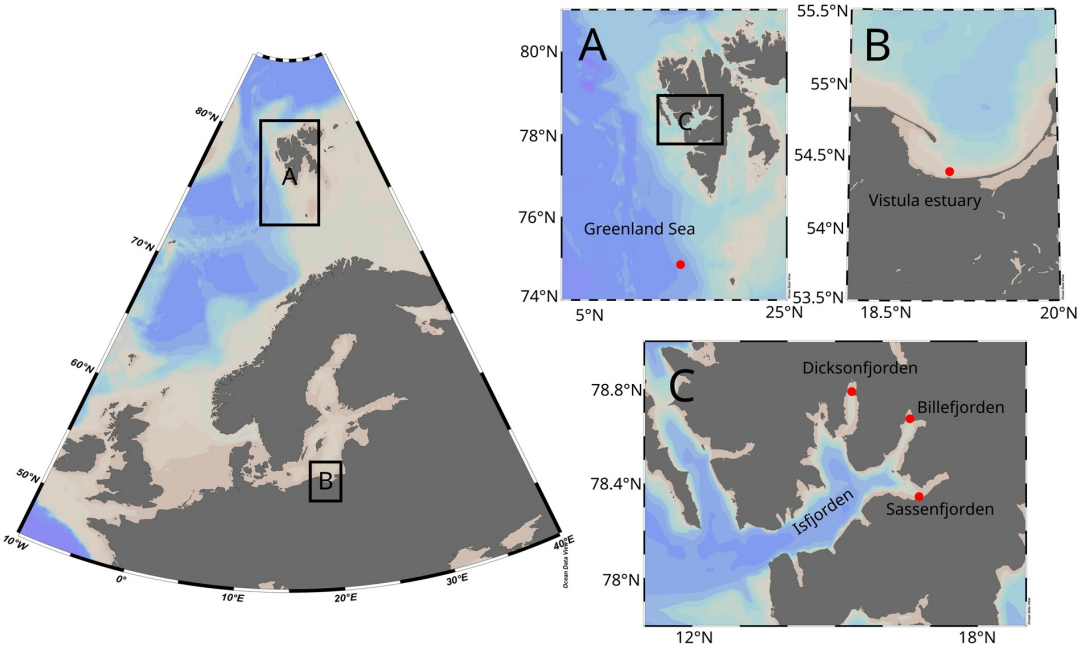

Figure 2. Location of the sampling stations (red dots). A) Greenland Sea. B) Baltic Sea. C) Svalbard fjords.

tion constants used in this study were extracted from Orr et al. (2018).

2.4 Sampling strategy and study area

For this study, sampling was conducted in three different areas, resulting in a total of eight water column profiles collected. Two study areas were located in stratified coastal systems (the Svalbard archipelago and the southern Baltic Sea), and one was located in the open waters of the Greenland Sea (Figure 2). The open ocean profile was sampled in July 2024 (74°59'58.2"N; 13°10'56.9"E), away from continental waters, where the marine CO_2 system is well characterized and where good consistency between measured and calculated values was expected based on previous studies (Aguado Gonzalo et al., 2024). These features enabled us to evaluate the sampling system's ability to simultaneously obtain thermodynamically coherent results for pCO_2, TA, and pH in the water column and verify the quality of the measured pCO_2 by comparing it with the pCO_2 calculated from TA and pH measurements.

In the coastal areas, the tests of the carbonate profiler have been performed in regions known for their highly stratified waters with sharp biogeochemical gradients. These sampling areas enabled us to evaluate the operability and capability of the carbonate profiler in resolving complex vertical variability. Four profiles were collected during spring 2024 within the Vistula River estuary (54°22'40.8"N; 18°55'30.0"E), located in the southern Baltic Sea (Figure 2). This region is characterized by the influence of TA-rich river waters and large gradients in the carbonate system parameters caused by the changing extent of the river plume and thus variable water stratification (Stokowski et al., 2021b). All four profiles were taken in the same location, but at six-hour intervals. The reason for that was to estimate the short-term variability of the carbonate system in the region and assess the reproducibility of the freshwater TA end member from the extrapolated dependency against salinity, which should be relatively conservative in such a short time period.

Additionally, three more profiles were obtained in August 2022 in the high Arctic fjords within the Svalbard archipelago (Figure 2). The sampling locations were selected in areas with a strong influence of freshwater turbid plumes. These plumes are produced by continental runoff, mainly fed by meltwater from land-terminating glaciers, and abrupt biogeochemical gradients are expected within the first 10 meters of the water column (e.g., Meslard et al., 2018; Szeligowska et al., 2020).

3. Results and discussion

3.1 Estimated quality of the carbonate profiler measurements

To demonstrate the system's capability to obtain accurate measurements of carbonate system variables in the water column, we compared measured and calculated (from pH and TA) values of pCO_2 in the oceanic waters of the Greenland Sea. These results, along with their uncertainties, are presented in Figure 3, which also shows the absolute differences between measured and calculated values, ΔpCO_2(meas-calc). Our results indicate that the first five samples collected in the water column (down to a water depth of 40 m) exhibited small variability (SD= $\pm$3.6 µatm) with an average measured pCO_2 of 308.8 µatm. On

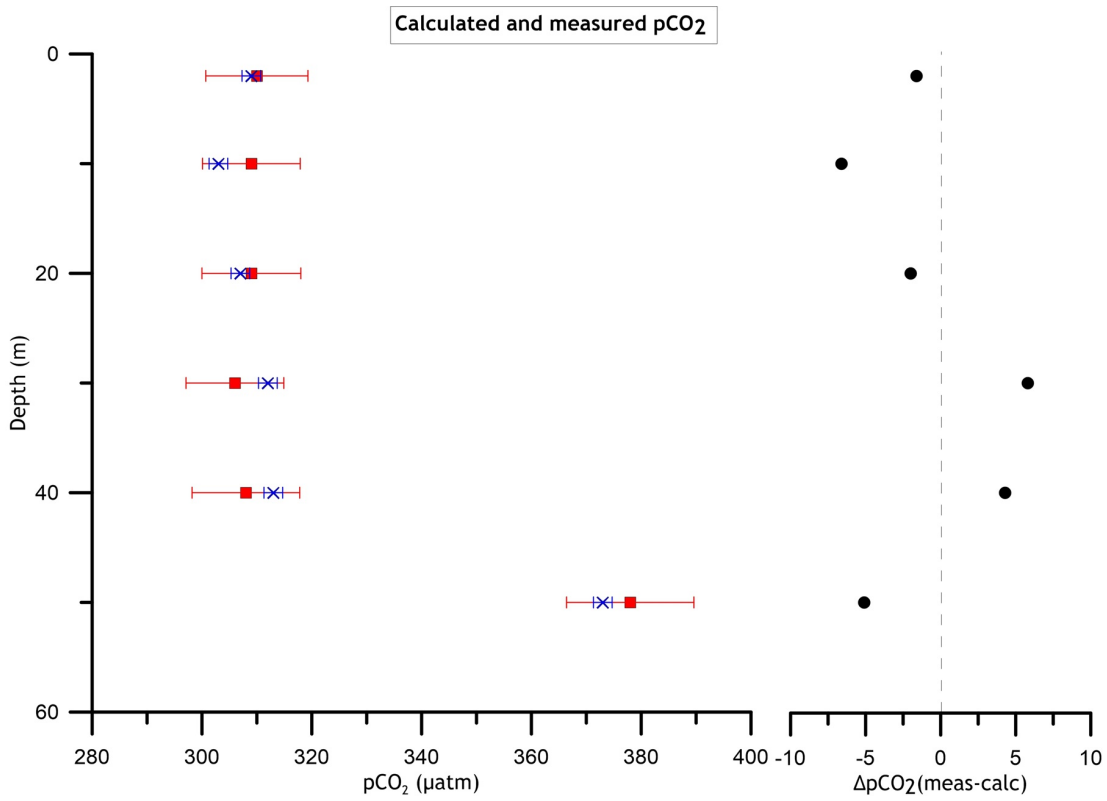

Figure 3. Left: measured (blue cross) and calculated (red square) pCO_2. The error bars indicate the uncertainty in the measured/calculated values. Right: the absolute differences between pCO_2 measured and calculated out of TA and pH.

the other hand, at a water depth of 50 m, the pCO_2 was significantly higher, amounting to 373 µatm, indicating a rapid increase of 64 µatm (Figure 3). The abrupt pCO_2 gradient between 50 and 60 m water depth was also successfully captured by TA and pH sampling, as indicated by the perfect agreement between the measured and calculated pCO_2 values. Hence, the ΔpCO_2(meas-calc) exhibited a low average of $\overline{x}(\mathrm{SD}) = 0.9(\pm 4.5)$ µatm, indicating an excellent performance of the carbonate profiler that enables consistent sampling of different carbonate system parameters despite differences in measurement methodologies requiring either continuous water flow or discrete sampling.

A similar exercise, as presented here, but using only surface data, was presented by Carter et al. (2024). In their study, the authors collected state-of-the-art surface open-ocean pCO_2, pH, and TA data from the Global Ocean Data Analysis Project 2022 update (GLODAPv2.2022) to estimate the (in)consistency between measured and calculated variables of the marine carbonate system. Their results show that the average of the relative difference between measured and calculated (from TA and pH) fCO_2 (fugacity of CO_2) was 1.8% of the measured fCO2 (equivalent to $\pm$ 5.6 µatm for 308.8 µatm). Following the calculation method described by Carter et al. (2024), we transferred our water column results to fCO_2 and presented them as a percentage of the measured value. Our results indicated a relative difference of 1.4 ($\pm$ 4.5 µatm), which is a better agreement than the one previously reported. Similarly to the study by Carter et al. (2024), but restricted to Arctic Oceanic surface waters, Woosley et al. (2017) and Aguado Gonzalo et al. (2024) reported discrepancies between measured and calculated pCO_2 of $\pm$ 5.3 and $\pm$ 5 µatm, respectively, which are slightly worse than the ones reported here ($\pm$ 4.5 µatm). Furthermore, the real observed uncertainty of $\pm$ 4.5 µatm for the difference between measured and calculated pCO_2 was significantly lower than the theoretical one ($\pm$ 9 µatm) derived from the propagation of all the initial uncertainties (see methods). This difference in the uncertainty suggests that any deviations in pCO_2 measured versus pCO2 calculated, ΔpCO_2(meas-calc), are solely due to uncertainties in the thermodynamic model of the marine CO_2 system, while the carbonate profiler guarantees high-quality, continuous pCO_2 measurements that are perfectly consistent with semi-continuous pH measurements and discrete sampling for TA.

This profile took about 25 minutes to complete in total. This time was a result of sampling at each depth and the time required to move the system between sampling levels. The time needed to obtain a complete set of results from a given depth was estimated based on the response time of the pCO_2 equilibrator, which was previously mea-

sured by Stokowski et al. (2021a), where the time to reach 63% of the equlibration (T63) was 68 seconds and an the effective equilibration time (T99) was 1 minute and 44 seconds (approx. 2 min). Thus, we maintained the PUMP-CTD for at least 3 minutes at each depth to ensure that measurements were taken after the equilibrium was reached. The excellent results from the consistency exercise demonstrated that this time was certainly sufficient to reach equilibrium. Based on calculations and earlier estimations by Stokowski et al. (2021a), we believe there is still room to optimize sampling time. Unfortunately, due to operational constraints of the open ocean cruise, no further tests were performed.

Nevertheless, the sampling time was satisfactorily short, especially since samples for additional parameters were taken in parallel. Commercially available submersible CO2 sensors offer a range of response times and effective measurement intervals. However, all of them are slower than the carbonate profiler, which allows easy adaptation of underway surface pCO2 measurement systems for water column sampling. For example, CO2 sensors based on pH indicators (e.g., Sunburst sensors, SAMI-CO_2) have a response time of approximately 5 minutes (Lai et al., 2018). In comparison, sensors based on non-dispersive infrared (NDIR) gas analyzers equipped with hydrophobic equilibration membranes (e.g., Pro-Oceanus Systems Inc. PSI CO_2-ProTM, C-Sense pCO_2, CONTROS HydroC CO_2) have typical measurement intervals and equilibration times of 10 to 15 minutes (Fietzek et al., 2014; Jiang et al., 2014; Schar et al., 2010b; Signori et al., 2021).

In addition to the higher sampling speed, the carbonate profiler system presented here shows excellent pCO2 measurement accuracy (reported above and by Stokowski et al. (2021a)), which is hardly achievable with submersible sensors. For instance, the SAMI-CO2 sensor was able to collect data with an accuracy of $+40 \pm 13$ µatm (x and SD) during a field test (Schar et al., 2010b). In the case of Pro-Oceanus Systems Inc. PSI CO2-ProTM, a similar test reported a $\bar{x}$ and SD of $+9 \pm 14$ µatm (Schar et al., 2010a), while Fietzek et al. (2014) reported an x and SD of -0.6 ± 3.0 µatm using a CONTROS HydroC CO_2.

To sum up, the high-quality water column pCO_2 results obtained in this study, along with the rapid sampling, including the possibility of collecting other carbonate system parameters in parallel, demonstrate the excellent performance of the carbonate profiler we designed, which is currently unachievable for sensor-based measurements on research vessels.

3.2 Performance of the carbonate profiler in highly stratified waters

3.2.1 Test 1: The mid-latitude estuary system of the Vistula River plume

The variability of TA, DIC, pH, and pCO_2, as well as salinity and temperature observed in the first 10 meters of the water column in the estuarine system of the Vistula River plume, is presented in Figure 4. In all the profiles, salinity and pCO_2 increased with depth, while pH, DIC, and TA decreased, indicating that the Vistula River water affecting this area had higher DIC, TA, and pH, and lower pCO_2. These results demonstrate that, thanks to the carbonate profiler, it was possible to resolve steep biogeochemical gradients, with ranges spanning up to 2050 µmol kg^{-1} for TA, approximately 1700 µmol kg^{-1} for DIC, 166 µatm for pCO_2, and 0.58 for pH, respectively. Herewith, DIC, TA and salinity were characterized by rapid changes within the first two meters of the water column and apparently varied among profiles, showing the spectrum of variability in riverine plume dynamics at a single location within the 24-hour sampling period. On the other hand, pCO_2 showed only slight changes within the first two meters, with comparable values between profiles (ranging from 217 to 246 µatm), suggesting strong primary production in the surface water layer, regardless of the scale of the Vistula River impact. Below this level, the pCO_2 increased significantly with depth, reaching values of up to 413 µatm at 10 m. Apart from being the first insight into the carbonate system structure in the water column of the region, these results clearly demonstrate the complexity and the vertical variability in stratified waters. Special attention should be paid to the vertical distribution of pCO_2, which highlights the importance of the sampling depth from which pCO_2 results are obtained for estimating air-sea CO_2 diffusive fluxes, a feature also discussed earlier by Ahmed et al. (2020) and Azevedo et al. (2024). Thus, underway pCO_2 measurements describing horizontal variability should always be combined with vertical profiling in stratified waters. For this, the carbonate profiler designed and described in this study provides an easy-to-use and low-cost solution that can significantly improve the estimation of air-sea CO_2 fluxes.

The relationship between TA and salinity exhibited a conservative behavior during sampling (Figure 5), with an excellent correlation ($R^2 = 0.98$). It demonstrates that the carbonate profiler attached to the CTD (PUMP-CTD) enabled the collection of water from a precise depth where salinity was measured, providing reliable vertical accuracy of sampling for carbonate system parameters. We took water samples at every half-meter interval in the first two meters of the water column and at every meter interval in the deeper water layer. This vertical resolution was sufficient to record the changes in the marine carbonate system parameters in the water column of this stratified area. However, the good correlation between salinity and TA suggests that even higher vertical resolution could be achieved. The freshwater TA end member estimated from the linear regression between salinity and TA collected for all four profiles amounted to 4069 µmol kg^{-1} (SD=12 µmol kg^{-1}). This value exceeds the previously reported range for the Vistula River (from 3136 to 3746 µmol kg^{-1}) by Stokowski

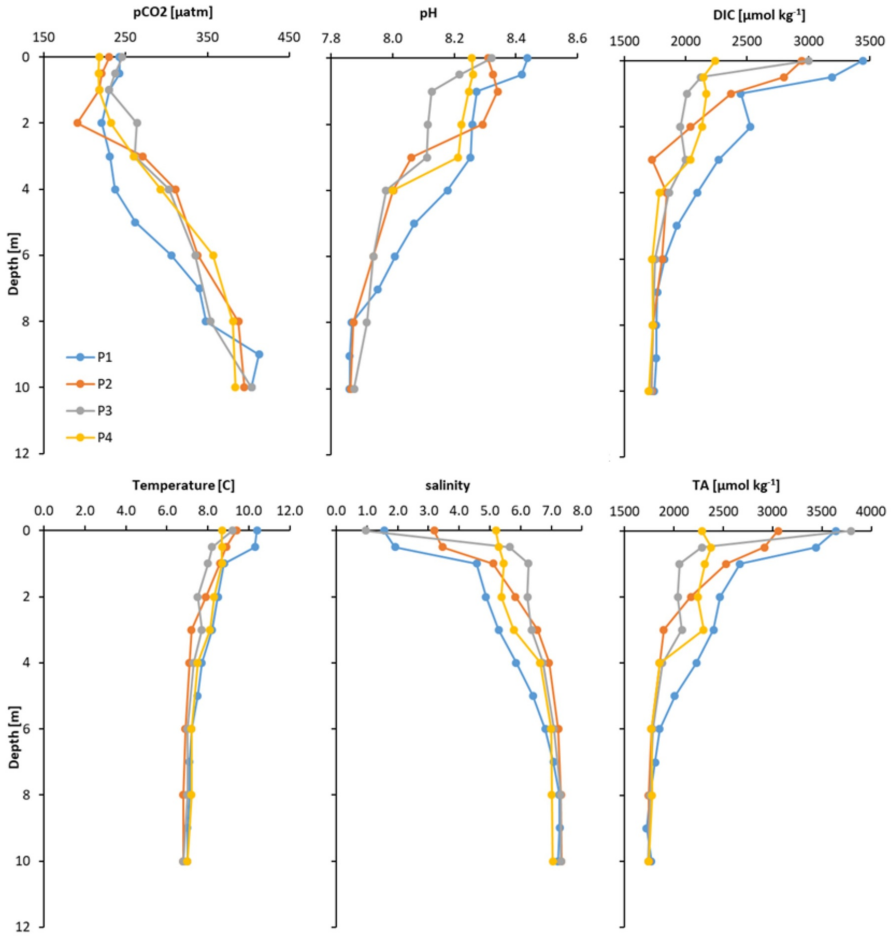

Figure 4. Vertical distribution of pCO2, pH, DIC, TA, temperature, and salinity during four samplings (P1–P4) performed in one spot in the Vistula River plume in 6-hour intervals.

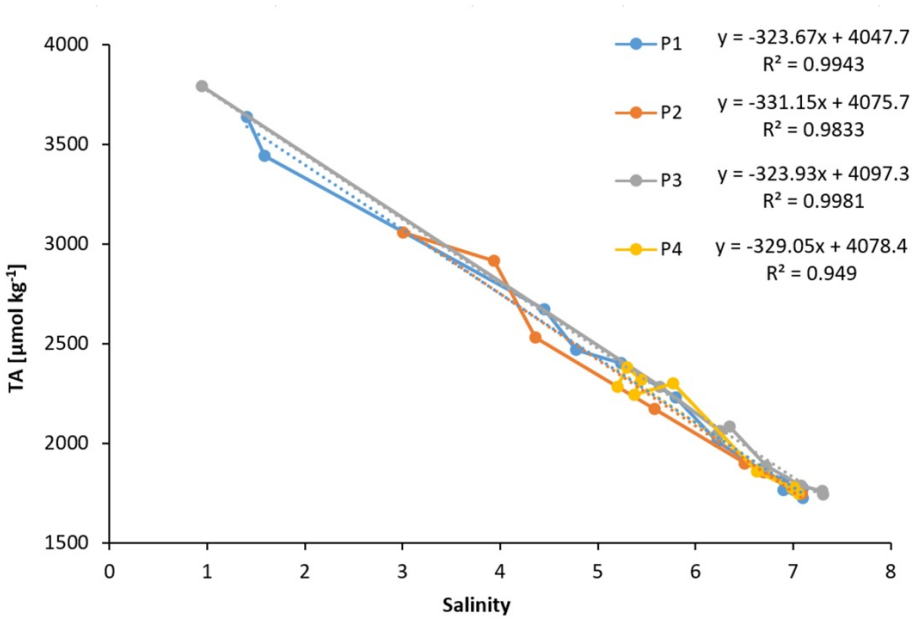

Figure 5. Linear correlation between salinity and TA during the four vertical profiles performed in one spot in the Vistula River plume at 6-hour intervals.

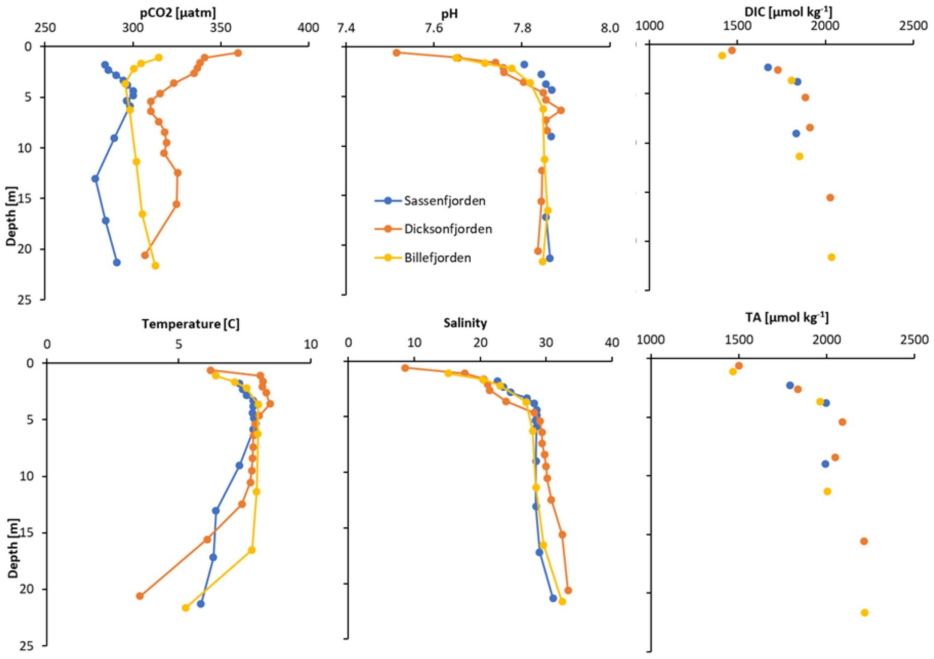

Figure 6. Vertical distribution of the marine carbonate system parameters (pCO2, pH, DIC, TA), temperature, and salinity in the three Spitsbergen fjords.

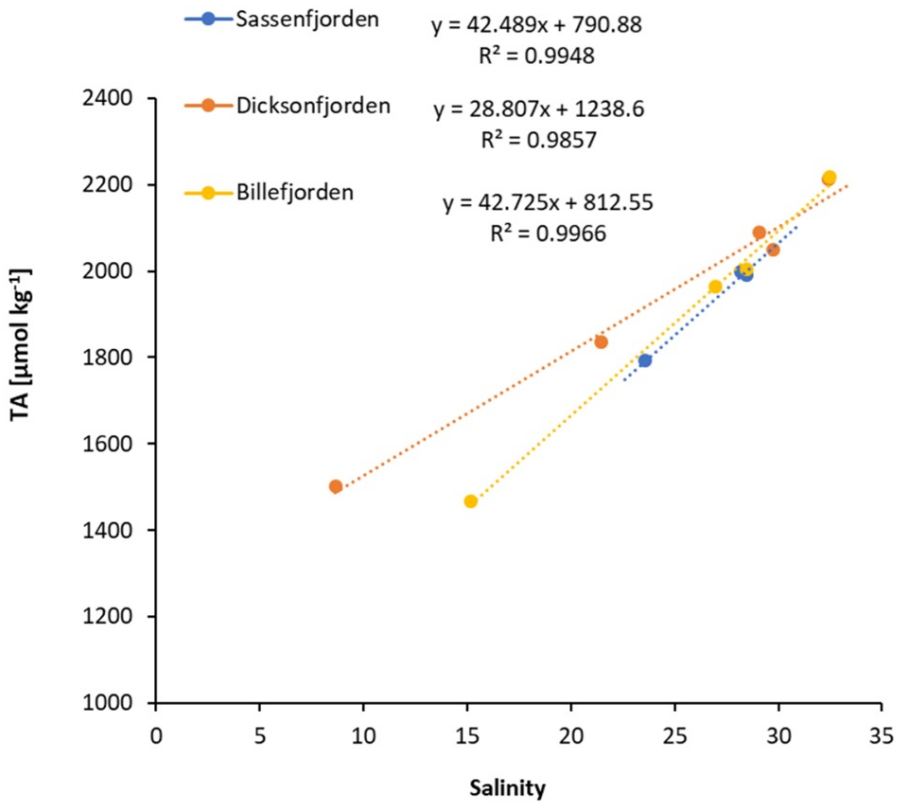

Figure 7. Linear correlation between salinity and TA collected using the carbonate profiler in the high-Arctic fjords of Sassenfjorden, Dicksonfjorden, and Billefjorden.

et al. (2021b), suggesting that the TA freshwater end member varies here in an even broader range than expected. This finding was possible thanks to the application of the carbonate profiler, which allowed for a precise sampling of the surface water layer (where the freshwater spreads) for carbonate system parameters, including TA. Although this result was achieved during operability tests of the carbonate profiler, it is an important contribution towards understanding the role of TA input from continental rivers (the Vistula River is the largest one) in mitigating Ocean Acidification in the Baltic Sea. At the same time, this very high freshwater TA end member (reported in this study for the first time for this region) indicates the need for further research in this area towards better resolving TA loads from the southern Baltic Sea catchment, which is in turn necessary to understand the alkalinity budget in the Baltic (Kuliński et al., 2022). All this demonstrates the utility of the carbonate profiler in resolving complex biogeochemical profiles in stratified waters and in obtaining accurate estimations of freshwater end-member properties by performing only a vertical profile in the vicinity of the estuaries.

3.2.2 Test 2: The turbid plumes of the Arctic fjords

The results from pCO_2, TA, DIC, pH, temperature, and salinity measurements at the three profiles collected within the turbid plumes in the fjord waters are presented in Figure 6. The sampling covered the first 20 meters of the water column in all the locations. The largest biogeochemical gradients, as reflected in all the measured parameters, were recorded in the surface water layer and were clearly related to the water freshening (see Figure 6). The measured salinity varied significantly across all profiles (ranging from 8.66 to 33.31), increasing from the surface to the deeper waters. Out of this range, most of the variability (79% in the Diksonfjorden profile, 74% in Billefjorden, and 71% in Sassenfjorden) occurred in the upper 5 m of the water column. Along with salinity changes, TA, DIC, pCO_2, and pH also exhibited the strongest variation in the uppermost layer. However, in contrast to the Vistula River plume, the freshwater inflow to the fjords diluted the seawater with respect to DIC and TA, which had a pronounced effect on decreasing surface pH, thus enhancing Ocean Acidification in the region.

The abrupt gradients measured in the surface layer of the water column with the vertical variance of TA, DIC, pH, and pCO_2 of up to 588 µmol kg^{-1}, 416 µmol kg^{-1}, 0.34, and 44 µatm, respectively, result from the outflow of turbid water plumes formed in the land-ocean transitional zone (Meslard et al., 2018; Szeligowska et al., 2020). These turbid water plumes usually cover only the first meters of the water column, creating steep biogeochemical gradients that the carbonate profiler has successfully recorded. This seemingly simple task would be unapproachable when using other sampling methods, such as a bathometer. In fact, if we were to collect water from 1 m depth using a 1 m long bathometer, we would collect water from a depth between 0.5 m and 1.5 m. Considering the variability identified in Dicksonfjorden (Figure 6), the water inside the bathometer would have a pH range of 7.51 at the top to 7.74 at the bottom. Thus, measured pH (and any other parameter) would vary significantly depending on the water subsample within the bathometer volume. In contrast, the carbonate profiler offers a straightforward tool for investigating steep biogeochemical gradients by collecting water samples and measuring in situ parameters (e.g., salinity, temperature, turbidity, fluorescence) with a significantly higher vertical resolution. For example, in this exercise, a resolution of 0.5 m was easily achieved.

As shown already for the Vistula River plume (section 5.2.1), it is possible to use the vertical variability of TA and salinity to estimate the TA concentration in freshwater end members with great accuracy. In Spitsbergen fjords, the relationships between TA and salinity revealed different freshwater TA in different fjords, namely 791 µmol kg^{-1} in Sassenfjorden, 813 µmol kg^{-1} in Billefjorden, and 1239 µmol kg^{-1} in Dicksonfjorden (Figure 7). These concentrations fall within the range of previously reported values for Svalbard fjords, which range from 232 to 1412 µmol kg^{-1} (Ericson et al., 2018; Fransson et al., 2015; Koziorowska-Makuch et al., 2023). All this data, including this study, proves that continental runoff in Arctic fjords reduces the TA in surface waters and thus lowers its capacity to absorb atmospheric CO_2 and enhances Ocean Acidification.

Moreover, the measured pCO2 in surface waters (Figure 6) was higher in Dicksonfjorden (360 µatm) and Billefjorden (314 µatm) than in the deeper water layer (approx. 303 µatm), but in Sassenfjorden, the surface pCO_2 was lower (284 µatm). These significant changes may be attributed to the different freshwater sources that influence the fjords. While Dicksonfjorden and Billefjorden are both heavily glaciated catchments, Sassenfjorden is primarily influenced by Sassenelva, a river that drains a permafrost-rich valley (McGovern et al., 2020). Overall, the carbonate profiler allowed us to highlight the complex stratification patterns in the Arctic fjords, which have a direct impact on biogeochemical changes and the structure of the marine carbonate system. Moreover, the data show that continental runoff in the Svalbard archipelago enhances ocean acidification in coastal areas, where its surface waters have a lower capacity to uptake atmospheric CO_2.

4. Conclusion

In this study, we designed a low-cost and easy-to-set-up upper water column sampler that can be easily incorporated into measurement systems on research vessels (and beyond). Combined with the ship's CTD profiler, they form a PUMP-CTD system that can be easily deployed on a variety of vessels regardless of their size and technical sophistication. Just by switching the water source to this PUMP-CTD, it can be used to feed the commonly used systems for

equilibrator-based continuous pCO_2 measurements (typically using the ship's pumping system having the water inlet at a Vfixed depth between 2 and 10 m) and extend their applicability also towards the water column sampling, including the precise sampling of the surface water layer. This is of great importance for accurately measuring seawater pCO_2 at the surface in stratified coastal water bodies (having often strong vertical biogeochemical gradients), which are to be used further for air/sea CO_2 flux calculations. As the water supply from the submersible pump is sufficient to be split, in addition to supplying the equilibrator-based continuous pCO_2 measurements, it also serves other receivers. The system allows for precise sampling of the full set of marine carbonate system parameters, namely TA, DIC, pH, and pCO_2. This feature is extremely useful in coastal waters, which, due to ion anomalies and the significant influence of non-parameterized acid-base constituents of seawater, often require a complete set of data on the structure of the marine carbonate system – a requirement that is considered excessive in open ocean waters.

The test performed in the open waters of the Greenland Sea shows that the system was able to obtain rapid and more accurate pCO_2 measurements in the water column than any other commercial method. Measurements of pCO_2 in the estuarine system of the Baltic Sea and the Spitsbergen fjords show that measurements using the carbonate profiler can be utilized as an easy tool to obtain the vertical distribution of pCO_2, including near-surface results, and thus improve estimations of air-sea CO_2 fluxes in stratified regions. The profiles also demonstrate an excellent capacity to obtain, in parallel with the continuous pCO_2 measurements, automated or discrete pH measurements and discrete samples for TA and DIC, with excellent correlation to in situ measured parameters. We also demonstrated the carbonate profiler's applicability in obtaining accurate estimations of the freshwater end-members' properties by only performing a vertical profile in the vicinity of the estuaries. For this, we used the correlation between precisely sampled TA and in situ salinity. The results from the Baltic Sea showed not only an excellent correlation in the four profiles ($R2 = 0.98$) but also a good reproducibility, i.e., the freshwater TA of 4069 µmol kg^{-1} estimated with the variation of only ± 12 µmol kg^{-1} (less than 1% of the estimated value). These TA results confirm the important role of the Vistula River as a net source of TA for the Baltic and reveal very high TA concentrations in the Vistula River that have not been reported before for this region. A similar utility of the carbonate profiler has been observed for the Spitsbergen fjords. However, the estimated TA freshwater end members were much lower and highly variable between the individual fjords (ranging from 790 to 1240 µmol kg^{-1}). Still, all of them demonstrated that the continental runoff in the Svalbard archipelago lowers the buffer capacity of the seawater, reduces its potential to uptake atmospheric CO_2, and enhances Ocean Acidification. To sum up, the carbonate profiler we designed represents an easy-to-implement and low-cost tool allowing the scientific community to obtain state-of-the-art measurements of all the marine carbonate parameters with a vertical resolution better than 0.5 meters, and providing new possibilities for observations and quantifications of ocean acidification, carbon inventory, and air-sea CO_2 fluxes in highly stratified environments.

Data availability

The data presented in this study are publicly available in the online data repositories of GeoNetwork (Aguado Gonzalo et al., 2025b; https://doi.org/10.48457/IOPAN.2025.515).

Funding sources

The author(s) declare that financial support was received for the research, authorship, and/or publication of this article. The study was conducted within the framework of Grant No. 2019/34/E/ST10/00167 (Arctic data), 2021/41/B/ST10/00946 (Baltic Sea pCO2 data), and 2023/49/B/ST10/02690 (TA, DIC, and pH data); all three of them financed by the Polish National Science Centre. The interpretation of the results in terms of their contextualization was supported by the European Union's Horizon Europe research and innovation programme under Grant Agreement No. 101136480 (SEA-Quester).

Authors contribution

Author contributions: CRediT FG: Conceptualization, Methodology, Writing – review & editing, Data curation, Formal analysis, Investigation, Methodology, Visualization, Writing – original draft. KKo: Data curation, Writing – review & editing. LB: Data curation. AL: Writing – review & editing. KKu: Conceptualization, Methodology, Funding acquisition, Project administration, Supervision, Validation, Writing – review & editing.

Acknowledgments

We would like to thank the captain and crew of the r/v *Oceania* for their enthusiasm and support throughout the sampling process, as well as the manuscript reviewers for their valuable comments.

Conflict of interest

None declared.

References

Aguado Gonzalo, F., Koziorowska, K., Szymczycha, B., Kuliński, K., 2025. *The Consistency between Calculated*

and Measured Variables of the Marine Carbonate System in Arctic Open and Coastal Waters. Mar. Chem. (pre-print).
https://doi.org/10.2139/ssrn.5205880

Aguado Gonzalo, F., Koziorowska, K., Bromboszcz-Szczypior, L., Kulinski, K., 2025b. *High resolution, vertical distribution of the marine carbonate system in estuarine waters of the Baltic Sea and Arctic fjords (Svalbard Archipelago)*. [Dataset]. Geonetwork.
https://doi.org/10.48457/IOPAN.2025.515

Aguado Gonzalo, F., Stokowski, M., Koziorowska-Makuch, K., Makuch, P., Beszczyńska-Möller, A., Kukliński, P., Kuliński, K., 2024. *Key processes controlling the variability of the summer marine CO2 system in Fram Strait surface waters*. Front. Mar. Sci. 11, 1–19.
https://doi.org/10.3389/fmars.2024.1464653

Ahmed, M.M.M., Else, B.G.T., Capelle, D., Miller, L.A., Papakyriakou, T., 2020. *Underestimation of surface pCO2 and air-sea CO2 fluxes due to freshwater stratification in an Arctic shelf sea, Hudson Bay*. Elementa 8.
https://doi.org/10.1525/elementa.084

Arruda, R., Atamanchuk, D., Cronin, M., Steinhoff, T., Wallace, D.W.R., 2020. *At-sea intercomparison of three underway pCO2 systems*. Limnol. Oceanogr. Methods 18, 63–76.
https://doi.org/10.1002/lom3.10346

Azevedo, C.C., González-Dávila, M., Santana-Casiano, J.M., González-Santana, D., Caldeira, R.M.A., 2024. *Impact of sampling depth on CO2 flux estimates*. Sci. Rep. 14, 1–9.
https://doi.org/10.1038/s41598-024-69177-x

Bauer, J.E., Cai, W.J., Raymond, P.A., Bianchi, T.S., Hopkinson, C.S., Regnier, P.A.G., 2013. *The changing carbon cycle of the coastal ocean*. Nature 504, 61–70.
https://doi.org/10.1038/nature12857

Bresnahan, P.J., Martz, T.R., Takeshita, Y., Johnson, K.S., LaShomb, M., 2014. *Best practices for autonomous measurement of seawater pH with the Honeywell Durafet*. Methods Oceanogr. 9, 44–60.
https://doi.org/10.1016/j.mio.2014.08.003

Cai, W.J., 2011. *Estuarine and coastal ocean carbon paradox: CO2 sinks or sites of terrestrial carbon incineration?* Ann. Rev. Mar. Sci. 3, 123–145.
https://doi.org/10.1146/annurev-marine-120709-142723

Carter, B.R., Radich, J.A., Doyle, H.L., Dickson, A.G., 2013. *An automated system for spectrophotometric seawater pH measurements*. Limnol. Oceanogr. Methods 11, 16–27.
https://doi.org/10.4319/lom.2013.11.16

Carter, B.R., Sharp, J.D., García-ib, M.I., Woosley, R.J., Fong, M.B., Alvarez, M., Barbero, L., Clegg, S.L., Easley, R., Fassbender, A.J., Li, X., Schockman, K.M., Wang, Z.A., 2024., *Review Random and systematic uncertainty in ship-based seawater carbonate chemistry observations*, 1–16.
https://doi.org/10.1002/lno.12674

Chen, B., Cai, W.J., Chen, L., 2015. *The marine carbonate system of the Arctic Ocean: Assessment of internal consistency and sampling considerations, summer 2010*. Mar. Chem. 176, 174–188.
https://doi.org/10.1016/j.marchem.2015.09.007

Clarke, J.S., Achterberg, E.P., Connelly, D.P., Schuster, U., Mowlem, M., 2017. *Developments in marine pCO2 measurement technology; towards sustained in situ observations*. TrAC – Trends Anal. Chem. 88, 53–61.
https://doi.org/10.1016/j.trac.2016.12.008

Clayton, T.D., Byrne, R.H., 1993. *Spectrophotometric seawater pH measurements: total hydrogen ion concentration scale calibration of m-cresol purple and at-sea results*. Deep. Res. Pt. I 40, 2115–2129.
https://doi.org/10.1016/0967-0637(93)90048-8

Cross, J.N., Mathis, J.T., Pickart, R.S., Bates, N.R., 2018. *Formation and transport of corrosive water in the Pacific Arctic region*. Deep. Res. Pt. II Top. Stud. Oceanogr. 152, 67–81.
https://doi.org/10.1016/j.dsr2.2018.05.020

Dai, M., Su, J., Zhao, Y., Hofmann, E.E., Cao, Z., Cai, W.J., Gan, J., Lacroix, F., Laruelle, G.G., Meng, F., Mudieller, J.D., Regnier, P.A.G., Wang, G., Wang, Z., 2022. *Carbon Fluxes in the Coastal Ocean: Synthesis, Boundary Processes, and Future Trends*. Annu. Rev. Earth Planet. Sci. 50, 593–626.
https://doi.org/10.1146/annurev-earth-032320-090746

Dickson, A.G.; Sabine, C.L. and Christian, J.R., 2007. *Guide to best practices for ocean CO2 measurement*. Sidney, British Columbia, North Pacific Marine Science Organization, 191 pp. (PICES Special Publication 3; IOCCP Report 8).
https://doi.org/10.25607/OBP-1342

Dickson, A.G., 1981. *An exact definition of total alkalinity and a procedure for the estimation of alkalinity and total inorganic carbon from titration data*. Deep Sea Res. Pt. A, Oceanogr. Res. Pap. 28, 609–623.
https://doi.org/10.1016/0198-0149(81)90121-7

Dickson, A.G., Afghan, J.D., Anderson, G.C., 2003. *Reference materials for oceanic CO2 analysis: A method for the certification of total alkalinity*. Mar. Chem. 80, 185–197.
https://doi.org/10.1016/S0304-4203(02)00133-0

Dickson, A.G., Wesolowski, D.J., Palmer, D.A., Mesmer, R.E., 1990. *Dissociation constant of bisulfate ion in aqueous sodium chloride solutions to 250°C*. J. Phys. Chem. 94, 7978–7985.
https://doi.org/10.1021/j100383a042

Ericson, Y., Falck, E., Chierici, M., Fransson, A., Kristiansen, S., Platt, S.M., Hermansen, O., Myhre, C.L., 2018. *Temporal Variability in Surface Water pCO2 in Adventfjorden (West Spitsbergen) With Emphasis on Physical and Biogeochemical Drivers*. J. Geophys. Res. Ocean. 123, 4888–4905.

https://doi.org/10.1029/2018JC014073

Fietzek, P., Fiedler, B., Steinhoff, T., Körtzinger, A., 2014. *In situ quality assessment of a novel underwater pCO 2 sensor based on membrane equilibration and NDIR spectrometry*. J. Atmos. Ocean. Technol. 31, 181–196. https://doi.org/10.1175/JTECH-D-13-00083.1

Fransson, A., Chierici, M., Nomura, D., Granskog, M.A., Kristiansen, S., Martma, T., Nehrke, G., 2015. *Effect of glacial drainage water on the CO2 system and ocean acidification state in an Arctic tidewater-glacier fjord during two contrasting years*. J. Geophys. Res. Ocean. https://doi.org/10.1002/2014JC010320

Friedlingstein, P., O'Sullivan, M., Jones, M.W., Andrew, R.M., Hauck, J., Landschützer, P., Le Quéré, C., Li, H., Luijkx, I.T., Olsen, A., Peters, G.P., 2025. *Global carbon budget*. Earth Syst. Sci. Data 17, 965–1039. https://doi.org/10.5194/essd-17-965-2025

Humphreys, M. P. and Matthews, R. S. 2024. *Calkulate: total alkalinity from titration data in Python*. Zenodo. https://doi.org/10.5281/zenodo.2634304

Jiang, Z.P., Hydes, D.J., Hartman, S.E., Hartman, M.C., Campbell, J.M., Johnson, B.D., Schofield, B., Turk, D., Wallace, D., Burt, W.J., Thomas, H., Cosca, C., Feely, R., 2014. *Application and assessment of a membrane-based pCO2 sensor under field and laboratory conditions*. Limnol. Oceanogr. Methods 12, 264–280. https://doi.org/10.4319/lom.2014.12.264

Johengen, T., Smith, G.J., Schar, D., Atkinson, M., Purcell, H., Loewensteiner, D., Epperson, Z., Tamburri, M., 2015. *Performance Verification Statement for the Sunburst SAMI-pH Sensor*. Solomons, MD, Alliance for Coastal Technologies, 63 pp. (ACTVS15-06). http://doi.org/10.25607/OBP-306

Kerr, D.E., Turner, C., Grey, A., Keogh, J., Brown, P.J., Kelleher, B.P., 2023. *OrgAlkCalc: Estimation of organic alkalinity quantities and acid-base properties with proof of concept in Dublin Bay*. Mar. Chem. 251, 104234. https://doi.org/10.1016/j.marchem.2023.104234

Koziorowska-Makuch, K., Szymczycha, B., Thomas, H., Kuliński, K., 2023. *The marine carbonate system variability in high meltwater season (Spitsbergen Fjords, Svalbard)*. Prog. Oceanogr. 211. https://doi.org/10.1016/j.pocean.2023.102977

Kuliński, K., Hammer, K., Schneider, B., Schulz-Bull, D., 2016. *Remineralization of terrestrial dissolved organic carbon in the Baltic Sea*. Mar. Chem. 181, 10–17. https://doi.org/10.1016/j.marchem.2016.03.002

Kuliński, K., Rehder, G., Asmala, E., Bartosova, A., Carstensen, J., Gustafsson, B., Hall, P.O.J., Humborg, C., Jilbert, T., Jürgens, K., Meier, H.E.M., Müller-Karulis, B., Naumann, M., Olesen, J.E., Savchuk, O., Schramm, A., Slomp, C.P., Sofiev, M., Sobek, A., Szymczycha, B., Undeman, E., 2022. *Biogeochemical functioning of the Baltic Sea*. Earth Syst. Dynam. 13, 633–685. https://doi.org/10.5194/esd-13-633-2022

Kuliński, K., Schneider, B., Szymczycha, B., Stokowski, M., 2017. *Structure and functioning of the acid-base system in the Baltic Sea*. Earth Syst. Dynam. 8, 1107–1120. https://doi.org/10.5194/esd-8-1107-2017

Lai, C.Z., DeGrandpre, M.D., Darlington, R.C., 2018. *Autonomous optofluidic chemical analyzers for marine applications: Insights from the Submersible Autonomous Moored Instruments (SAMI) for pH and pCO2*. Front. Mar. Sci. 4, 1–11. https://doi.org/10.3389/fmars.2017.00438

Lee, K., Kim, T.W., Byrne, R.H., Millero, F.J., Feely, R.A., Liu, Y.M., 2010. *The universal ratio of boron to chlorinity for the North Pacific and North Atlantic oceans*. Geochim. Cosmochim. Acta 74, 1801–1811. https://doi.org/10.1016/j.gca.2009.12.027

Lewis, E., Wallace, D., and Allison, L. J., 1998. Program developed for CO2 system calculations (TN (United States: Brookhaven Natl. Lab., Dept. Appl. Sci., Upton, NY; Oak Ridge Natl. Lab., Carbon Dioxide Information Analysis Center). No. ORNL/CDIAC-105).

Liu, P., He, S., Wei, H., Wang, J., Sun, C., 2015. *Characterization of α-Fe2O3/γ-Al2O3 catalysts for catalytic wet peroxide oxidation of m-Cresol*. Ind. Eng. Chem. Res. 54, 130–136. https://doi.org/10.1021/ie5037897

Lueker, T.J., Dickson, A.G., Keeling, C.D., 2000. *Ocean pCO2 calculated from dissolved inorganic carbon, alkalinity, and equations for K1 and K2: validation based on laboratory measurements of CO2 in gas and seawater at equilibrium*. Marine Chem. 70(1–3), 105–119.

McGovern, M., Pavlov, A.K., Deininger, A., Granskog, M.A., Leu, E., Søreide, J.E., Poste, A.E., 2020. *Terrestrial Inputs Drive Seasonality in Organic Matter and Nutrient Biogeochemistry in a High Arctic Fjord System (Isfjorden, Svalbard)*. Front. Mar. Sci. 7, 1–15. https://doi.org/10.3389/fmars.2020.542563

Meslard, F., Bourrin, F., Many, G., Kerhervé, P., 2018. *Suspended particle dynamics and fluxes in an Arctic fjord (Kongsfjorden, Svalbard)*. Estuar. Coast. Shelf Sci. 204, 212–224. https://doi.org/10.1016/j.ecss.2018.02.020

Millero, F.J., 2007. *The marine inorganic carbon cycle*. Chem. Rev. 107, 308–341. https://doi.org/10.1021/cr0503557

Mosley, L.M., Husheer, S.L.G., Hunter, K.A., 2004. *Spectrophotometric pH measurement in estuaries using thymol blue and m-cresol purple*. Mar. Chem. 91, 175–186. https://doi.org/10.1016/j.marchem.2004.06.008

Mosley, L.M., Liss, P.S., 2020. *Particle aggregation, pH changes and metal behaviour during estuarine mixing: Review and integration*. Mar. Freshw. Res. 71, 300–310. https://doi.org/10.1071/MF19195

Orr, J.C., Epitalon, J.M., Dickson, A.G., Gattuso, J.P., 2018. *Routine uncertainty propagation for the marine carbon*

dioxide system. Mar. Chem. 207, 84–107. https://doi.org/10.1016/j.marchem.2018.10.006

Perez, F.F., Fraga, F., 1987. *Association constant of fluoride and hydrogen ions in seawater*. Mar. Chem. 21, 161–168. https://doi.org/10.1016/0304-4203(87)90036-3

Pierrot, D., Lewis, E., Wallace, D.W.R., 2006. *MS Excel Program Developed for CO2 System Calculations*. Tech. Rep. Carbon Dioxide Inf. Anal. Cent. Oak Ridge Natl. Lab., U.S. DOE, Oak Ridge, Tenn.

Regnier, P., Resplandy, L., Najjar, R.G., Ciais, P., 2022. *The land-to-ocean loops of the global carbon cycle*. Nature 603, 401–410. https://doi.org/10.1038/s41586-021-04339-9

Resplandy, L., Keeling, R.F., Rödenbeck, C., Stephens, B.B., Khatiwala, S., Rodgers, K.B., Long, M.C., Bopp, L., Tans, P.P., 2018. *Revision of global carbon fluxes based on a reassessment of oceanic and riverine carbon transport*. Nat. Geosci. 11, 504–509. https://doi.org/10.1038/s41561-018-0151-3

Schar, D., Atkinson, M., Johengen, T., Pinchuk, A., Purcell, H., Robertson, C., Smith, G.J., 2010a. Pro-Oceanus Systems Inc. PSI CO2-Pro TM. Situ 1–24.

Schar, D., Atkinson, M., Johengen, T., Pinchuk, A., Purcell, H., Robertson, C., Smith, G.J., Tamburri, M., 2010b. *Performance Demonstration Statement Sunburst Sensors SAMI-CO sub(2)*. ACT Technol. Eval. Reports DS10-04, 1–23.

Signori, R.T., de Souza, S.A., Ferreira, R.B., da Silva, J.T., de Andrade, A.M.D., dos Reis, G.C.G., 2021. *Data acquisiton and transmission system for carbon dioxide analysis*. Rev. Bras. Meteorol. 36, 115–123. https://doi.org/10.1590/0102-77863610003

Stokowski, M., Makuch, P., Rutkowski, K., Wichorowski, M., Kuliński, K., 2021a. *A system for the determination of surface water pCO2 in a highly variable environment, exemplified in the southern Baltic Sea*. Oceanologia 63(2), 276–282. https://doi.org/10.1016/j.oceano.2021.01.001

Stokowski, M., Winogradow, A., Szymczycha, B., Carstensen, J., Kuliński, K., 2021b. *The CO2 system dynamics in the vicinity of the Vistula River mouth (the southern Baltic Sea): A baseline investigation*. Estuar. Coast. Shelf Sci. 258, 2–11. https://doi.org/10.1016/j.ecss.2021.107444

Strady, E., Pohl, C., Yakushev, E. V., Krüger, S., Hennings, U., 2008. *PUMP-CTD-System for trace metal sampling with a high vertical resolution. A test in the Gotland Basin, Baltic Sea*. Chemosphere 70, 1309–1319. https://doi.org/10.1016/j.chemosphere.2007.07.051

Szeligowska, M., Trudnowska, E., Boehnke, R., Dąbrowska, A.M., Wiktor, J.M., Sagan, S., Błachowiak-Samołyk, K., 2020. *Spatial Patterns of Particles and Plankton in the Warming Arctic Fjord (Isfjorden, West Spitsbergen) in Seven Consecutive Mid-Summers (2013–2019)*. Front. Mar. Sci. 7, 1–18. https://doi.org/10.3389/fmars.2020.00584

Takahashi, T., Olafsson, J., Goddard, J.G., Chipman, D.W., Sutherland, S.C., 1993. *Seasonal variation of CO2 and nutrients in the high-latitude oceans: A comparative study*. Global Biogeochem. Cycles 7, 843–878.

Ulfsbo, A., Kuliński, K., Anderson, L.G., Turner, D.R., 2015. *Modelling organic alkalinity in the Baltic Sea using a Humic-Pitzer approach*. Mar. Chem. 168, 18–26. https://doi.org/10.1016/j.marchem.2014.10.013

Woosley, R.J., Millero, F.J., Takahashi, T., 2017. *Internal consistency of the inorganic carbon system in the Arctic Ocean*. Limnol. Oceanogr. Methods 15, 887–896. https://doi.org/10.1002/lom3.10208

Statement of co-authors

Sopot, 18/03/2026

MSc Fernando Aguado Gonzalo

Institute of Oceanology of the Polish Academy of Sciences

Laboratory of marine biogeochemistry

Author contribution statement

I declare that my contribution to the publication:

Gonzalo, F. A., Koziorowska, K., Bromboszcz-Szczypior, L., Loginova, A., & Kuliński, K. (2026). High vertical resolution measurements of pH, pCO 2, Total Alkalinity and Dissolved Inorganic Carbon using a new approach: the carbonate profile. Oceanologia, 68(1), 68101.

Involved: Conceptualization, Methodology, Writing– review & editing, Data curation, Formal analysis, Investigation, Methodology, Visualization, Writing– original draft.

and accounted for 70% of the total work needed for the realization of this publication.

Sopot, 18/03/2026

Dr Katarzyna Koziorowska

Institute of Oceanology of the Polish Academy of Sciences

Laboratory of marine biogeochemistry

Author contribution statement

I declare that my contribution to the publication:

Gonzalo, F. A., Koziorowska, K., Bromboszcz-Szczypior, L., Loginova, A., & Kuliński, K. (2026). High vertical resolution measurements of pH, pCO 2, Total Alkalinity and Dissolved Inorganic Carbon using a new approach: the carbonate profile. Oceanologia, 68(1), 68101.

Involved: Data curation, Writing– review &editing.

and accounted for 5% of the total work needed for the realization of this publication.

Katarzyna Koziorowska

Sopot, 18/03/2026

MSc Laura Bromboszcz-Szczypior

Institute of Oceanology of the Polish Academy of Sciences

Laboratory of marine biogeochemistry

Author contribution statement

I declare that my contribution to the publication:

Gonzalo, F. A., Koziorowska, K., Bromboszcz-Szczypior, L., Loginova, A., & Kuliński, K. (2026). High vertical resolution measurements of pH, pCO 2, Total Alkalinity and Dissolved Inorganic Carbon using a new approach: the carbonate profile. Oceanologia, 68(1), 68101.

Involved: Data curation.

and accounted for 5% of the total work needed for the realization of this publication.

Laura Bromboszcz-Szczypior

Sopot, 18/03/2026

Dr Alexandra Loginova

Institute of Oceanology of the Polish Academy of Sciences

Laboratory of remote sensing

Author contribution statement

I declare that my contribution to the publication:

Gonzalo, F. A., Koziorowska, K., Bromboszcz-Szczypior, L., Loginova, A., & Kuliński, K. (2026). High vertical resolution measurements of pH, pCO 2, Total Alkalinity and Dissolved Inorganic Carbon using a new approach: the carbonate profile. Oceanologia, 68(1), 68101.

Involved: Writing – review & editing.

and accounted for 5% of the total work needed for the realization of this publication.

(Loginova)

Sopot, 18/03/2026

Dr. hab. Karol Kuliński

Institute of Oceanology of the Polish Academy of Sciences

Laboratory of marine biogeochemistry

Author contribution statement

I declare that my contribution to the publication:

Gonzalo, F. A., Koziorowska, K., Bromboszcz-Szczypior, L., Loginova, A., & Kuliński, K. (2026). High vertical resolution measurements of pH, pCO 2, Total Alkalinity and Dissolved Inorganic Carbon using a new approach: the carbonate profile. Oceanologia, 68(1), 68101.

Involved: Conceptualization, Methodology, Funding acquisition, Project administration, Supervision, Validation, Writing– review & editing.

and accounted for 15% of the total work needed for the realization of this publication.

Karol Kuliński